A Helicopter Observation Platform for Atmospheric Boundary Layer Studies

by

Heidi Eichinger Holder

Department of Civil and Environmental Engineering
Duke University

April 1, 2009
Approved:

____
Roni Avissar, Supervisor

____
Donald Bliss

____
Andrey Khystov

____
Amilcare Porporato

Dissertation submitted in partial fulfillment of
the requirements for the degree of Doctor
of Philosophy in the Department of
Civil and Environmental Engineering in the Graduate School
of Duke University

2009

ABSTRACT

A Helicopter Observation Platform for Atmospheric Boundary Layer Studies

by

Heidi Eichinger Holder

Department of Civil and Environmental Engineering
Duke University

Date: April 1, 2009
Approved:

____
Roni Avissar, Supervisor

____
Donald Bliss

____
Andrey Khlystov

____
Amilcare Porporato

An abstract of a dissertation submitted in partial
fulfilment of the requirements for the degree
of Doctor of Philosophy in the Department of
Civil and Environmental Engineering in the Graduate School
of Duke University

2009

Abstract

Spatial variability of the Earth's surface has a considerable impact on the atmosphere at all scales and understanding the mechanisms involved in land-atmosphere interactions is hindered by the scarcity of appropriate observations. A measurement gap exists between traditional point sensors and large aircraft and satellite-based sensors in collecting measurements of atmospheric quantities. Point sensors are capable of making long time series of measurements, but cannot make measurements of spatial variability. Large aircraft and satellites make measurements over large spatial areas, but with poor spatial and temporal resolution. A helicopter-based platform can make measurements on scales relevant for towers, especially close to the Earth's surface, and can extend these measurements to account for spatial variability. Thus, the Duke University Helicopter Observation Platform (HOP) is designed to fill the existing measurement gap.

Because measurements must be made in such a way that they are as uncontaminated by the platform itself as much as is possible, it is necessary to quantify the aerodynamic envelope of the HOP. The results of an analytical analysis of the location of the main rotor wake at various airspeeds are shown. Similarly, the results of a numerical analysis using the commercial Computational Fluid Dynamics software Fluent are shown. The optimal flight speed for the sampling of turbulent fluxes is found to be around 30 m/s. At this airspeed, the sensors located in front of the nose of the HOP are in advance of the wake generated by the main rotor. This airspeed is also low enough that the region of high pressure due to the stagnation point on the nose of the HOP does not

protrude far enough forward to affect the sensors. Measurements of differential pressures, variables and turbulent fluxes made while flying the HOP at different airspeeds support these results. No systematic effects of the platform are seen at airspeeds above about 10 m/s.

Processing of HOP data collected using the current set of sensors is discussed, including the novel use of the Empirical Mode Decomposition (EMD) to detrend and filter the data. The EMD separates the data into a finite number of Intrinsic Mode Functions (IMFs), each of which is unique and orthogonal. The basis is determined by the data itself, so that it need not be known *a priori*, and it is adaptive. The EMD is shown to be an ideal tool for the filtering and detrending of the HOP data gathered during the Cloud and Land Surface Interaction Campaign (CLASIC).

The ability of the HOP to accurately measure atmospheric profiles of atmospheric variables is demonstrated. During experiments conducted in the marine boundary layer (MBL) and the convective boundary layer (CBL), HOP profiles of potential temperature are evaluated using an elastic backscatter lidar. The HOP and the lidar agree on the height of the boundary layer in both cases, and the HOP effectively locates other atmospheric structures.

Atmospheric sensible and latent heat fluxes, turbulence kinetic energy (TKE) and horizontal momentum fluxes are also measured, and the resulting information is used to provide context to tower-based data collected concurrently. A brief comparison made over homogeneous ocean conditions yields good results. A more exhaustive evaluation is made using short HOP flights performed above an orchard during the Canopy Horizontal Turbulence Study (CHATS). Randomly selected one-minute sections of tower data are used to calculate fluxes to which the HOP fluxes can be more directly compared, with good results. Profiles of atmospheric fluxes are used to provide context to tower-based measurements.

In conclusion, the research conducted here demonstrates unambiguously that the HOP is a unique platform that fills an important gap in observation facilities for the atmospheric boundary layer. It is now available to the scientific community for performing research, which is likely to help bridging existing knowledge gaps in various aspects of Earth surface (continental and maritime) – atmosphere interactions.

Dedication

For Chris, love always.

Contents

List of Tables

List of Figures

Acknowledgements

Many, many thanks go out to my advisor, Dr. Roni Avissar, for all of his guidance and encouragement. This was definitely not always an easy process, but I have learned an amazing amount, both professionally and personally. It says a lot that I can finally drive past the Burlington airport exit without cringing.

I am also greatly indebted to the members of my graduate committee, Drs. Donald Bliss, Andrey Khlystov and Amilcare Porporato. I appreciate your advice and feedback. I would also like to thank the members of the Avissar group. I will miss all of the discussions and arguments held in our office from which I also learned a lot both professionally and personally.

Finally, I would like to thank my family and friends (especially Chris and Darrow Holder and Leanne and Bill Eichinger) for their support, encouragement and patience. Now I have no excuse for not returning phone calls and emails.

This research was funded by the National Science Foundation Award Number 0623182 and the National Aeronautics and Space Administration Award Number NNX07AJ60G-S01. Additional support was provided by a James B. Duke Fellowship.

1. Introduction

As pointed out by many researchers and studies, e.g., Avissar and Pielke (1989), Avissar and Schmidt (1998), Schmid (2002), Avissar and Werth (2005), Kim et al (2006), and also emphasized in a recent report of the National Research Council on Integrating Multiscale Observations of U.S. Waters (NRC, 2008), spatial variability of the Earth's surface has a considerable impact on the atmosphere at all scales. While much has been accomplished with conventional point instruments, they are inadequate for the study of three dimensional, heterogeneous processes over large areas. Understanding the mechanisms involved in land-atmosphere interactions in a highly heterogeneous environment is hindered by the scarcity of appropriate observations. Observing the physical and chemical properties of the atmosphere near the Earth's surface, both over land and water, remains a great challenge. This is particularly true for the turbulent fluxes of water, energy, trace gases and aerosols. In order to understand the cycles of these quantities through the atmosphere and thus to predict them accurately, it is essential to find a way to link inexpensive, long-term, point measurements with large scale remotely-sensed quantities. For decades, the benefits of using aircraft to sample the Earth's boundary layer and to extend surface measurements have been clear. The development and use of a helicopter-based observation platform (HOP) dedicated to such a task is described here.

1.1 The Need for Aircraft Measurements

Long time series of measurements of atmospheric variables over land are easily and relatively inexpensively made using tower-based sensors. As a result, most theories and model parameterizations are developed using this kind of data. However, fixed-point sensors provide only a limited number of points in the lower atmosphere, and most practical applications of atmospheric data are spatial in nature. Weather forecasting, climate prediction and satellite measurement validation, for example, require highly resolved spatial coverage of measurements. Aircraft-based sensors are ideal for the study of spatial phenomena, such as mesoscale motions or the effects of heterogeneous land surfaces on the PBL. The spatial nature of aircraft data is also valuable for use in the improvement of satellite algorithms (Desjardins et al 1995) and climate modeling (Heinemann and Kerschgens 2006). Even using a high-density network of towers (which is practical only at the microscale), deciphering the footprints of spatial variability in the atmospheric variables has had only very limited success (e.g., Schmid 2002). Combining towers and remote sensing techniques (from space and/or the ground) helps mitigate the obvious deficiency of point observations, yet many of the processes linking the two methods are empirical in nature and the fundamental mechanisms needed to use such an approach more efficiently and more accurately remain to be elucidated (Kim et al 2006).

Many different types and sizes of aircraft have been used to make spatio-temporal observations of the atmosphere. As aircraft have a limited flight time capability and are expensive to operate, they are used only in relatively short missions, typically as part of dedicated intensive field campaigns. Yet, in spite of these obvious limitations, they fulfill a key role in our observation strategy, making in situ measurements covering areas from tower-scales to satellite-scales. An overview of fixed point *versus* airborne observations is provided in Muschinski et al (2001).

Aircraft are capable of making measurements throughout almost the entire atmosphere, and certainly throughout the entirety of the Earth's Planetary Boundary Layer (PBL). Not only are aircraft able to probe a large vertical extent, but they are capable of covering horizontal spatial scales ranging from a few kilometers to a few hundred kilometers in a relatively short time. They may travel with a parcel of air moved by the wind, or they may travel at any angle or speed relative to it (Lenschow 1986). This allows a wide variety of atmospheric phenomena to be studied in situ and as they evolve, such as industrial plumes or boundary layer dynamics.

In particular, airborne measurements of atmospheric fluxes are especially interesting over heterogeneous terrain. Such measurements improve understanding of land-atmosphere interactions and PBL development, and complement tower-based measurements. Small aircraft, particularly helicopters, have the ability to sample quickly at several altitudes, leading to a better concept of the propagation of land surface effects throughout the PBL. Ultimately, these advances in knowledge will improve the way that heterogeneity is treated in numerical models (Mahrt, MacPherson and Desjardins 1994). With a better understanding of land-atmosphere interactions, models will be able to simply use remotely-sensed measurements of land surface parameters, rather than directly measured atmospheric fluxes, which have far less coverage spatially and/or temporally, for boundary conditions and forcing.

In the early 1970's, measurements of turbulent fluxes made from aircraft over the ocean at various altitudes began to be made with good results (Warner 1972; Donelan and Miyake 1973; Pennell and LeMone 1974; Nicholls 1978). Several platforms have been used with much success, including the Canadian National Research Council (NRC) Twin Otter research airplane (Guo et al 1995; Desjardins et al 1992; Ogunjemiyo et al 1997; Ogunjemiyo et al 2003; Mahrt, Vickers and Sun 2001, among others). The National Oceanic and Atmospheric Administration has successfully collected atmospheric measurements using a Rutan "Long-EZ" aircraft (Oechel et al 1998; Dobosy et al 1997) and the National Center for Atmospheric Research has a established record of measurements based a Lockheed Electra (Lenschow et al 1991; Dobosy et al 1997; Burns et al 1999; Nichols et al 1983). Many studies have been made using a Beechcraft King Air developed by the University of Wyoming (Dobosy et al 1997; Kang et al 2007; LeMone et al 2003; Kelly et al 1992; LeMone et al 2007). Many other platforms have been used with success.

1.2 Advantages of Helicopter-Based Platforms

In general, large airplanes have expensive costs for fuel, maintenance, and personnel, but may house a full complement of scientific investigators. They have long flight durations, large payloads, and fast transit speeds. But at the airspeeds needed for large airplanes to maintain lift (at least 60-70 m/s), turbulent fluxes are measured with poor accuracy. While it is possible for them to fly low (as they do, obviously, on landing and takeoff), it is not practical and a quite risky maneuver outside of an airport environment. Furthermore, the USA Federal Aviation Regulation (FAR §91.119) essentially prohibits low-level flights (i.e., less than 500 ft above ground level (AGL)) with airplanes over much of the continental USA, as it is difficult in practice to find a long enough flight leg without operating "*...closer than 500 feet to any person, vessel, vehicle, or structure.*"

Small airplanes have lower costs, but they also have limitations on duration, speed and maximum payload. The slower speed (as compared to large airplanes) is an advantage for aerosol sampling and for measuring turbulent fluxes, but it prohibits the use of small airplanes in areas more than ~100 km from an airport since the transit time will often require 50% or more of the allowable flight duration. This limitation is particularly relevant for off-shore research missions. To alleviate the payload limit, the Network of Airborne Environmental Research Scientists (see www.naers.org) suggests simultaneously using well-coordinated aircraft, each one dedicated to a particular instrument. An important point to note is that there is no distinction in FAR §91.119 between types of airplanes, and they are all subject to the same altitude restrictions, no matter how small they are.

The main advantage of the helicopter is that it combines slow airspeed and near-surface flight capability (Muschinski et al 2001, Siebert et al 2006). The importance of slow airspeed measurements, which has been discussed in detail by Siebert et al (2006), is perhaps best illustrated with a realistic example. Assuming that a helicopter flies at an airspeed that is 1/3 that of an airplane (say, 25 m/s *vs* 75 m/s), it measures atmospheric variables at a spatial resolution three times higher than that obtained by the airplane if both use the exact same sensors. This is important for measuring the high-frequency turbulent perturbations that can be an important component of the turbulent fluxes in the PBL. The importance of low-altitude flight capability is illustrated in Figure 1, which shows a characteristic vertical profile of sensible heat flux in the convective boundary layer (CBL).

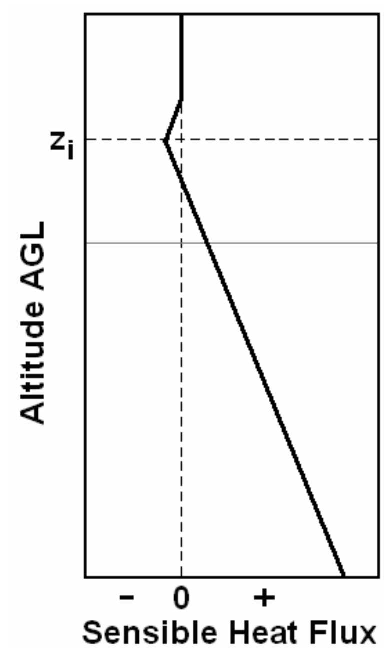

Figure 1: Schematic profile of turbulent sensible heat flux in a typical CBL (z_i indicates its top). The grey, horizontal (solid) line illustrates an example of minimum allowed flight altitude for airplanes.

Understandably, an airplane not allowed to fly below the altitude illustrated with the grey line would be limited to sampling the CBL at heights where the absolute value of the flux is small. The loss of accuracy and precision associated with the loss of high-frequency turbulent motions due to high airspeed (Siebert et al 2006) could result in measurements that generate an error in the flux calculation that is at least of the same magnitude as the flux itself.

Given that the sensible heat flux decreases linearly with height in the mixed layer, the entire profile could, in principle, be assessed from two altitudes, yet minor absolute errors at two altitudes near the CBL top could result in large errors in derived surface fluxes. On the other hand, a sampling just above the atmospheric surface layer and near the top of the CBL results in a much more reliable flux profile. It is worth noting that during the Cloud and Land Surface Interaction Campaign (CLASIC) in June 2007, surface sensible heat fluxes of less than 30 W/m^2 and PBL heights of 200-300 m were frequently observed. Thus, airplane measurements of that variable would not have been very useful given the precision and sampling frequency of even the most sophisticated, state-of-the-art sensors currently available. A similar case could be made for any turbulent flux that varies with height in the PBL. This is even more crucial when the surface flux is dependent on the land-cover type (as is the case for heat, momentum, moisture, CO_2 and many trace gases and aerosols), in which case it is unrealistic to expect reasonable estimates of surface fluxes from airplane observations. The importance of low-level flights is also important for the stable boundary layer, which is typically much shallower than the CBL and is often dominated by transient waves and instabilities, and by intermittent, small-scale turbulence that is neither homogeneous nor stationary.

Lenschow et al (1994) investigated the errors obtained in flight legs. They found that the maximum systematic and random errors could be estimated by $2.2z_i(z/z_i)^{0.5}/L$ and $1.75(z/z_i)^{0.25}(z_i/L)^{0.5}$, respectively, where z_i is the height of the convective boundary layer, z is the flight altitude, and L is the length of the flight leg. Accordingly, they estimated that flying a 4,000-m leg at an altitude of 100 m AGL in a 1,000-m deep boundary layer resulted in a maximum systematic error of 17% and a maximum random error of 49%. Flying a 10-km leg at a height of 30 m AGL, as can easily be done with a helicopter, reduces these theoretical errors (which cannot be reached in real flight conditions) to about 1% and 7%, respectively.

The helicopter platform can also enjoy an effectively longer duration at the designated sampling area, since it can land and refuel at locations inaccessible to fixed-wing aircraft, removing the waste of fuel and time that occurs in transit. Indeed, it is logistically possible to bring a fuel truck to a landing site at or near the sampling area where the helicopter could stop regularly for refueling. Perhaps the biggest advantage of all, which has been demonstrated with the "Helipod" (a gliding pod towed by a helicopter) described by Muschinski and Wode (1998), is the opportunity to perform marine observations far from shore using a helipad aboard a ship. Such a helipad is available, for instance, on the NOAA *David Starr Jordan* and could be adapted to fit other research vessels to make remote marine locations requiring a US Class I research ship accessible, with effectively all of the flight hours available on station for observations. Modern commercial cruisers are also typically equipped with helipads, and cooperation with the scientific community, as may be best demonstrated with the past research missions conducted on the *Explorer of the Seas* (see www.royalcaribbean.com) is feasible. It is therefore conceivable to deploy a properly equipped HOP for marine operation in collaboration with passenger and/or cargo ships. Unlike even large aircraft that can remain on station for a few hours before heading back to shore, a helicopter on a ship could stay at sea for extensive periods thus providing the opportunity for long marine atmospheric campaigns. The magnitude of turbulent fluxes, aerosols and atmospheric chemistry above the oceans remain uncertain, and a HOP has the potential to revolutionize the quality and quantity of scientific information that could be gathered there.

Despite these advantages, helicopters have been used mostly for remote sensing applications (e.g., Babin 1996), and only sporadically for in-situ atmospheric sampling. One helicopter platform has been used to monitor air quality in Belgium (Roeckens et al 1992; De Saeger et al 1993). The Tennessee Valley Authority (TVA) has also operated a helicopter-based platform, based on a Bell 205 helicopter (Hubler et al 1998). This helicopter is mainly equipped with instrumentation to measure gaseous and particulate atmospheric pollutants, as well as temperature, pressure, relative humidity and aircraft position and attitude (Luria et al 1999; Imhoff et al 2001; Imhoff et al 2000; Gillani et al 1998; Valente et al 1998; Imhoff et al 1995).

More recently, the Helipod has measured atmospheric properties using a pod towed on a 15 m cable underneath the main cabin (Muschinski and Wode 1998; Roth, Hofmann and Wode 1999a; Roth, Hofmann and Wode 1999b; Roth 1999; Wolff and Bange 2000). The HELIPOD has been successfully used to measure turbulent fluxes under a variety of conditions, including in the nocturnal boundary layer (Bange and Roth 1999), over a heterogeneous land surface (Bange et al 2006b), and in the polar region (van den Kroonenberg and Bange 2007). HELIPOD measurements compare favorably to ground-based and remote sensing measurements (Bange et al 2002) and to the results of numerical models (Bange et al 2006a; Heinemann and Kerschgens 2006).

In part, the infrequent use of helicopters can be attributed to the popular belief in our scientific community that atmospheric sampling on a helicopter is not feasible because of the main rotor “downwash.” But as illustrated in Figure 2 and discussed by Siebert et al (2006), even at low airspeed, the wake created by the main rotor is skewed backward and has practically no impact on the air in front of the helicopter nose.

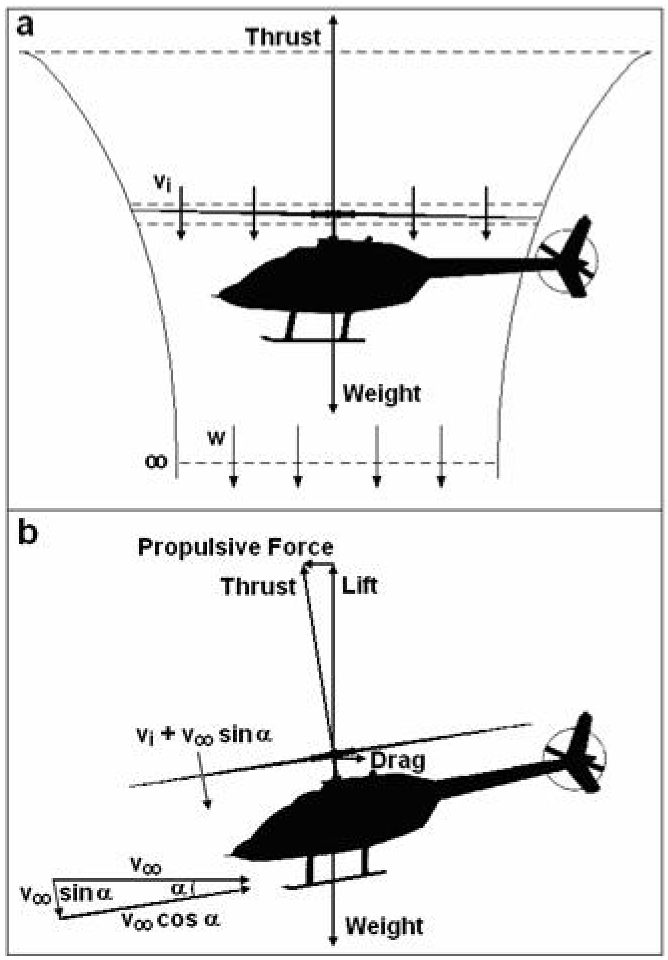

Figure 2: Schematic representation of Glauert’s (1935) rotor-wake model (a) at hover, and (b) in forward flight (adapted from Leishman 2006, e.g., Figure11.7, Page 661, among many other examples in that textbook).

This is why the pitot tube of many helicopters is installed at that location (including on the Jet Ranger, which is the helicopter adopted for the Duke Helicopter Observation Platform) so that even at airspeeds as low as 6-7 m/s the rotor wake has no significant impact on the helicopter instrument readings. Obviously, accurate flight instrument readings are essential for flight safety so that measuring the rotor wake instead of the undisturbed atmosphere would be unacceptable.

2. The Duke University Helicopter Observation Platform

Given the obvious usefulness of a helicopter-based atmospheric measurement system, Duke University purchased and equipped a Bell 206B Jet Ranger helicopter. The first step, however, towards accomplishing the task of making accurate atmospheric measurements is to understand the capabilities and limitations of the platform. It is essential to quantify the aerodynamic envelope of the helicopter in order to make informed decisions about where to place instruments and how to best design field campaigns.

2.1 Aerodynamic Envelope

There is abundant professional literature that describes the theory, experiments, and physical and numerical models that have been developed and applied to explain the wake generated by the main rotor and its interactions with the helicopter frame while hovering and in forward flight (e.g., Leishman 2006). In part to dispel the above-mentioned "downwash" misconception, but primarily to identify the range of airspeeds that provide the best results for measuring fluxes and aerosols (which is essential for research mission planning), the problem was examined from several directions. These included an analytical model, numerical simulations, and observations collected on board the HOP. These studies are summarized below.

2.1.1 Analytical Study

Rotor performance in flight was first derived and explained by Glauert (1935) based on the analysis of marine propellers proposed by Rankine (1865) that was further developed by Froude (1878) and Froude (1889). It is often referred to as the "Rankine-Froude Momentum Theory." It is thoroughly described in most introductory textbooks on helicopter aerodynamics (e.g., Leishman, 2006) and a simplification of this flow model is adopted here.

Figure 3 shows the magnitude of the airflow velocity through the rotor, and the resultant airflow velocity and the angle of the rotor wake obtained with this model at various airspeeds, from hover to 30 m/s. It is interesting to note that the induced-air velocity decreases rapidly with airspeed and, as a result, the wake angle switches from vertical at hover to about 68^{o} at an airspeed of 15 m/s. The angle between the tip of the blade (when aligned with the front of the helicopter) and the nose of the helicopter is about 57^{o}, which is clear of the rotor wake at an airspeed of about 10 m/s. This very simple analysis is clearly supported by the observations of Leishman and Bagai (1991).

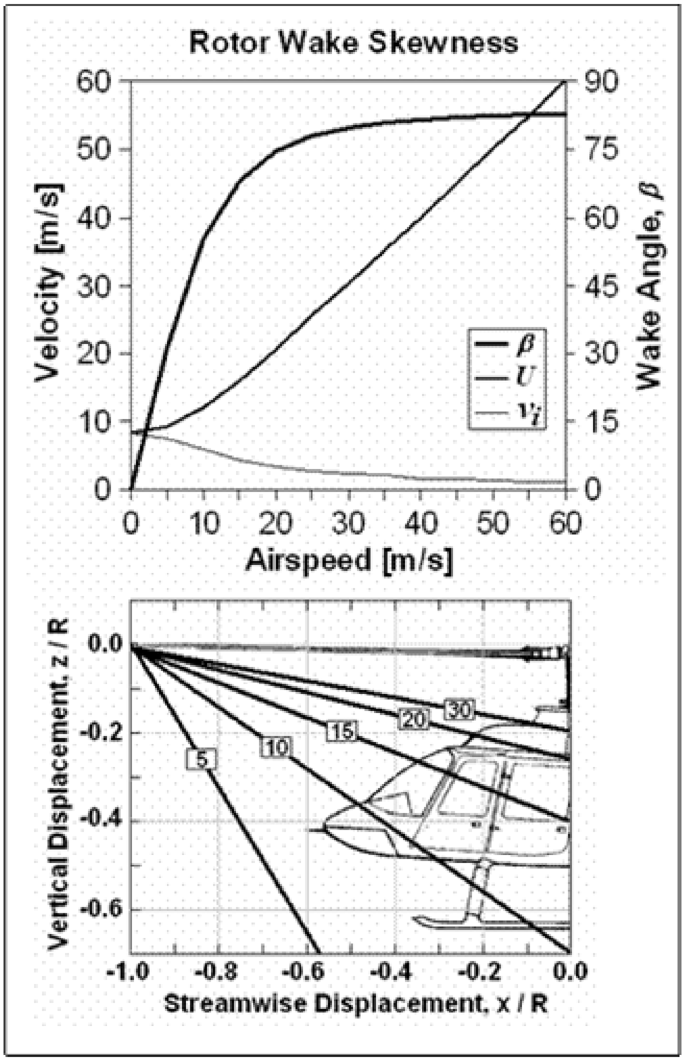

Figure 3: (Upper frame) Induced velocity (v_i), resultant velocity (U), and resultant wake angle (β) defined from the normal to the plane of rotation at the tip of the rotor blade when aligned with the longitudinal axis of the helicopter and above its nose {$\beta = \text{arctg}[v_\infty \cos\alpha/(v_i + v_\infty \sin\alpha)]$; v_∞ is the free-stream velocity and α is the angle between the rotor plane of rotation and the free-stream direction} for the Jet Ranger at various airspeeds. (Lower frame) Location of the wake leading edge as a function of distance from the blade root (x) and plan of rotation (z) normalized by the rotor radius (R) at airspeeds of 5 m/s, 10 m/s, 15 m/s, 20 m/s, and 30 m/s. Note, all calculations take into account that the rotor diameter of the Jet Ranger is 10.16 m, and with one pilot on board, fully fueled, and with its current sensors and data acquisition system, the HOP mass is about 1,400 kg. We assumed $\alpha = 6^o$, which is the mast tilt angle on the Jet Ranger.

2.1.2 Numerical Study

FLUENT (www.fluent.com), a state-of-the-art commercial computational fluid dynamics (CFD) software, was used to simulate the Jet Ranger in flight at different airspeeds. Figure 4 illustrates some of the simulation results. Initially, the streamlines are horizontal and the background airspeed is constant in space and time. Therefore, any impact from the helicopter on the airflow is seen on these graphs as a departure of the streamlines from horizontal and/or a change of color.

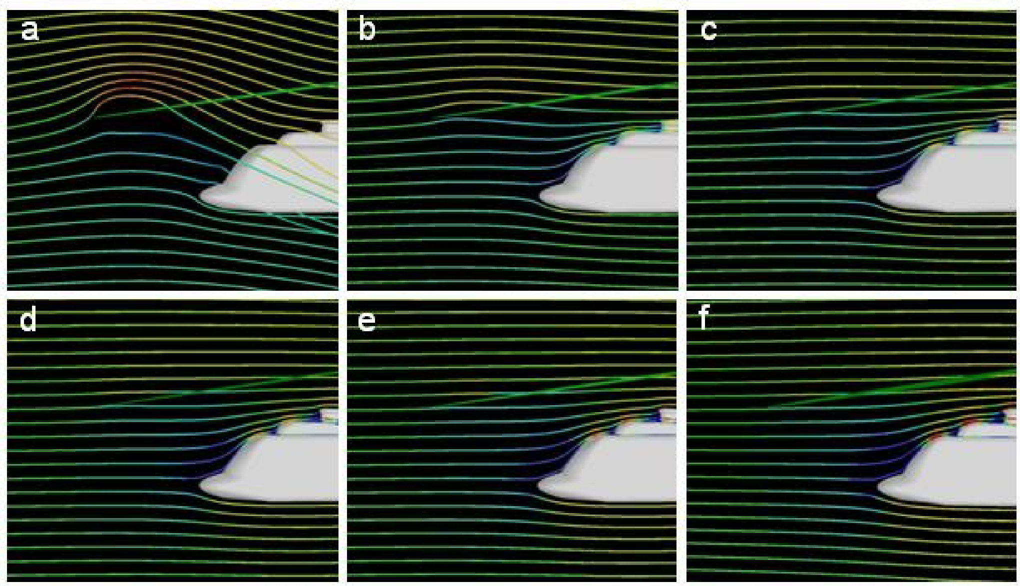

Figure 4: FLUENT simulations of streamlines near the front of the Jet Ranger flying at airspeeds of (a) 10 m/s, (b) 20 m/s, (c) 30 m/s, (d) 40 m/s, (e) 50 m/s, and (f) 60 m/s. The dark blue and red colors indicate airflow velocities that are significantly lower (-10 m/s) and higher (+10 m/s) than the undisturbed air, respectively.

It is interesting to note that, concerning the main-rotor wake position at different airspeeds, there is no conceptual difference between these results and those obtained with the simpler analytical study discussed in the previous section. This emphasizes the robustness of the assumptions and simplifications made in our analytical study.

However, an important result of the CFD simulations shows that as the helicopter flies faster and faster, a “pocket” of compressed air develops and grows in front of it, creating another zone of air disturbance that is independent of the main rotor. This additional disturbance is similar to that observed in front of airplanes, and it is affected by the shape of the aircraft as well as its airspeed. This is well simulated with the CFD but ignored in the analytical study. Figure 5 shows the relative disturbance created by the rotor versus the airframe of the helicopter at different airspeeds and distances from its nose. This disturbance is defined, similar to turbulence kinetic energy, as half the sum of the velocity perturbation variances in the three directions relative to the aircraft movement (i.e., longitudinal, lateral, and vertical). For comparison, we also simulated the disturbance in front of an airplane about the size of a Twin Otter flying at 60 m/s. This type of airplane, whose propellers are located on its wings far away from its nose, is frequently used for research missions (see, e.g., the Center for Inter-Disciplinary Remotely Piloted Aircraft Studies – CIRPAS – at http://www.cirpas.org).

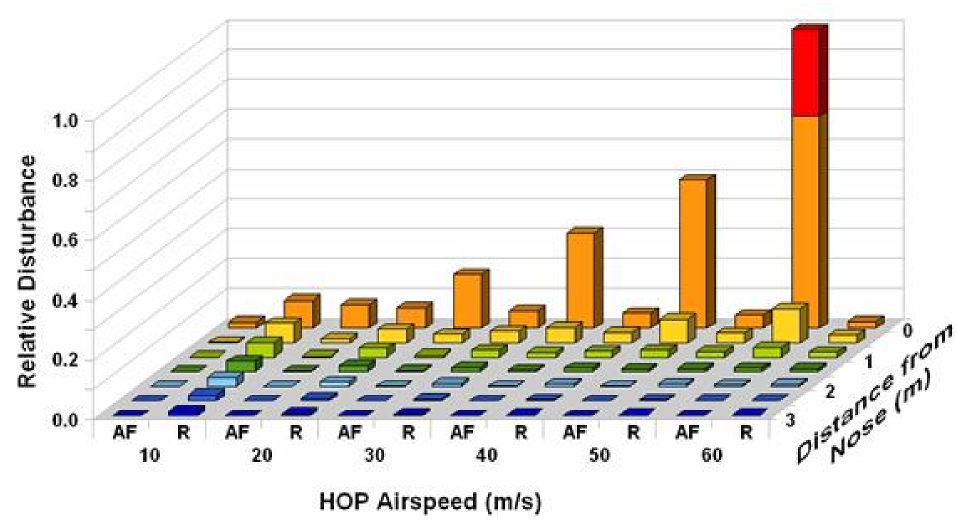

Figure 5: Airspeed disturbance generated by the rotor alone (R) and the airframe alone (AF) of the Jet Ranger relative to the disturbance generated near the tip of an airplane nose (similar in size to a Twin Otter) flying at an airspeed of 60 m/s (red column). All results are derived from FLUENT simulations and are averaged values for a 2-m wide and 1-m high area centered at the tip of the nose of the aircraft. The various colors are for different distances from the tip of the nose (0, 0.5, 1, …, and 3 m).

All results in Figure 5 are normalized by the disturbance near the nose[1] of the airplane and one can see that at a speed of 60 m/s, the helicopter airframe disturbance is only about 70% that of the Twin Otter. Of course, the size of the cabin and the shape of the nose are important factors in this relation and this only indicates that given the small size of the helicopter, it is less disturbing than a larger research airplane. Interestingly, however, the sum of the airframe and rotor disturbances is still much smaller than that of the airplane airframe. Also, at airspeeds of 20 – 40 m/s, the total disturbance in front of the helicopter nose is much smaller than that obtained in front of the airplane flying at 60

[1] A 2-m^2 plan (2-m wide and 1-m high) perpendicular to, and centered at, the tip of the nose of the aircraft is used.

m/s, especially within the first meter from the tip of the nose, where it is easiest to install most sensors and inlets. At these airspeeds, neither the main-rotor wake nor the airframe of the Duke HOP significantly disturbs the atmosphere at this location. In a practical sense, these studies show that there is a minimum flight speed necessary to minimize the rotor effects (more than 20 m/s), but that there is also a maximum speed (less than 60 m/s) which must not be exceeded in order to minimize pressure-drag effects.

2.2 Platform Description

The Bell 206B Jet Ranger adopted for the Duke HOP is a light, single engine (turbine) helicopter that was originally designed as a light observation helicopter for the US Army. Its first commercial version was certified in 1966, and while many of its components have been improved over the past 40+ years, its conceptual design dates back to the early sixties. It is simple, robust, and nimble, and based on the US National Transportation Safety Board (NTSB) statistics, it is the safest, single-engine aircraft (including airplanes!) flying today. It has been used extensively for military, police, news gathering, and many other applications all over the world. As a result, it benefits from a very broad international network of technical support.

A full description of the Jet Ranger characteristics and performance is available on the manufacturer's website at www.bellhelicopters.com, and only the most relevant characteristics for its use as the Duke HOP are summarized in Table 1.

Table 1: Main characteristics and performance of the Duke HOP.

Characteristics	Duke HOP
Maximum Gross Weight (MGW)	3350 lbs
Base Operating Weight (BOW)	2900 lbs
Additional Payload Capability (APC)	450 lbs
Aft Cabin and Baggage Cargo Volume	56 ft^3
Maximum Altitude for Research Mission	12,000 ft
Maximum Endurance for Research Mission	3.67 hrs

While its available payload capability (APC) for scientific instrumentation is limited, when compared to its hourly fuel consumption, it is one of the most efficient turbine helicopters. Thus, it is comparatively cheap to operate, which was another reason (in addition to safety record and technical support) to adopt it as the Duke HOP.

Seats, all unnecessary plastic covers and sound-proofing material were removed from the 40-ft^3 aft cabin to reduce its weight and to make room for instrument and computer racks. This resulted in an increase of the APC by nearly 120 lbs. The co-pilot/passenger seat in the forward cabin was also eliminated to make room (~18 ft^3) for an Atmospheric Chemistry Package (ACP) with inlets going straight through the helicopter nose. The ACP is expected to become available for research missions in 2009.

There is also a 16-ft^3 baggage compartment located behind the aft cabin that can be exploited for additional instruments and computers, if needed.

The Jet Ranger DC generator provides 105A (28V) on a continuous basis (200A for 5 s and 170A for 2 min). In its configuration as the Duke HOP, the navigation and communication systems use ~42A in cruise flight, thus leaving up to ~63A for the continuous operation of the research equipment. This equipment consists of a Data Acquisition System (DAS), instruments, and sensors. In an upcoming upgrade scheduled for Spring 2009, an alternator capable of generating an additional 100A will be installed on the platform. It will be dedicated for research equipment. Two independent power inverters (from 28V DC to 110V AC) provide ~4 KW of standard 110V AC power for the research equipment. The DAS and all instruments and sensors are controlled by switches located in the cockpit and operated by the pilot.

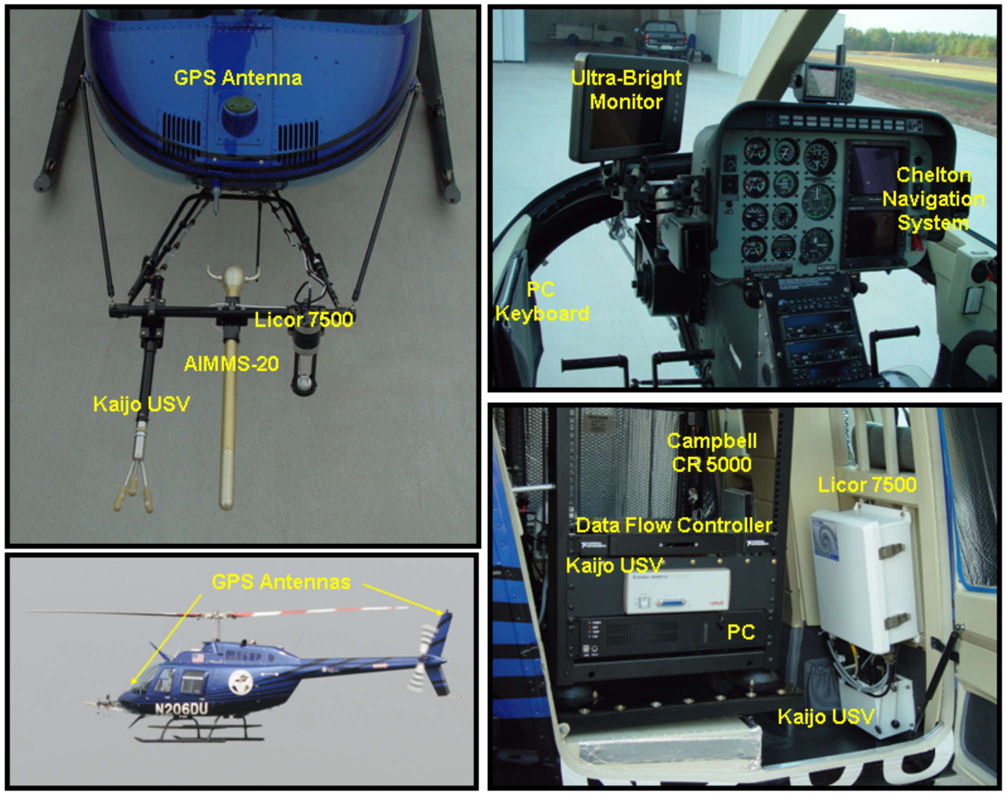

Figure 6: (Left) Permanent sensors mounted on the Duke HOP; (Upper Right) Pilot cockpit; And (Lower Right) aft cabin seen from the right side.

Figure 6 shows pictures of the HOP as it is currently equipped with its permanent scientific instrumentation, i.e., the sensors that are expected to be used for any scientific mission. This set of sensors consists of an Aventech Research Inc. (www.aventech.com) AIMMS-20 that measures the three components of the wind, temperature and relative humidity, a Licor (www.licor.com) LI-7500 that measures water vapor and CO_2 concentrations, and an Ultrasonic Velocimeter (USV) prototype developed by the Kaijo Sonic Corporation in collaboration with Japan Aerospace Exploration Agency (JAXA) (Matayoshi et al 2005). This USV also measures the three components of the wind and the virtual temperature. As this information is crucial for the calculation of all turbulent fluxes, it is beneficial to have this duplication, especially because the two sensors are based on different technologies. Both the AIMMS-20 and USV have a data output rate of 40 Hz and the Licor has an output rate of 160 Hz, which is reduced to 40 Hz for consistency with the other sensors when calculating fluxes.

The AIMMS-20 consists of four modules: (1) An air-data probe (located on the nose of the HOP) that senses temperature, humidity, barometric pressure, the three-dimensional aircraft-relative airflow vector and the three-axis acceleration and magnetic field measurement; (2) An inertial measurement unit that provides three-axis acceleration and three-axis angular rates; (3) A dual processor global positioning system that includes dual antenna inputs for differential carrier-phase measurement (one antenna is located on the nose and the other one is on the tail of the HOP); And (4) a central processing module that, among other functions, converts the inertial and GPS phase/position/velocity data into precise attitude data (roll, pitch, true heading). This processed information is shared with all other sensors and, therefore, the AIMMS-20 is operated during all research missions. It is also used to coordinate the clock between the different sensors and to trigger data storage (see below).

The LI-7500 Open Path CO_2/H_2O gas analyzer consists of two components: (1) The analyzer sensor head that is mounted on the nose of the HOP, and (2) the control box, which houses the electronics and is located in the aft cabin (Figure 6). The sensor head has a 12.5 cm open path, with single-pass optics and a large 1 cm diameter optical beam. Reference filters centered at 3.95 μm and 2.40 μm provide for attenuation corrections at non-absorbing wavelengths. Absorption at wavelengths centered at 4.26 μm and 2.59 μm provide for measurement of CO_2 and water vapor, respectively. These features minimize sensitivity to drift and dust, which can accumulate during normal operation.

The USV is based on a conventional ultrasonic anemometer that consists of two main components: (1) A probe (also located on the nose of the HOP), which senses the three-dimensional aircraft-relative airflow vector and ambient temperature by measuring ultrasonic pulse transit time between three mounts (Figure 6); And (2) a control box and a junction box (located in the aft cabin), which control ultrasonic pulse emissions and output the measured data via RS-232C. The main advantage of the USV as compared to a pitot-static system is that it can provide accurate measurements at low speed and in crosswinds. This is obviously important for helicopters. Unlike conventional ultrasonic anemometers, the USV uses high-frequency (200 kHz) ultrasonic pulses to reduce acoustic noise, and its probe shape minimizes airflow disturbance at high airspeeds. These modifications allow a broad range of airflow measurements, from 0 to 70 m/s, which covers the entire flight envelope of the HOP.

A PC is used to run a National Instruments LabVIEW (www.ni.com/labview) program that reads the data input from each instrument, parses and displays data, and controls the logging of the data to files. The AIMMS-20 and USV communicate via individual RS232 serial lines to the PC. The Licor outputs two 0-10V analog signals (proportional to water vapor and CO_2) that are connected to the PC through a National Instruments USB-6008 Data Acquisition (DAQ) Card. An independent pressure sensor (with its own static port located under the HOP) that is used to calculate potential temperature in real time provides a 0-10V analog signal that is also wired to the DAQ

Card. Finally, a 0-5V signal is fed through a switch in the cockpit and back to the DAQ card so that the pilot can easily mark the beginning and the end of a measurement flight leg by creating a signal in the log file. This is a useful marker when processing the data after the flight.

The real-time visualization that is displayed on the monitor located in the cockpit includes the potential temperature profile, which is calculated from the temperature measured with the USV and the pressure sensor. This real-time profiling capability is useful for the assessment of the height of the various atmospheric layers and, accordingly, for the selection (in real time) of relevant flight altitudes. It also displays the DAS information in graphic form and a series of green/red virtual buttons indicating the functioning status of the various sensors and instruments.

Section 3.2 below describes in more detail the principles upon which these sensors are based and how their outputs are treated to extract high-frequency atmospheric turbulence variables. Finally, it should be mentioned that the Duke HOP is equipped with the Chelton Flight Systems (www.cheltonflightsystems.com), which is a state-of-the-art navigation system that provides three-dimensional synthetic vision of the terrain with all its obstructions (including antennas, buildings, etc), a complete flight/navigation instrumentation system, and the “Highway-In-The-Sky” (HITS), which depicts the programmable flight track in a perspective-like tunnel. This system helps perform very precise flights according to preset altitudes and coordinates of the path to be flown. It also includes traffic awareness and real-time satellite weather for enhanced safety. It is backed-up by a battery-operated portable GPS Garmin 496 (www.garmin.com) in case of electrical power loss.

2.3 Measurement System

2.3.1 Wind Measurement from Aircraft

2.3.1.1 Transformation from Platform to Earth-Based Coordinates

In order to measure winds from a moving aircraft, it is necessary to measure both the winds relative to the aircraft, and the motion of the aircraft relative to the earth. The aircraft motion and the winds must then be transformed into an Earth-fixed coordinate system. An excellent detailed description of the transformations involved can be found in Lenschow (1972), and is slightly corrected in Lenschow (1986). The explanation found there is based on the more general development of the Eulerian equations of motion of classical physics by Etkin (1959) and the similar development of Axford (1968). Letting an arrow denote a vector, the wind velocity vector, $\vec{v}$, is equal to:

$$\vec{v}_i = \overrightarrow{v_a} + \overrightarrow{v_p} + \overrightarrow{\Omega_p} \times \vec{R} \qquad (1)$$

where $\overrightarrow{v_p}$ is the velocity of the platform with respect to the earth and $\overrightarrow{v_a}$ is the velocity of the air relative to the aircraft. $\overrightarrow{\Omega_p} \times \vec{R}$, where $\overrightarrow{\Omega_p}$ is the angular acceleration of the platform and $\vec{R} = \vec{i}X + \vec{j}Y + \vec{k}Z$, is a required term when the point of measurement of the attitude information (e.g. accelerometers, gyrometer, GPS) is located some distance (X,Y,Z) away from the point of measurement of the winds.

This treatment defines a convenient right-handed Earth-based coordinate system, where x is positive toward East, y is positive toward North and z is positive up, although any right-handed Cartesian coordinate system is equally valid. The aircraft has three degrees of freedom with respect to this coordinate system: heading, pitch and roll. Heading, Ψ, is defined as the angle that the longitudinal axis of the aircraft makes with the Earth-fixed y axis (North), in the x-y (horizontal) plane of the earth, and is positive clockwise from North. Pitch, Q, is defined as the angle that the longitudinal axis of the aircraft makes with the x-y plane, and is positive upwards from horizontal. Roll, Φ, is defined as the angle that the latitudinal axis of the aircraft makes with the horizontal plane; this is positive with the right side of the aircraft (facing it) rotating upwards. Similarly, the wind direction with respect to the aircraft is defined by two angles. The sideslip angle, β, is the angle that the wind makes with the longitudinal axis, in the horizontal plane of the aircraft. Like the heading, the sideslip angle is positive clockwise from the longitudinal axis of the platform. The angle of attack, α, is the angle that the wind makes with the horizontal plane of the aircraft, and so represents the vertical component of the wind. The angle of attack is positive downward.

Since most of the systems used to measure attitude information give this information in an Earth-fixed frame, it is reasonable to assume that the motion of the aircraft is already in an Earth-fixed frame. What is left then is to transform the wind relative to the aircraft into first a platform-based frame, and then an Earth-based one, and to deal with the moment caused by non-co-located measurements. In the frame of reference of the platform, the components of the air velocity, [$v_a^{'}$], are (using the more convenient matrix notation):

$$\left[v_a^{'}\right] = -U\begin{bmatrix}\cos\alpha\cos\beta \\ \sin\beta \\ \sin\alpha\cos\beta\end{bmatrix} \tag{2}$$

where U is the airspeed.

The order of the rotation is important in performing the transformation to Earth-based coordinates, although the final outcome should be the same regardless of the order. In this development, the first rotation is the heading, ψ, made about the z-axis of the Earth-fixed frame of reference. The second rotation is made using the pitch, θ, about the y-axis rotated in the horizontal plane by the angle ψ, and the third rotation is by the roll, ϕ, about the x-axis of the aircraft-based coordinate system (the longitudinal axis). With this order of rotation, the transformation

$$\left[v_a\right] = \left[T_{ij}\right]\cdot\left[v_a^{'}\right] \tag{3}$$

has the transformation matrix (the Jacobean):

$$\left[T_{ij}\right] = \begin{bmatrix}\cos\psi\cos\theta & -\sin\psi\cos\phi + \cos\psi\sin\theta\sin\phi & \sin\psi\sin\phi + \cos\psi\sin\theta\cos\phi \\ \sin\psi\cos\theta & \cos\psi\cos\phi + \sin\psi\sin\theta\sin\phi & \sin\psi\sin\theta\cos\phi - \cos\psi\sin\phi \\ -\sin\theta & \cos\theta\sin\phi & \cos\theta\cos\phi\end{bmatrix}$$

Similarly,

$$\left[R_i\right] = \left[T_{ij}\right]\cdot\begin{bmatrix}X \\ Y \\ Z\end{bmatrix} \quad \text{and } \Omega_{p_i} = \left[T_{ij}\right]\cdot\begin{bmatrix}\dot{\phi} \\ \dot{\theta} \\ \dot{\psi}\end{bmatrix} \tag{4}$$

where $\dot{\phi}$, $\dot{\theta}$ and $\dot{\psi}$ are the angular accelerations associated with ϕ, θ and ψ, respectively.

2.3.1.2 Measurement of Platform Location and Attitude

In order to obtain accurate wind velocity measurements, the position, attitude and groundspeed of the aircraft must be measured with a high degree of accuracy, with a frequency at least as high as that of the wind measurements. Inaccuracy and imprecision of the aircraft attitude information is a major limitation to the accurate measurement of wind velocity (Tjernstrom and Friehe 1991; Foster 2003). A combination of an inertial navigation system (INS) and Global Position System (GPS), usually differential GPS, is most often used in modern aircraft measurement platforms, in a method similar to that presented in Khelif, Burns and Friehe (1999). Neither INS nor GPS are sufficient alone, and the two methods provide complementary measurements. INS, consisting of accelerometers and a gyrometer, is subject to drift and to the Schuler oscillation. The Schuler oscillation is an amplifying error with a period around 84 minutes, and is basically the motion of an undamped pendulum in response to the curvature of the Earth (King 1998). GPS has a relatively low updating frequency, around 1 Hz, and the data is also subject to dropouts whenever the aircraft maneuvers or moves so that a sufficient number of satellites cannot be seen by the receiver, or when the aircraft body or other objects move in between the aircraft and the satellites. Therefore, using the faster and more accurate INS, corrected with the absolute information from the GPS to eliminate drift and the Schuler oscillation, leads to a more accurate solution (Matejka and Lewis 1997).

2.3.1.3 Measurement of Wind Velocity

There are several methods of measuring the wind velocity relative to the aircraft. A hemispherical differential pressure-based wind speed sensor is often used to obtain measurements of wind speed and direction with respect to the aircraft. This technology is based on theory which is well described in the literature (Brown et al 1983, Lenschow 1986, Crawford and Dobosy 1992, Wood et al 1997). Probes such as the Aventech AIMMS-20 (Foster 2003) and the NOAA-ATDD "Best Aircraft Turbulence" (BAT) probe (Crawford and Dobosy 1992; Garman et al 2006) use this theory of operation. These probes use differential pressure measurements made around the hemispherical tip of the probe to determine the three components of the wind, along with the magnitude. Also necessary are measurements of the barometric pressure and 3-D acceleration. Along with differential GPS and a gyroscope to give the absolute position, including the pitch, heading, roll and yaw, the ground speed and the airspeed of the aircraft, the winds can be calculated using a method similar to that described in Khelif et al (1999). The air temperature and relative humidity are also required to calculate the density of the air. Sensors of this type use relatively inexpensive components and are robust, a must for airborne applications (Crawford and Dobosy 1992).

Essentially, wind flowing over a hemisphere creates a pressure distribution over the hemisphere's surface. For fully turbulent flow, this distribution is given by:

$$P_{\Theta} - P_{\infty} = \frac{1}{2}\rho U^{2}\left(1 - \frac{9}{4}\sin^{2}\Theta\right) \tag{5}$$

where P_θ is the pressure at angle Θ (measured from the stagnation point), P_∞ is the static pressure, ρ is the density of air and U is again the speed of the airflow relative to the aircraft (the airspeed). From Bernoulli's equation, the free stream velocity is related to the dynamic (or pitot-static) pressure, ΔP_{ps}, by:

$$\Delta P_{ps} = \frac{1}{2}\rho U^2 . \tag{6}$$

If the pressure is measured at Θ=45 degrees above and below the stagnation point (which is the case for the AIMMS-20), the pressure difference between the ports, ΔP_α is related to the vertical flow angle by:

$$\alpha = -\frac{1}{2}\sin^{-1}\left(\frac{4}{9}\frac{\Delta P_\alpha}{\Delta P_{ps}}\right) \tag{7}$$

where α is the angle of attack that the flow makes with the probe. Similarly, the horizontal flow angle (for ΔP_β measured from pressure ports at 45 degrees on either side of the stagnation point) is given by:

$$\beta = -\frac{1}{2}\sin^{-1}\left(\frac{4}{9}\frac{\Delta P_\beta}{\Delta P_{ps}}\right) \tag{8}$$

where β is the sideslip angle.

In the past, it was common to use wind vanes, either fixed or rotating, to measure the direction of the wind relative to the aircraft, while the magnitude of the airspeed was measured using the pitot-static pressure as in the differential pressure probes (Axford 1968; Lenschow 1986). These wind vanes are fragile and require frequent calibration. In addition, to avoid the effects of the airflow distortion by the aircraft, they must be located on long booms (Crawford and Dobosy 1992). Ultrasonic anemometers have also been used more recently to measure wind speed and direction on aircraft (Marillier et al 1991; Cruette et al 2000), including helicopters (Yazawa et al 2001; Matayoshi et al 2005). In fact, these ultrasonic anemometers are particularly well-suited for helicopter use, since unlike differential pressure-based sensors, they work at low airspeeds. They also work well in high crosswinds, another advantage over pressure-based sensors. In addition, as with the Japan Aerospace Exploration Agency ultrasonic velocimeter (USV), the probes can be designed to be simple and robust (Yazawa, Tamaru and Hashiguchi 2001; Matayoshi et al 2005).

Suomi and Businger (1959) first presented the theory of operation of the ultrasonic anemometer; the technology was developed for practical use shortly thereafter (Mitsuta 1966). Simply, a sonic source emits a short ultrasonic pulse which is detected by a receiver located at a fixed distance *L* away. The time it takes for the pulse to cross this distance, *t*, is measured. With two emitter/receiver pairs whose signal paths cross, the relative wind speed can be calculated:

$$V = \frac{L}{2}\left(\frac{1}{t_1} - \frac{1}{t_2}\right) \tag{9}$$

With three pairs, the full three-dimensional relative wind speed and direction can be calculated. Similarly, the dry-air temperature can be calculated:

$$T = \frac{L^2}{2\gamma_a R_a}\left(\frac{1}{t_1^2} + \frac{1}{t_2^2}\right) \tag{10}$$

In this equation, $\gamma_a = c_{pa} / c_{va}$, the ratio of the specific heat of dry air at constant pressure to the specific heat of dry air at constant volume and $R_a = R^* / M_a$, the specific gas constant of dry air, where R* is the universal gas constant (5.32 kg/m K) and M_a is the molecular weight of dry air. Because this temperature applies to dry air only, it must be corrected using measurements of air humidity, *q*. The relationship between *T*, the measured temperature, and *T′*, the actual temperature, is given by:

$$T' = T(1 - 0.518q) \tag{11}$$

For aircraft use, several adjustments must be made to the traditional ultrasonic anemometer. Traditional tower-based sensors are not designed for the constant high-flow conditions experienced by sensors mounted on aircraft, and experience negative aerodynamic effects (Cruette et al 2000). The instrument's signal-to-noise ratio is decreased at higher airspeeds by an increase in acoustic noise, requiring some method of noise reduction. In addition, the signal must be amplified and/or the aerodynamics of the sensor and the paths between transmitter/receiver pairs must be modified, because as the airspeed increases, more of the energy in the pulses is carried downstream, away from the receiver (Matayoshi et al 2005).

3. Data Processing

3.1 Data Preprocessing

3.1.1 Calibration

Airborne wind velocity sensors must be calibrated in-flight, due to the unpredictability of the airflow distortions caused by the aircraft. Sensors are rarely calibrated in wind tunnels, due to the difficulty of simulating actual flight conditions (Lenschow 1986), although recently a wind tunnel test was performed on the BAT probe, primarily to ensure that the basis flow model is appropriate (Garman et al 2006). Calibration maneuvers entail making changes in the aircraft's attitude and speed and are usually flown in air that is as smooth as possible, typically above the top of the atmospheric boundary layer. For example, if the heading is held steady, and the pitch of the aircraft is varied in a systematic way (usually oscillatory), a systematic error will be present in the uncalibrated data. Often maneuvers are done so that the aircraft flies through the same airspace in different directions; if the maneuver is done quickly enough that the winds can be considered to be constant, the system should measure the same values regardless of heading. Many studies have used a variety of similar flight maneuvers to determine the extent of errors that are present, and the corrections necessary to rectify them as much as possible (Axford 1968; Telford and Wagner 1974; Telford, Wagner, and Vaziri 1977; Nicholls, Shaw, and Hauf 1983; Bogel and Baumann 1991; Tjernstrom and Friehe 1991; Crawford, Dobosy, and Dumas 1996; Kalogiros and Wang 2002a; Kalogiros and Wang 2002b; Strunin and Hiyama 2004; and Garman et al 2006). A potentially more efficient, although similar in concept, calibration method is described and applied to a helicopter-based platform by Hui and Baillie (1996). As technology improves, especially technology relating to measurement of aircraft attitude, the quality and precision of sensor calibration improves.

While it can be easily understood from Equations 2-5 that the position of the AIMMS-20 and the USV in flight relative to the local Cartesian coordinate system is crucial for obtaining accurate readings of the three components of the wind, that of the LI-7500 does not seem to play a significant role (except for possible aerodynamic disturbances). Since the distance between the LI-7500 and the wind velocity sensors is less than the size of the smallest atmospheric structure that the HOP can measure, the orientation of the sensor should not be an issue. A series of calibration flights similar to those described above were conducted to correct as much as possible for the effects of the HOP pitch, roll and yaw when flying at different airspeeds and in crosswinds. These maneuvers followed the procedures suggested by the manufacturers of the respective wind-measurement instruments, who developed and provided the calibration algorithms. It should be noted that there is no need to repeat the calibration flights as long as the position of the AIMMS-20 or the USV on the HOP remains unchanged. Yet the first step in preprocessing the data collected by the AIMMS-20 and the USV consists of applying this calibration algorithm.

The LI-7500 data is calibrated for water mixing ratio and carbon dioxide concentration in laboratory conditions, according to a procedure described by the manufacturer. This procedure is repeated before each field campaign as it involves replacing chemicals whose properties change with time. As part of the above-mentioned calibration flights, the LI-7500 was oriented in different directions relative to its mount (Figure 3), including parallel and perpendicular to the AIMMS-20 (and, therefore, the flight direction). However, no noticeable impact of orientation was identified and there is no specific preprocessing procedure required for that sensor.

3.1.2 Preprocessing

Occasionally, during a high wind gust that may cause the HOP to pitch, roll and/or yaw excessively and rapidly, the attitude of the HOP is outside the range in which the calibration algorithm is applicable. Indeed, due to the aerodynamics of the hemispherical differential pressure sensor, the optimal operating range of the AIMMS-20 is within a sideslip of ±5 degrees. The USV is also calibrated to perform optimally within this range. Therefore, as part of our data preprocessing, an algorithm which automatically flags the data for such occurrences, which are typically not more than a few seconds long, was developed. To maintain the continuity of the data series, this algorithm substitutes the “damaged” data with randomly-generated data with the same mean and variance as the immediate previous and subsequent 0.25 seconds of data. While not perfect, it seems that the error incurred by this substitution is much less significant than the error present in the flawed data, especially when such events are only occasional. For similar reasons, the data collected during steep turns, rapid climbs or descents is typically ignored.

A very large disturbance is incurred in the temperature data collected with the AIMMS-20 when the HOP radio is activated for communication. Similarly, when flying nearby radio and TV towers, data is contaminated. However, these disturbances are easily identified in the time series, and the dataset is correspondingly adjusted.

The AIMMS-20 sensor, to which all other sensors are referenced due to its measurement of the precise timing and attitude information, protrudes about 0.25 m ahead of the LI-7500 (Figure 3). For research missions aimed at measuring the atmospheric variables needed to calculate fluxes using the eddy-correlation technique, it is most practical to fly the HOP at a 30-m/s airspeed. This is slow enough to sample the atmosphere at a high resolution yet fast enough to perform a reasonably long flight leg. As detailed in Section 2.2, this speed is also somewhat optimal to clear the sensors from the HOP main-rotor wake and yet to avoid the distortion of airflow due to its airframe. At this speed, the distance between the AIMMS-20 and the LI-7500 is flown in ~8 milliseconds. However, the AIMMS-20 records a data point only every 25 milliseconds and this discrepancy, which could have an impact on the covariances and co-spectra between the wind components and the water mixing ratio or the carbon dioxide concentration, cannot be captured by the current system. Similarly, the electronic reaction time between the actual sampling and data registering could be a factor that affects such covariances and co-spectra. In general, there is no a priori correlation between the variables measured by the two sensors, and thus estimating this potential bias is problematic. Because of this, the current system relies on the manufacturers' information about the instrument delays.

3.2 Empirical Mode Decomposition

Aircraft observations in the turbulent PBL are contaminated by aircraft movements, which are occasionally erratic and difficult to dissociate from the turbulence signals that are being measured. Additional data contamination sources include aircraft vibrations (typically producing high-frequency noise) and the non-stationarity of the atmosphere along the flight path and during the period of sampling. Therefore, it is essential to use an algorithm to "decontaminate" the observed data series.

The focus of the present study is on the methodology that is used to process the data collected on-board the HOP. It is largely based on the Empirical Mode Decomposition (EMD) introduced by Huang et al (1996) and further discussed by Huang et al (1998, 1999, and 2003). The purpose of the EMD is to separate a signal into its component frequencies, each of which is unique, adaptive and orthogonal. As explained below, this method appears to be particularly appropriate for processing data collected on-board aircraft. While it does not seem to have been used previously for that purpose, the EMD coupled with the Hilbert Spectral Analysis (HSA), which is known as the Hilbert-Huang Transform (HHT), has been used to analyze many different types of datasets. Among others, Lundquist (2003) used it to separate stationary waves and intermittent events in temperature time series, Veltcheva and Soares (2004) and Datig and Schlurmann (2004) applied it in ocean wave analysis, Duffy (2004), Pan et al (2002), and Salisbury and Wimbush (2002) applied it to climatological datasets and Huang et al (2003) analyzed financial records with it. More recently, it was used to study the spectral properties of turbulent heat and carbon dioxide fluxes (Zhaoyang et al 2006). In almost all cases, the HHT provided signals that are much sharper than any of the traditional analysis methods in time-frequency-energy representation. Importantly, it provides true physical meaning to many of the datasets examined.

Here, the EMD method is briefly described. Rather than coupling it to the HSA as has been done by others, here the EMD is used together with the Fourier Transform (FT). While there are advantages of using the HHT method (e.g., Huang et al 1998 and

Zhaoyang et al 2006), turbulence has been studied very extensively with the FT and much theoretical and empirical knowledge is available for comparison with our data.

3.2.1 Method

Using the EMD method, any complicated data set can be decomposed into a finite and often small number of components, which is a collection of so-called intrinsic mode functions (IMFs). An IMF represents a generally simple oscillatory mode as a counterpart to the simple harmonic function. By definition, an IMF is any function with the same number of extrema and zero crossings, with its envelopes being symmetric with respect to zero. This decomposition method operating in the time domain is adaptive and highly efficient. Since the decomposition is based on the local characteristic time scale of the data, it can be applied to non-linear and non-stationary processes.

The method is adaptive, which is especially important over long flights, when the data is unlikely to be stationary. Unlike the empirical orthogonal function (EOF) expansion, which also has an adaptive basis, the results of the EMD are unique and typically have a physical interpretation (Huang et al 1998). The advantage of an IMF over a Fourier Transform is that both the amplitude and frequency of the IMF are allowed to change. These requirements for a Fourier transform are highly restrictive and certainly not true for real data sets.

From a practical point of view, the method consists of "sifting" the data into IMFs. It progresses by first determining the local maxima and minima of the time series $X(t)$. A spline fit to each of the maxima and to the minima of the time series is calculated, making an envelope containing all of the data. The mean of the envelope, m_1, is calculated and subtracted from $X(t)$, resulting in the first mode, h_1:

$$X(t) - m_1 = h_1 \tag{12}$$

This process is repeated with h_i replacing $X(t)$ in each successive sifting step, generating a series of IMFs, which each represent a mode in the data (Huang et al 1998). It should be noted that using the usual HHT notation, the first results of the EMD contain higher-frequency modes; IMF_0, for example, contains the highest-frequency mode (Lundquist 2003). In the notation used here, the IMF containing the lowest-frequency mode is IMF_ℓ, the next lowest-frequency one is $IMF_{\ell-1}$, etc.

3.2.2 Demonstration of EMD

3.2.2.1 Description of Experiment

A flight performed during CLASIC on June 19, 2007 is used to illustrate the issues involved in collecting turbulence data on-board the HOP and to demonstrate the use of the EMD method. A triangular pattern, 10 km on each side, was flown at different altitudes, as demonstrated in Figure 7.

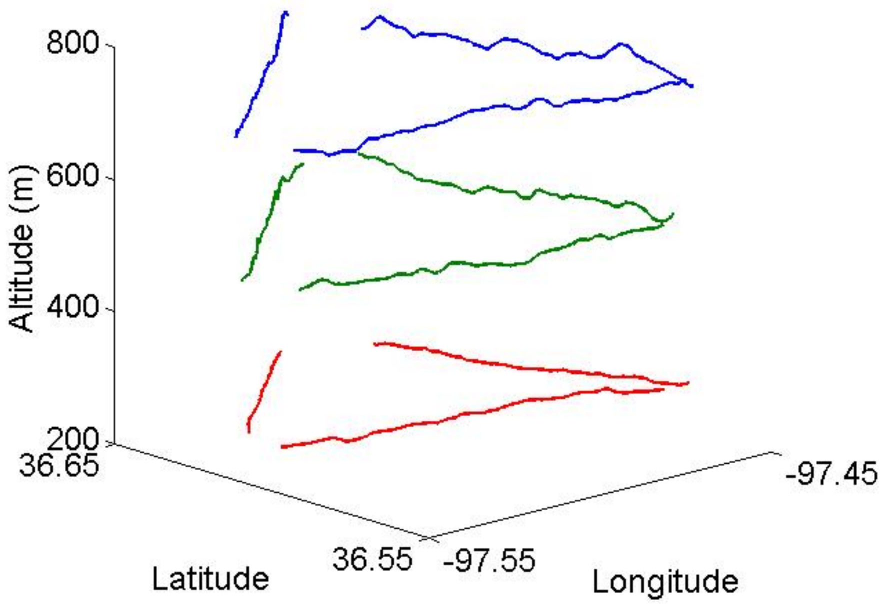

Figure 7: Example triangles flown during the CLASIC campaign. The z-axis represents the altitude above sea level, so that the flight was made a few tens of meters above the surface.

In addition, two "profiling" flight segments aimed at characterizing the vertical structure of the atmosphere were performed. The vertical climb rate during such profiling segments is about 100 m per minute and, therefore, the data collected probably cannot be used reliably for flux calculation. However, the real-time display of potential temperature is accurate enough to provide a good estimate of the top of the convective boundary layer (CBL), which is then used to establish the various altitudes at which the triangular patterns are performed. Typically, if the CBL is less than 300-m high, three triangles are performed: one near the ground surface, one near (i.e., 30-50 m below) the top of the CBL, and one near the middle of the CBL. When the CBL is higher, the near-surface and near-top CBL triangles are performed, and more triangles are flown in between these levels with a separation of 100-150 m.

Figure 8 depicts the time series of the flight altitude and of the preprocessed wind components and scalars collected by the AIMMS-20 and the LI-7500 in this flight. The altitude provides a clear history of this specific flight. During the first ~800 s, a climb was performed by ~100-m high “steps,” starting near the ground surface up to the last layer below the top of the CBL, maintaining a nearly constant altitude for about two minutes at each one of the steps. At the end of this pattern, the HOP climbed through the top of the CBL (which is identified by the real-time display of the potential temperature profile in the pilot cockpit), up to above the entrainment layer to provide information on the magnitude of the inversion layer capping the CBL. Next, three triangles were performed as explained above, i.e., one near the top, one near the middle and one near the bottom of the CBL. In this specific case, the three triangles were flown in about 47 minutes. Following these three triangles, a continuous climb and descent was performed to profile the CBL and to detect any changes in the height of the CBL. Then, two additional triangles were performed at intermediary altitudes to complete the full characterization of the CBL.

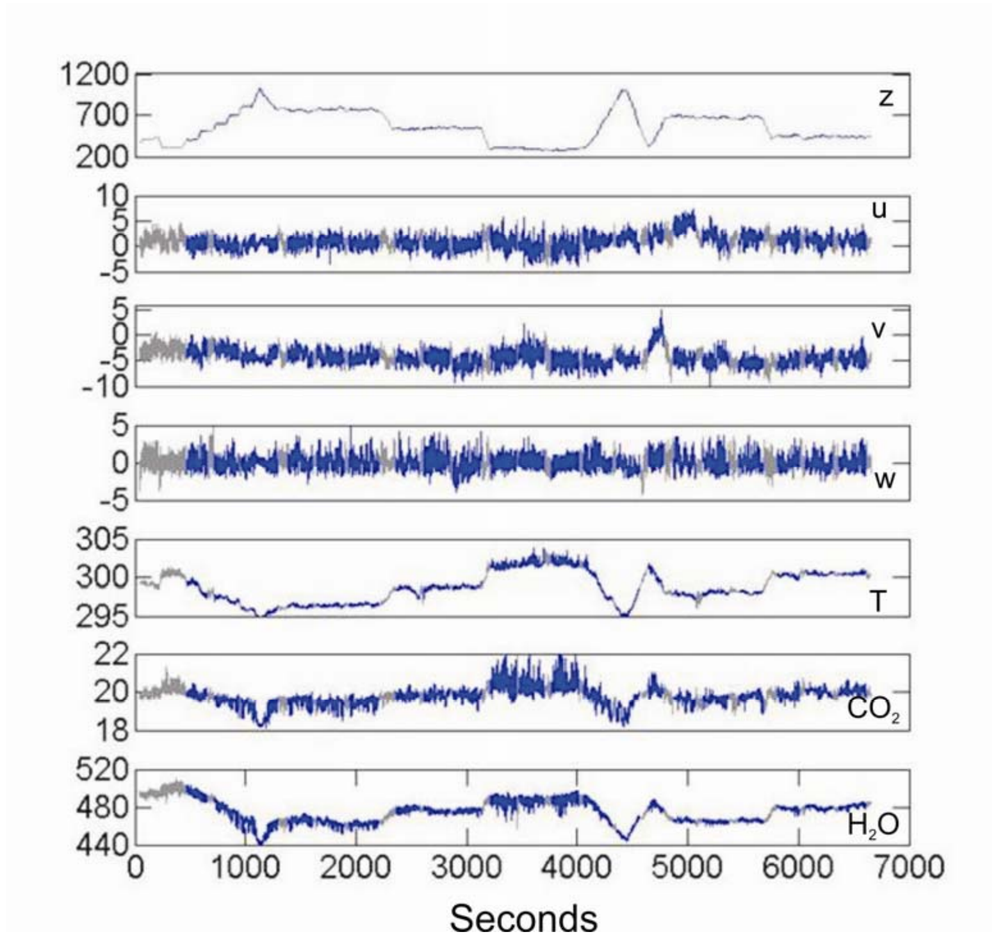

Figure 8: From top to bottom, altitude (z), three wind components (u, v, and w) (m/s), temperature (T) (K), water vapor concentration (g/m^3), and carbon dioxide concentration (C) (mg/m^3) collected on the HOP in a flight performed during CLASIC on June 19, 2007. The continuous grey lines are the raw data and blue lines indicate those data not affected by the HOP "undesirable" movements (including turns, rapid climbs and descents).

The collected data clearly illustrate the intensification of turbulence near the ground surface, which is generated by wind shear and buoyancy. This is particularly evident in the time series of the scalars. Furthermore, there is a visible correlation between altitude and the scalars, showing a decrease of temperature with height as expected in a CBL. Moisture and carbon dioxide also generally decrease with height although the carbon dioxide concentration very close to the surface increases slightly with height. This is consistent with the negative mean carbon dioxide flux at the lowest flight level, which indicates absorption of carbon dioxide by the land surface. The large moisture source at the surface (i.e., evapotranspiration) is consistent with the relatively low height of the CBL (~600 m), which is a consequence of a relatively low contribution of buoyancy (sensible heat flux) and strong latent heat flux. June 2007 was the wettest month of June on record in Oklahoma and, therefore, these observations are not surprising. The entire flight displayed in Figure 8 was performed between 1:45 p.m. and 3 p.m. At this time of the year, when the winter wheat crops are senescent and the summer corn crops are not yet growing, the vegetation photosynthesis activity is low and, correspondingly, the sink of carbon dioxide is small.

Figure 9 presents the spectra of atmospheric variables obtained in the first leg of the third triangle. The reason for selecting this specific leg is that the near-surface flights are the most challenging to process, given the variations of altitude due to topographical features as well as various obstacles on the ground that need to be avoided (e.g., power lines, trees, houses, etc). Furthermore, wind shear near the ground affects the stability of the HOP. Even more importantly, observations in the near-surface layer are the special niche of the HOP among airborne platforms, as discussed in Chapter 1.

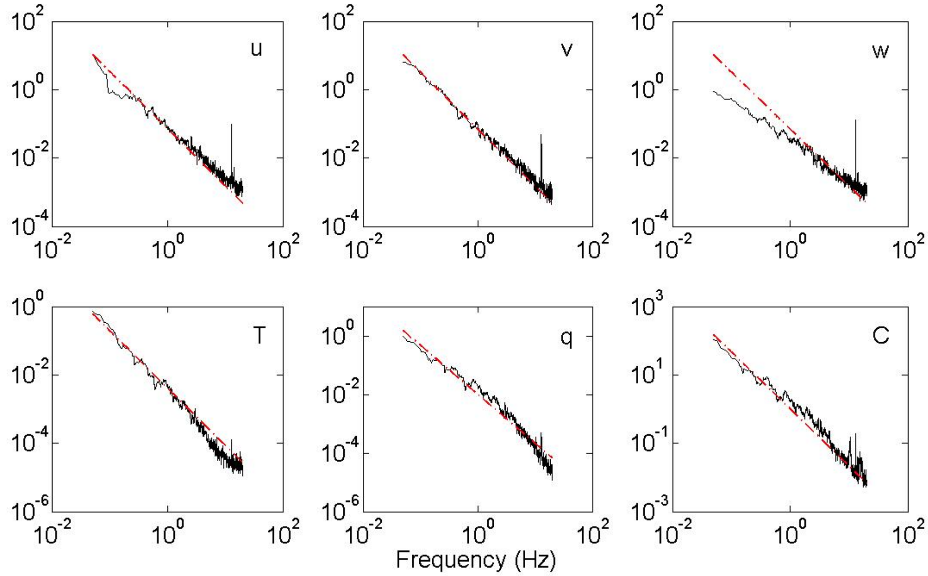

Figure 9: Power spectra of the three wind components (u, v, and w), temperature (T), water vapor concentration (q), and carbon dioxide concentration (C) collected on the HOP in a flight performed during CLASIC on June 19, 2007. Red dotted lines indicate -5/3 slopes. Units are those of the variable variance (e.g., K^2 for the temperature).

A few characteristics relevant to the HOP and its current set of sensors are worth mentioning. For instance, one can notice that due to sensor limitations, the highest frequency of valuable data that can be used for our studies is ~10 Hz. The main rotor of the Jet Ranger, which has two blades, has a constant 396 RPM (±1-2%) that generates the disturbance peak seen in all spectra at ~13 Hz. All spectra show an inertial sub-range with a slope of -5/3 up to sensor limit at ~10 Hz, as expected from Kolmogorov Theory. But the -5/3 slope of the *w* inertial sub-range starts at higher frequencies than that of the other two wind components and the scalars, giving the appearance of a “flatter” spectrum. This feature is a well-known phenomenon of the surface layer that is discussed extensively in Kaimal et al (1972). Yet it seems somewhat exacerbated here due to the short range of frequencies between the beginning of the inertial sub-range and the rotor disturbance peak.

A sensor capable of collecting data at much higher frequencies than the AIMMS-20, would probably show a continuation of the -5/3 slope at higher frequencies. However, flying near the ground surface is particularly destructive for the sensors (due to collision with insects and dust) and the choice of a robust sensor comes at the detriment of high sensitivity. As explained below, given the negligible impact that higher frequencies have on the calculation of the turbulent fluxes, this is an acceptable compromise for these types of missions.

Some of the cospectra between the wind components and the temperature, the water mixing ratio, and the carbon dioxide concentration are presented in Figure 10. The sub-range slopes of the co-spectra are close to -5/3. While Lumley (1964), Kaimal et al (1972) and Kader and Yaglom (1991) obtained sub-range slopes of -7/3, Wyngaard and Cote (1972) report a -3 slope, and, similarly to this study, Van Atta and Wyngaard (1975), Wyngaard et al (1978), and Antonia and Zhu (1994) observed a -5/3 slope. The differences between these empirical results are due to the difference of atmospheric stability prevailing during the different experiments, and our results are consistent with these prior findings.

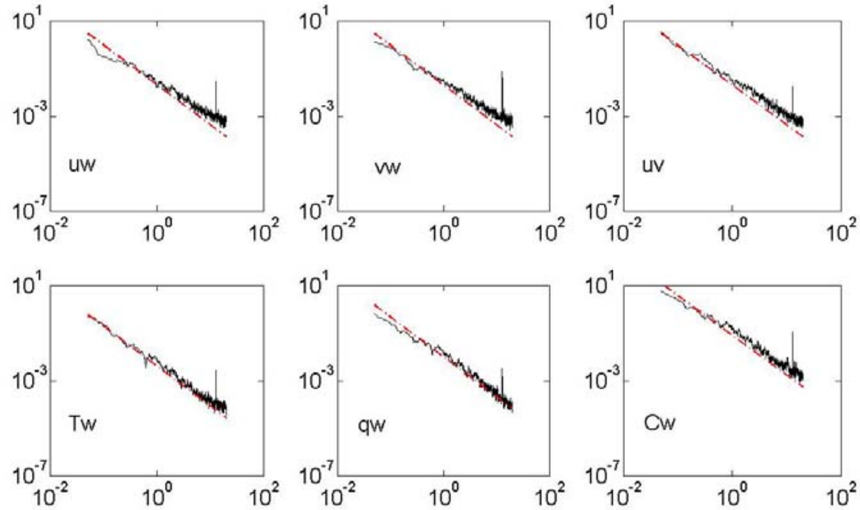

Figure 10: *:* **Power co-spectra between wind components (u, v, and w), temperature (T), water vapor concentration (q), and carbon dioxide concentration (c) collected on the HOP in a flight performed during CLASIC on June 19, 2007. Raw data for the entire flight are used. Red dotted lines indicate -5/3 slopes. Units are those of the variable covariance (e.g., $ms^{-1}K$ for the wT covariance).**

3.2.2.2 Results

Figures 11-13 show some of the IMFs obtained for the vertical component of the wind, the temperature and the water vapor concentration. This analysis was also performed for the other variables and for all flight legs, with similar results.

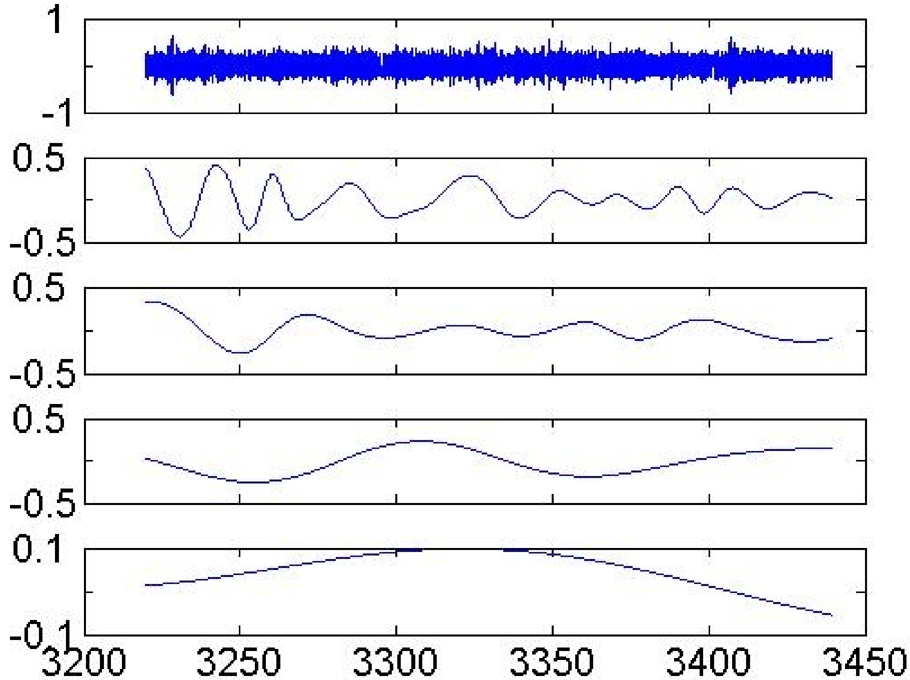

Figure 11: Graphical representation of (from top to bottom) IMF_0, $IMF_{\ell-3}$, $IMF_{\ell-2}$, $IMF_{\ell-1}$, and IMF_{ℓ} obtained for the vertical component of the wind collected on the HOP in one of the flight legs performed during CLASIC on June 19, 2007.

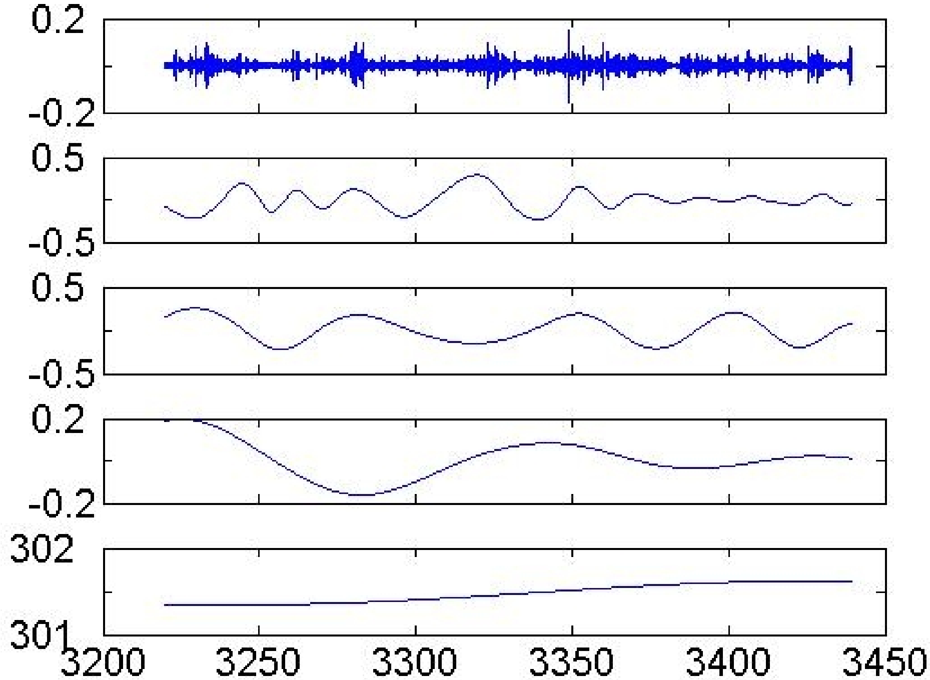

Figure 12: Graphical representation of (from top to bottom) IMF_0, $IMF_{\ell-3}$, $IMF_{\ell-2}$, $IMF_{\ell-1}$, and IMF_ℓ obtained for the temperature collected on the HOP in one of the flight legs performed during CLASIC on June 19, 2007.

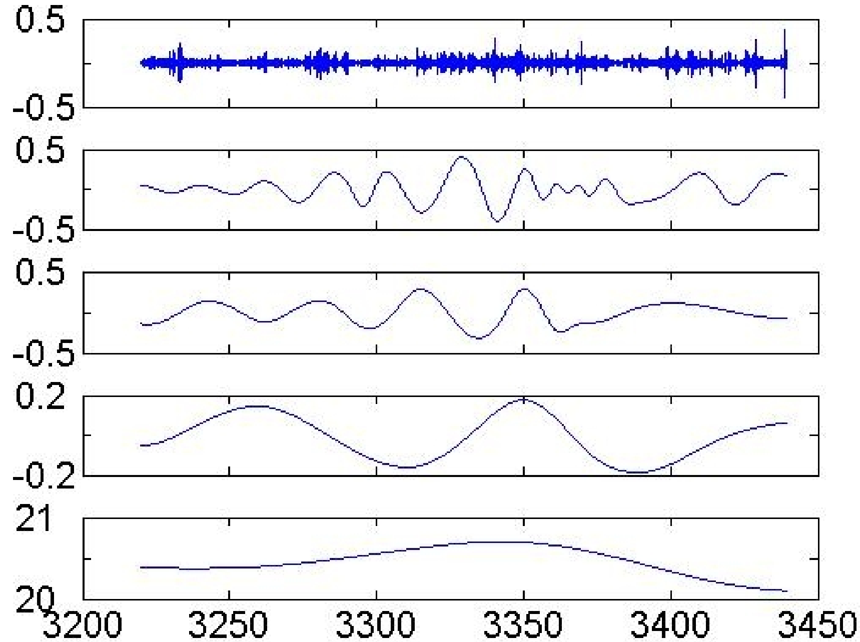

Figure 13: Graphical representation of (from top to bottom) IMF0, IMFℓ-3, IMFℓ-2, IMFℓ-1, and IMFℓ obtained for the water vapor concentration collected on the HOP in one of the flight legs performed during CLASIC on June 19, 2007.

IMF_0 represents the high-frequency noise that is associated with the sensor and has no physical meaning. Also included in IMF_0 is the noise created by the main rotor, which is seen as the peak in the energy spectra in Figure 9. Therefore, its elimination from the original time series, which in practice makes little or no difference to the variables, their variance and their covariances (i.e., kinematic fluxes), is straightforward. IMF_ℓ represents the general trend of the time series and its elimination has the effect of detrending the time series. Its impact on the variances and covariances is, however, quite significant. Physical justification is considered necessary for the elimination of any other IMF, and since it is not always straightforward to relate an IMF to the physics of the observed variable, this is the most obvious weakness of the method. Eventually, some subjectivity is used in the process.

Here, a correlation analysis is used to help in the decision to remove specific IMFs. As emphasized above, after detrending the time series with IMF_ℓ, it is anticipated that eliminating fluctuations caused by (i) non-stationarity of the atmosphere observed during the flight leg (possibly in addition to the series trend, depending on the distance/flight time of the leg), (ii) altitude variations, and (iii) pitch, roll and yaw movements of the HOP will be the most important corrections required to be made to the dataset. Since such fluctuations are expected to occur over time scales of at least a few seconds, the low frequency IMFs are expected to carry these fluctuations. Table 2 presents the correlation analysis between these parameters and the progressive sum of IMFs (i.e., IMF_ℓ, $IMF_\ell + IMF_{\ell-1}$, $IMF_\ell + IMF_{\ell-1} + IMF_{\ell-2}$, etc.) for the time series of some of the atmospheric variables obtained during the first leg of the third triangle of our flight. For example, the first line of the table shows the r^2 value as calculated from the roll of the platform and the successive IMFs of *u*. The minimum r^2 value necessary for a correlation to be significant at the 95% confidence level, for a dataset of this size, is 0.04. However, in most cases, this level of correlation is too low to be a guideline for IMF removal. Based on this straightforward analysis, and assuming subjectively that an $r^2 > 0.10$ justifies the elimination of a particular IMF, for this flight leg, eliminating $IMF_{\ell-1}$ (in addition to IMF_ℓ and IMF_0 as explained earlier) is justified for *u* and *q*, and further eliminating $IMF_{\ell-2}$ is justified for *v*, *w*, and *c*. The last four IMFs of temperature exhibit a correlation with yaw, so these IMFs should be eliminated as well. This correlation is likely due to the aerodynamics of the sensor mount, which is designed to protect the fragile thermistor.

Table 2: The impact of the various IMFs on the correlation (r^2) between some of the atmospheric variables observed on the HOP on June 19, 2007 and the HOP attitude (defined by pitch, roll, and yaw). Highlighted in bold are all $r^2 > 0.10$.

	IMF$_0$	IMF$_1$	IMF$_2$	…	IMF$_{\ell-4}$	IMF$_{\ell-3}$	IMF$_{\ell-2}$	IMF$_{\ell-1}$	IMF$_\ell$
u and z	0.09	0.00	0.00	…	0.00	0.01	0.06	0.10	0.01
v and z	0.01	0.00	0.00	…	0.01	0.00	**0.11**	**0.21**	0.00
w and z	0.02	0.00	0.00	…	0.00	0.00	**0.16**	0.04	**0.14**
T and z	0.00	0.00	0.00	…	0.01	0.00	**0.22**	**0.17**	0.00
Q and z	0.00	0.00	0.00	…	0.00	0.00	0.05	0.01	0.07
C and z	0.00	0.00	0.00	…	0.00	0.03	0.03	0.00	0.07
u and roll	0.00	0.00	0.00	…	0.00	0.04	0.08	0.01	0.02
v and roll	0.00	0.00	0.00	…	0.04	0.00	0.01	0.05	0.02
w and roll	0.00	0.00	0.00	…	0.00	0.01	0.00	0.01	0.01
T and roll	0.00	0.00	0.00	…	0.01	0.02	0.03	0.00	0.01
Q and roll	0.00	0.00	0.00	…	0.00	0.01	0.00	0.01	0.02
C and roll	0.00	0.00	0.00	…	0.01	0.00	**0.12**	0.03	0.04
u and pitch	0.00	0.00	0.00	…	0.04	0.01	0.03	**0.10**	0.02
v and pitch	0.00	0.00	0.00	…	0.07	0.01	0.02	0.01	0.02
w and pitch	0.00	0.00	0.00	…	0.00	0.01	**0.13**	**0.18**	0.00
T and pitch	0.00	0.00	0.00	…	0.00	0.00	0.00	0.01	0.02
q and pitch	0.00	0.00	0.00	…	0.00	0.02	0.01	**0.10**	0.00
C and pitch	0.00	0.00	0.00	…	0.05	0.02	0.00	0.02	0.02
u and yaw	0.00	0.00	0.00	…	0.00	0.01	0.05	**0.21**	0.03
v and yaw	0.00	0.00	0.00	…	0.00	0.05	0.05	**0.40**	0.01
w and yaw	0.00	0.00	0.00	…	0.00	0.03	0.02	**0.20**	**0.31**
T and yaw	0.00	0.00	0.00	…	0.00	**0.24**	**0.13**	**0.28**	0.00
q and yaw	0.00	0.00	0.00	…	0.00	0.00	0.04	**0.11**	**0.18**
c and yaw	0.00	0.00	0.00	…	0.00	0.01	0.02	0.03	**0.14**

Figure 14 illustrates the impact of removing various IMFs from the data on the variable spectra and Table 3 summarizes how the low-frequency IMFs affect the calculation of the turbulence fluxes.

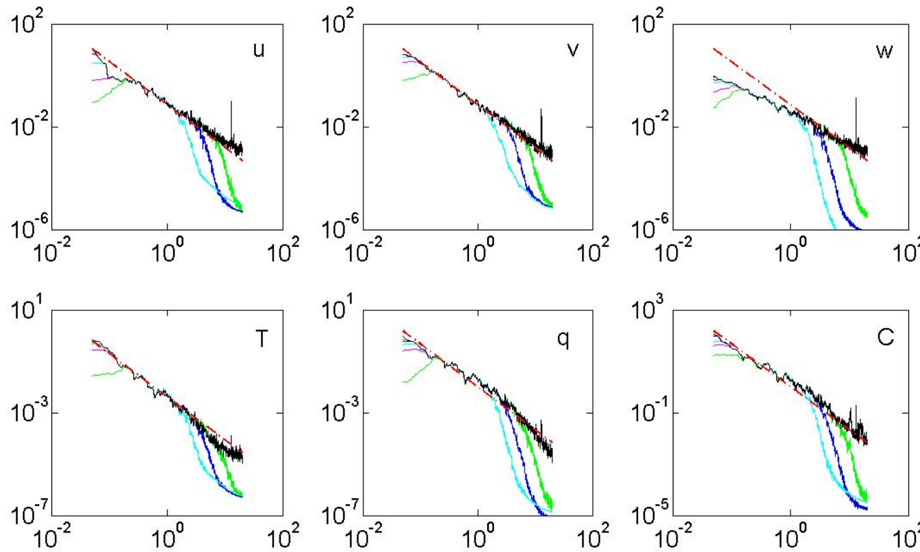

Figure 14: Same as Figure 14 but the various colored lines indicate the remaining spectra after successive IMFs have been eliminated on either side of the spectra. The black lines indicate the raw data shown in Figure 14.

It is interesting to note that the impact of the different IMFs is quite nonlinear and that it is not possible, *a priori*, to estimate the impact of eliminating a particular IMF on the fluxes. Indeed, in some cases the removal of a specific IMF decreases the variance of a given variable while the removal of that and the following IMF might increase it. From the results presented in Table 3, removal of successive IMFs decreases the magnitude of both the carbon dioxide flux and the TKE, as might be expected. However, the removal of the last two IMFs increases the magnitude of the sensible heat and latent energy fluxes. This result is not entirely surprising, as these IMFs are correlated with altitude and aircraft attitude. These erroneous signals are superposed on the physical turbulence signals, so their removal improves the quality of the data. This in turn improves the correlation between variables. The final row in the table shows the flux values obtained when the number of IMFs removed for each variable is determined by the variable's correlation with altitude and attitude, which are taken to be the best estimate values. This optimal value for the sensible heat flux falls between the value calculated by subtracting three IMFs from both w and T (three IMFs is the optimal number removed for w) and four IMFs for both w and T (four IMFs is the optimal number removed for T). This phenomenon is also true for TKE. Three IMFs are the optimal number removed for both w and carbon dioxide, so that the optimal value of carbon dioxide flux is the same as that calculated in row 4. The latent heat flux is also calculated with two variables whose ideal number of IMFs removed is 3, but the ideal value falls between the value where 2 and 3 IMFs are removed from all variables. To calculate the best estimate value, four IMFs were removed from temperature, which is also an indirect factor in the latent heat calculation, so this comparison is not completely straightforward. In addition, the IMFs are nonlinear, so any generalizations about specific flux values are difficult to make. This analysis shows the importance of removing the correct number of IMFs from each variable, as the resultant flux values are unpredictable.

Table 3: The impact of removing IMFs on the turbulence fluxes in the convective boundary layer observed on the HOP on June 19, 2007.

IMFs removed	SH [Wm^{-2}]	LH [Wm^{-2}]	CF [mg $m^{-2}s^{-1}$]	TKE [m^2s^{-2}]
None	60.1	118.5	-0.73	1.35
ℓ	67.1	107.8	-0.70	1.25
ℓ & ℓ-1	68.1	122.0	-0.64	1.11
ℓ & ℓ-1 & ℓ-2	59.4	108.8	-0.58	0.87
ℓ & ℓ-1 & ℓ-2 & ℓ-3	33.7	80.5	-0.41	0.65
Best Estimate	41.14	121.50	-0.58	1.05

Another type of fluctuation that can be seen in our dataset is that triggered by vibrations of the HOP. As explained above, the effect of the main rotor (which includes various vibrations) is well visible in all spectra. Other rotating components of the helicopter, e.g., the engine, the transmission, and the tail rotor have RPM that are much faster than the rotor and, therefore, are likely to have vibration peaks at much higher frequencies than those detected by our sensors. Here, it appears that all these vibrations are eliminated from the time series by subtracting the respective IMF_0 from them.

3.2.2.3 Conclusions

Here a typical (yet complex) research flight conducted with the HOP during the CLASIC experiment demonstrates the potential of the EMD method for airborne data processing. The capability to detrend the time series for non-stationarity and to eliminate the contamination that is typically found in airborne data, especially when flying in a stratified atmospheric layer is demonstrated. The main advantage of this method is that it is empirically based and does not need to make particular assumption about the data structure. In addition, the EMD is capable of handling nonlinear, non-stationary data, which makes it ideal for the analysis of atmospheric turbulence data. It is an especially useful technique for the analysis of HOP data, as it can identify and separate the signals due to vibrations and platform motions which have changing frequencies and amplitudes. Traditional Fourier methods use only a single frequency or range of frequencies at constant amplitude, and the frequency chosen must be a harmonic of the sampling frequency. In addition, Fourier methods are inappropriate for non-stationary data. Wavelet methods are also limited to a single frequency range and amplitude, both of which must be known a priori. Unlike the empirical orthogonal function (EOF) expansion, which also has an adaptive basis, the results of the EMD are unique, so that each one has a physical interpretation (Huang et al 1998).

Analyzing the impacts of the low-frequency IMFs on the correlations between the atmospheric variables being measured and the aircraft altitude and its pitch, yaw and roll helps eliminate disturbances in the time series, which are due to the aircraft movements and not to the atmospheric dynamics. As these disturbances have a significant impact on the turbulent fluxes, this is a very important contribution of this method. However, there is some subjectivity in the process of eliminating some of the IMFs and this is the most obvious weakness of this method.

4. Helicopter Observation Platform Evaluation

4.1 Evaluation of Aerodynamic Envelope

In chapter 2, the theoretical and computationally calculated aerodynamic limits of the HOP were shown. It is good practice to verify these limits empirically, as the aerodynamics of a real system flying in real conditions may depict features that are not necessarily represented by the theory or the numerical model, which typically simplify the real world. By comparison of the measurements made from the HOP while flying at different airspeeds, systematic flow distortion at a given speed can be ruled out. Here the aerodynamics while flying at slow speeds are tested to find the minimum flight speed for which the main rotor wake is behind the sensors, and the aerodynamics at high speeds are tested to rule out any effects of the high pressure due to the stagnation point on the nose.

4.1.1 Low Speed Aerodynamic Envelope

It is clear from examining Equations 7 and 8 that when moving forward and measuring undisturbed air, the ratio of ΔP_{α} (or ΔP_{β}) to ΔP_{PS} should be small. Because the HOP is constantly undergoing pitching and yawing motions, there is (by definition) some component of the forward flight speed contained in α and β, but for forward flight with the helicopter facing the direction of flight, the magnitude of the wind components should be smaller than the magnitude of the flight speed. If ΔP_{α}, in particular, is large compared to the forward flight speed, it is an indication that the sensor is in the rotor downwash.

4.1.1.1 Flight Description

Low–speed flights (20 m/s or less) were conducted over the runway at the Burlington airport, in Burlington, NC and at the Sanford airport, in Sanford, NC. The flight altitude was about 30 m, which is sufficiently high to ensure that no effects from the rotor wake interacting with the ground were felt. The flights, made on October 11, 2005, January 09, 2006 and February 02, 2006 in Burlington, and October 2, 2007 and October 9, 2007 in Sanford, all followed a general pattern: a period of hover, about 1-2 minutes, followed by a flight leg made the length of the runway. The helicopter turned, hovered for another period, and then the helicopter was flown back above the runway at the same speed. This was repeated two or three times, for increasing flight speeds.

4.1.1.2 Results

Figure 15 (upper) shows the ratio of ΔP_{α} to ΔP_{ps} (angle of attack differential pressure ratio) for a range of airspeeds. The values are averaged over 2-4 minutes of flight, as described above. It is clear from the figure that at airspeeds above about 10 m/s, the ratio is small, indicating that the downwash of the rotor is behind the front sensors.

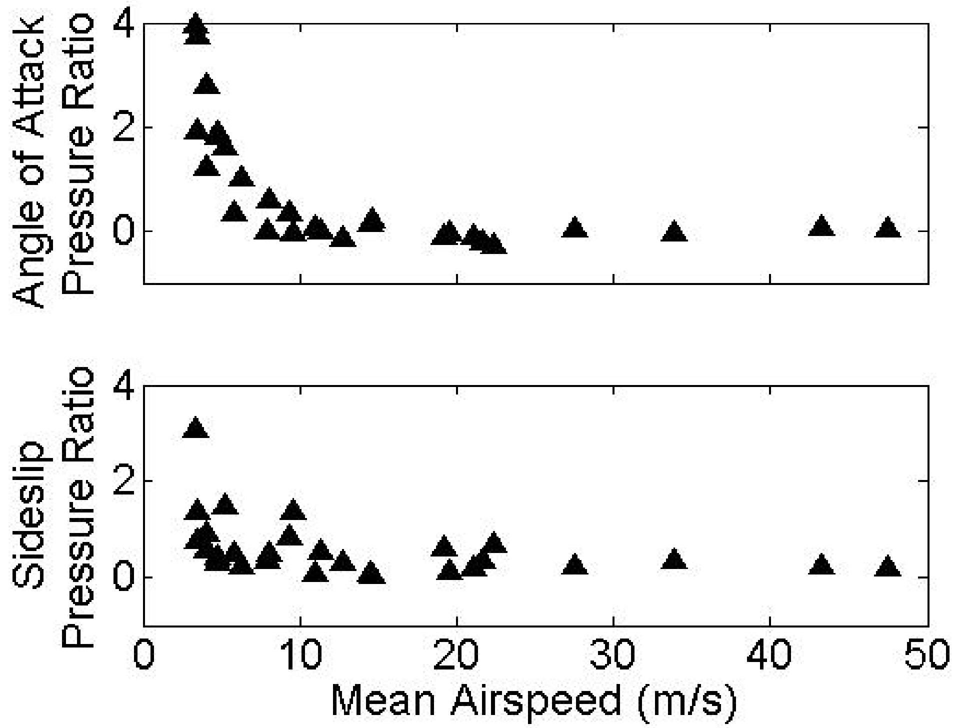

Figure 15: The ratio of the measured angle of attack differential pressure (upper figure) and the sideslip differential pressure (lower figure) to the pitot-static pressure, as a function of airspeed.

The ratio of to $\Delta P_{\beta} / \Delta P_{ps}$ (sideslip differential pressure ratio), shown in the lower part of figure 15, has a similar shape. There is more variation in this ratio for two reasons: first, the magnitude of the horizontal wind is an order of magnitude larger than the vertical wind, and second, the helicopter tends to have larger variances in its horizontal angle to the forward flight direction (i.e. yaw) than in its vertical angle (i.e. pitch). The AIMMS-20 calculation of the winds only becomes numerically stable when this ratio is larger than about 1 (personal communication, Steven Foster, Aventech Research). As with ΔP_{α}, this is achieved for airspeeds greater than 10 m/s.

4.1.2 High Speed Aerodynamic Envelope

4.1.2.1 Flight Description

Two low-level flights (i.e., 15-30 m ASL) were performed at various airspeeds along the Outer Banks of North Carolina, each lasting about 40 minutes. The marine boundary layer (MBL) is typically more homogeneous than the continental one, so the observations were carried out there to minimize the change of turbulence during the flights. On the day the flights were flown, the prevailing winds were easterly (i.e., from the sea) and the HOP was flown about 200 m offshore to minimize land effects. Each flight consisted of eight four- to five-minute legs, each one at a different airspeed, with the slowest one at ~18 m/s and the fastest one at ~55 m/s. All data were processed according to the methods introduced in Chapter 3.

4.1.2.2 Results

Figure 16 presents the spectra of the wind components and scalars measured with the AIMMS-20 and the LI-7500 during the above-mentioned two flights combined together. The raw data as well as the "filtered" data after different IMFs have been removed from them are shown.

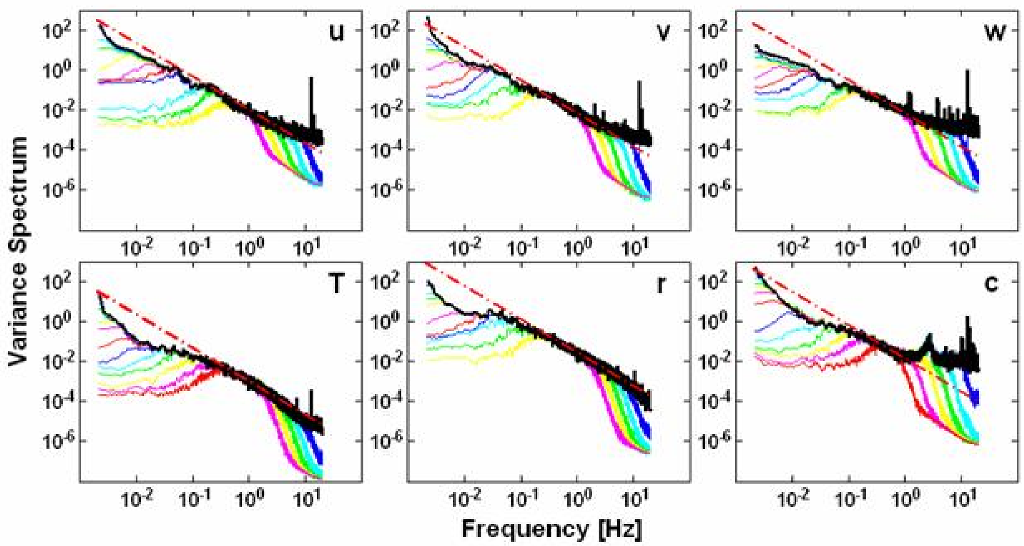

Figure 16: Power spectra of the three wind components (u, v, and w), temperature (T), water mixing ratio (r), and carbon dioxide (c) obtained from the sensors mounted on the nose of the HOP in a flight performed near the Atlantic Ocean surface (along the Outer Banks of North Carolina) at various airspeeds. The black lines indicate the raw data and the various colored lines indicate the remaining spectra after successive IMFs have been eliminated on either side of the spectra. Red dotted lines indicate -5/3 slopes. Units are those of the variable variance (e.g., K^2 for the temperature).

The spectra show an inertial sub-range with a slope of -5/3 up to about 5–10 Hz. Unlike the other variables, the carbon dioxide spectrum is noisy starting at about 1 Hz. Given that the same sensor simultaneously measures carbon dioxide and water mixing ratio (with the same signal processed differently) and that the water mixing ratio spectrum does not depict such a noisy response, this phenomenon can be attributed to the lack of carbon dioxide sources/sinks and a well-mixed carbon dioxide concentration at this location and time that does not generate much turbulence.

To evaluate the potential impact of the HOP airspeed on the collected data, Figure 17 shows the temperature raw data collected with the AIMMS-20, together with the temperature variances obtained in the different flight legs.

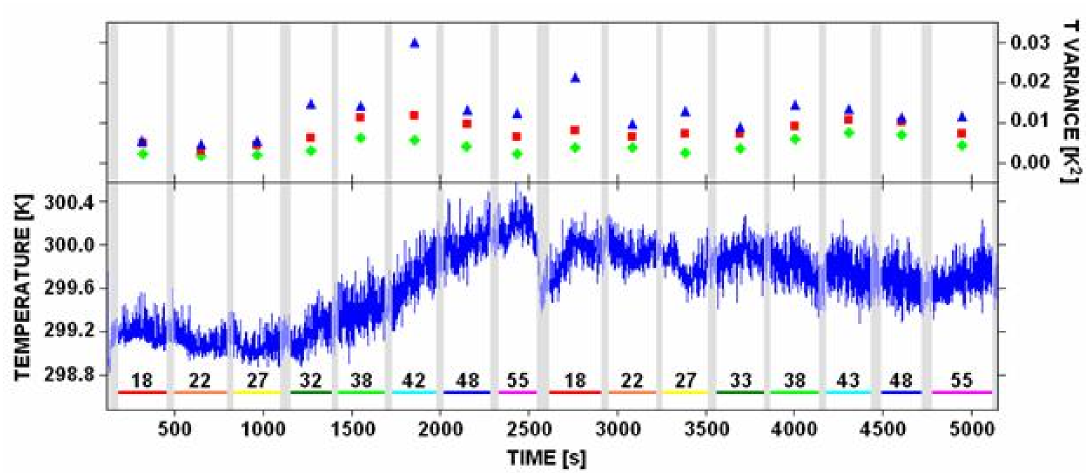

Figure 17: Temperature collected on the nose of the HOP in two low-level flights performed at various airspeeds along the Outer Banks of North Carolina on September 4, 2007. Each flight lasted about 2,500 s. The continuous blue line is the raw data, and shaded areas (light grey) indicate the time during which the HOP is accelerating between flight legs or turning and rapidly decelerating at the end of the first flight. Symbols indicate variances by flight legs (blue triangles – raw data; red squares – filtered at frequencies <0.01 Hz; and green diamonds – filtered at frequencies <0.1 Hz). The colored horizontal bars indicate the lengths of the flight legs and the numbers above them indicate the mean airspeed (m/s) of the HOP during the legs.

Figure 16 illustrates the impact of removing various IMFs from the raw data on the variables' spectra. While the flights presented here seem to have recorded a mesoscale event that would be interesting to study further, here low-frequency IMFs containing perturbations smaller than 0.01 Hz have been removed. Note that the measured inertial sub-range starts at ~0.1 Hz and, not surprisingly, cutting the production range has a significant impact on the temperature variance, in some legs reducing it by as much as half.

It is not possible to identify any clear impact of airspeed on the measurements in these two flights. The high variances seen in the raw data (Figure 17) in Leg 4 (dark green), Leg 6 (light blue) and Leg 9 (red) are well correlated with the obvious change (i.e., trend) of background conditions. These low-frequency changes are removed from the data series with the lowest IMFs. Also, one can notice an increase of the filtered variances (green diamonds and red squares in Figure 17) in Legs 5, 6, 13, 14, and 15. Quite interestingly, these occur at the same geographical location, just north of Duck, where land increases friction as compared to the open water of the Albemarle Sound, as shown in Figure 18.

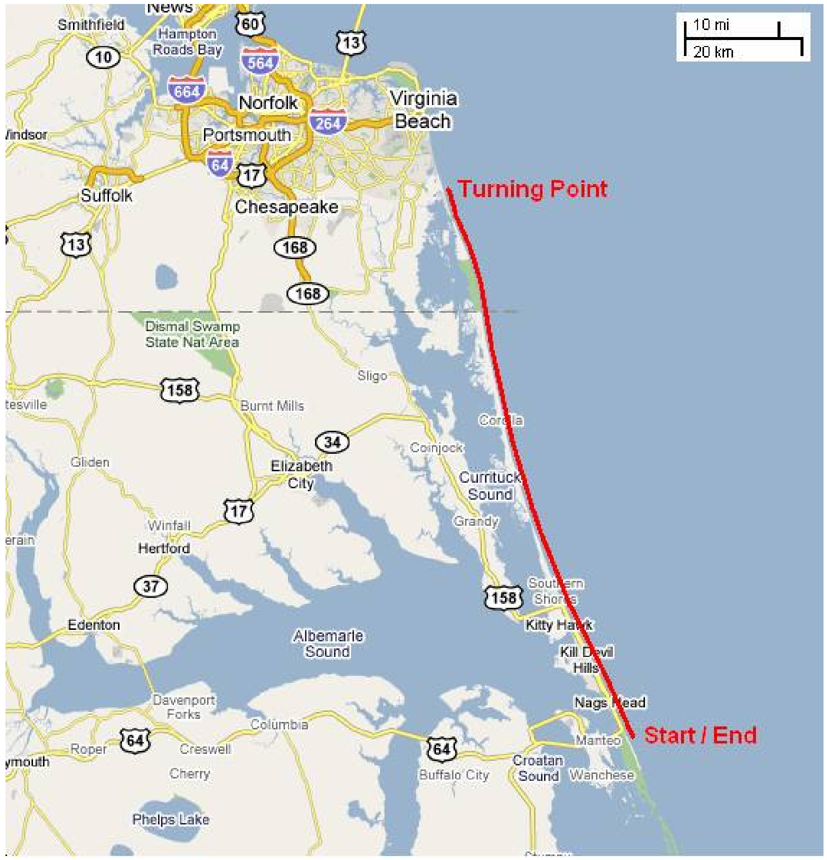

Figure 18: Experimental flight (red line) conducted along the Outer Banks of North Carolina on September 4, 2007 (from Google Map).

4.2 HOP Profiles

Another interesting application of the HOP is its ability to make vertical profiles of atmospheric variables. Typically ground-based sensors, either in-situ, such as tethersondes, or remote sensing, such as LIght Detection And Ranging (lidar) or radio acoustic sounding systems (RASS), are used to make vertical profiles of atmospheric variables. Exact, quantitative measurements are often difficult to obtain using remote sensing techniques. Non-manned aircraft, such as non-tethered balloons or gliders, are also used to make in-situ vertical profiles, although they are difficult to control. Many powered aircraft are also capable of making vertical profiles, from very close to the surface to high in the atmosphere. Helicopters are particularly useful for this application, since they can ascend and descend quickly, covering almost any sized spatial area desired. In addition, helicopters are able to begin profiles at the Earth's surface, an ability which is unparalleled for platforms carrying a complete set of micrometerological sensors. In particular, measurements of carbon dioxide concentration are problematic using balloons, as the sensors needed to make them are expensive, delicate and relatively large.

The height of the PBL is a product derived from vertical profiles that is especially useful. This variable is required for many atmospheric models and energy budgets. Gunter (2007) found that PBL heights determined from potential temperature profiles made with the National Oceanic and Atmospheric Administration (NOAA) Twin Otter aircraft over land and the ocean compare favorably with RASS measurements in most cases. Also recently, data from a long diurnal time series of lidar-derived PBL heights correlate highly with radiosonde measurements taken concurrently (Martucci et al 2007). PBL heights and other atmospheric structures measured using elastic lidar compare very well with those measured by radiosondes over rural (Bosenberg and Linne 2002) and urban areas (Cooper and Eichinger 1994). Lidar and radar wind-profiling radar measurements are found to correlate well also (Cohn and Angevine 2000). Eloranta and Forrest (1992) use lidar measurements of atmospheric structures to provide context to aircraft measurements, showing that structures found in instantaneous flux records are explained by structures seen by the lidar.

The capability of the HOP to make fast and accurate boundary layer profiles is demonstrated using two cases with very different surface and atmospheric conditions. Both cases show the ability of the HOP to capture interesting and complete boundary layer profiles, measuring structures and atmospheric layers and providing context to flux measurements made concurrently.

4.2.1 Methods

There are several methods of locating the top of the PBL, as well as identifying discrete structures and layers, and several studies have found that different methods compare favorably. Potential temperature measurements, whether made from aircraft or from balloons, detect the location of the capping inversion at the top of the PBL. The HOP has a real-time display so that the capping inversion can be located before a series of flights, enabling flights to be made accurately at various locations relative to the height of the PBL. The flexibility of the helicopter platform allows profiling flights to be made with a variety of patterns. In this case, over homogeneous surfaces, flights were made starting near the surface, climbing in a straight line until above the capping inversion and then descending back toward the surface. Over a smaller area, profiles can be made in a tight spiral pattern ascending or descending. For the flights shown here, with a shallow PBL, the HOP traversed the entire profile in about 3 minutes.

Remote sensing measurements rely on the fact that in general, there is a sharp gradient in the concentration of aerosols and/or water vapor at the top of the PBL. The lidar determines the top of the PBL with an edge detection method as in Kovalev and Eichinger (2004), taking the top of the PBL to be halfway through the entrainment zone, the region where the aerosol concentration (and thus the elastic backscatter) drops off sharply. In addition, the differences in elastic backscatter measured by the lidar illuminate different structures and layers in the atmosphere.

The lidar used is a vertically-staring elastic system belonging to the University of Iowa (for details of the instrument, see Eichinger et al 2005 or Eichinger and Cooper 2007), which was used to make vertical profiles of the boundary layer. This lidar sends out a pulse of light with a wavelength of 1064 nm, and collects the light backscattered by atmospheric aerosols with a 25 cm telescope. The laser beam is emitted parallel to the telescope, about 24 cm away, but the entire laser beam must be in the field of view of the telescope in order to obtain accurate data. Thus there is a minimum distance below which the lidar data is unusable. Data was collected using a transient digitizer operating at 60 Mhz, giving the system a 2.5 m range resolution. The data from 50 laser pulses were averaged to produce a single vertical profile allowing a one second time resolution.

4.2.2 Case Studies

4.2.2.1 Marine Boundary Layer (MBL)

A comparison between HOP-measured atmospheric profiles and profiles made with the vertically-staring elastic lidar belonging to the University of Iowa is made here. The experiment was performed March 31, 2007 in the Army Corps of Engineers Field Research Facility (FRF) in Duck, North Carolina. This facility is located toward the northern end of the Outer Banks, on the Atlantic Ocean side of a narrow island. Figure 19 shows a Google Earth satellite map of the region.

Figure 19 : The Field Research Facility at Duck, NC

The long FRF pier is circled in the figure. The lidar was set up midway down the pier, about 300 m from the coastline, over the open ocean. The pier is 25 ft above sea level.

When the experiment began, the winds were coming from the land (figure 20), but around 1 pm local time a frontal boundary pushed through the area.

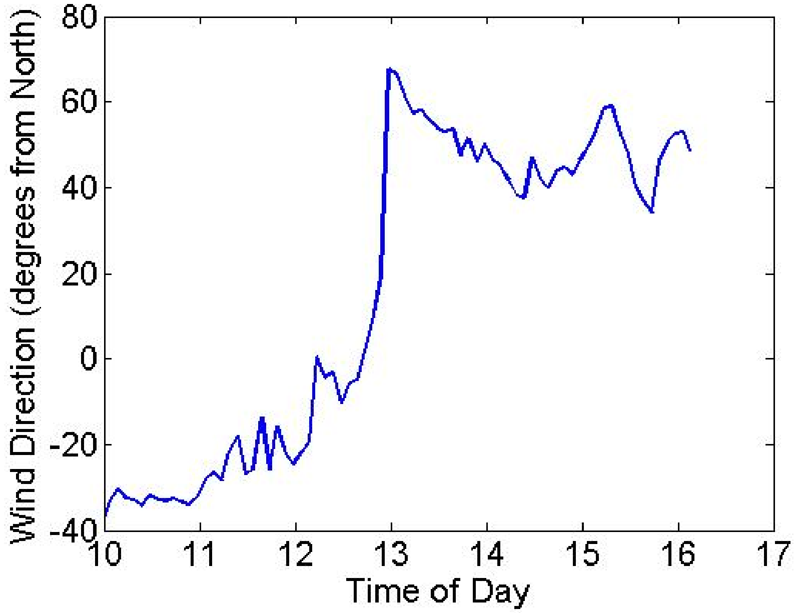

Figure 20: Wind direction during the Duck experiment

After this time, the winds were from the open ocean. Especially when the winds are from the open ocean, the surface can be considered to be homogeneous enough that measurements taken several hundreds of meters apart will represent the same surface type. The sea surface temperature during the experiment was fairly cold, around 11 degrees Celsius.

4.2.2.2 Convective Boundary Layer (CBL)

In this case, HOP profiles are compared with lidar profiles made June 19, 2007 at the Department of Energy Atmospheric Radiation Measurement (ARM) Southern Great Plains (SGP) site. The landscape consists of relatively homogeneous pasture land and wheat fields, which were mostly senescent at the time of this experiment. The lidar was technically identical to the one used in the MBL experiment, but was mounted in a truck to enable mobile measurements (Lewandowski et al 2008). A picture of the site taken on the day of the experiment is shown in figure 21.

Figure 21: The Southern Great Plains ARM site

This experiment was done as part of CLASIC and was done concurrently with the flux measurements described in Chapter 3. The weather during the entire month of June was extremely rainy, so much so that the ground was saturated and there was a great deal of flooding in the area. The weather on June 19 was warm, humid and sunny. Some convection did develop on this day, but because the ground was so saturated, the PBL stayed fairly low.

4.2.3 Experimental Results

4.2.3.1 MBL HOP-Lidar Comparison

Figure 22 shows the time series of lidar data of relative aerosol concentrations as a function of height (y axis) and time (x axis). Red denotes a higher aerosol concentration, and blue is a lower aerosol concentration. This long time series provides context to the individual profiles, an important contribution as the mesoscale motions affected the boundary layer dynamics to a large extent. In the lidar figures, strong changes in aerosol concentrations are indicative of changes in mixing properties, particularly changes in potential temperature. For example, sharp increases in potential temperature with height inhibit vertical mixing, so that the aerosol concentration is sharply less above the height of the increase in potential temperature. Figures 23, 24 and 25 show smaller sections of this time series with the HOP profiles so that details can be seen.

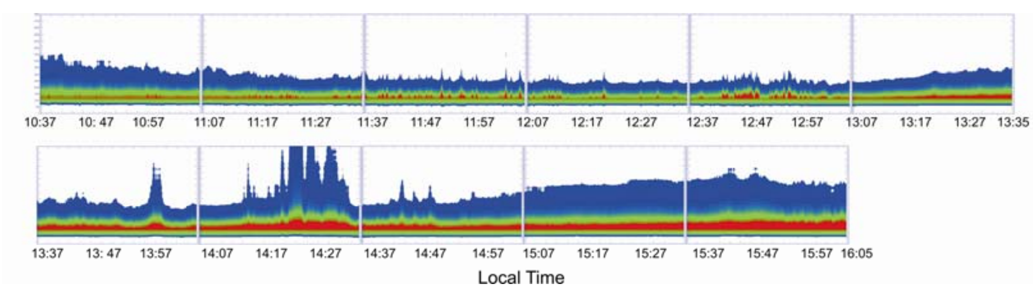

Figure 22: Background meteorology during the Duck Experiment

The first HOP profile was made at about 14:15 at the beginning of the period of rapid MBL growth (figure 23). The HOP profile shows an inversion at 150 m, where the lidar data shows the top of the MBL before the period of growth. The HOP profile was flown several hundred meters downwind of the lidar, so that it may have taken a few minutes for the change in the atmosphere to advect to that area. It was during this period that the frontal boundary was moving through the area, and the wind direction was shifting.

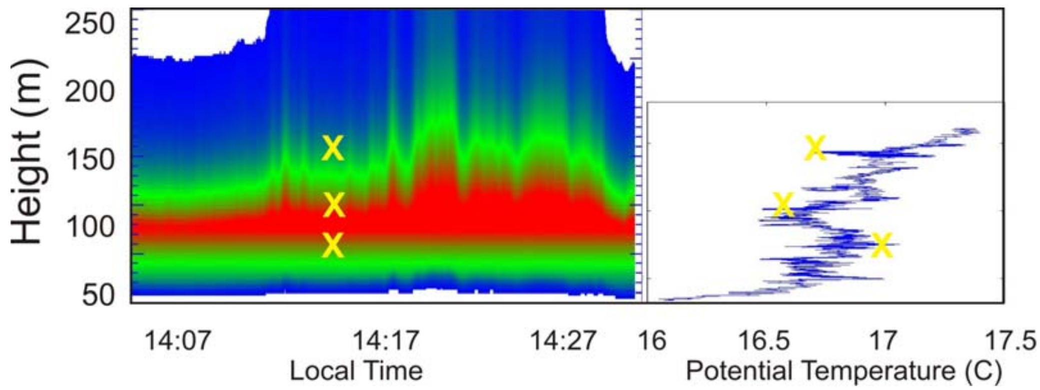

Figure 23: Comparison of lidar backscatter and HOP potential temperature profile showing inversions which create distinct atmospheric layers. Locations on the lidar image where HOP profiles made at that time show similar structures are marked with an x.

Figure 24 shows the next HOP profile, made at about 15:24. This profile shows excellent agreement with the lidar data. However, it appears that at this time, the top of the PBL, if it is taken to be the altitude to which a buoyant plume released at the surface will travel, is at about 35 m, where there is a large inversion. This is a highly unusual situation over the ocean which was probably caused by large-scale subsidence. The relatively cold sea surface temperatures also might be a factor in keeping this PBL unusually shallow. The inversion at around 150 m correlates well with the top of the high-aerosol layer detected by the lidar data. The top of the residual layer is a little under 400 m, and can be clearly seen in both datasets.

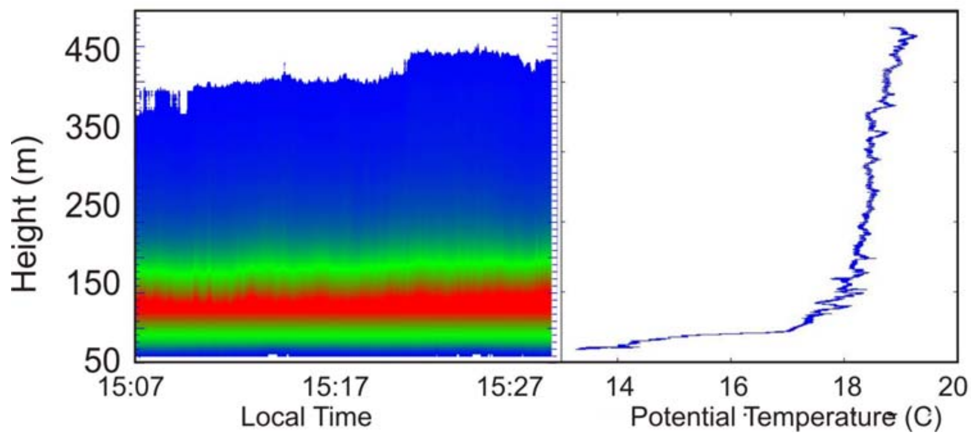

Figure 24: Comparison of HOP potential temperature profile with lidar backscatter showing the locations of three temperature inversions which create distinct atmospheric layers.

The final HOP profile (figure 25), made at 15:58, shows a similar agreement, although at this point, the height of the PBL has risen slightly.

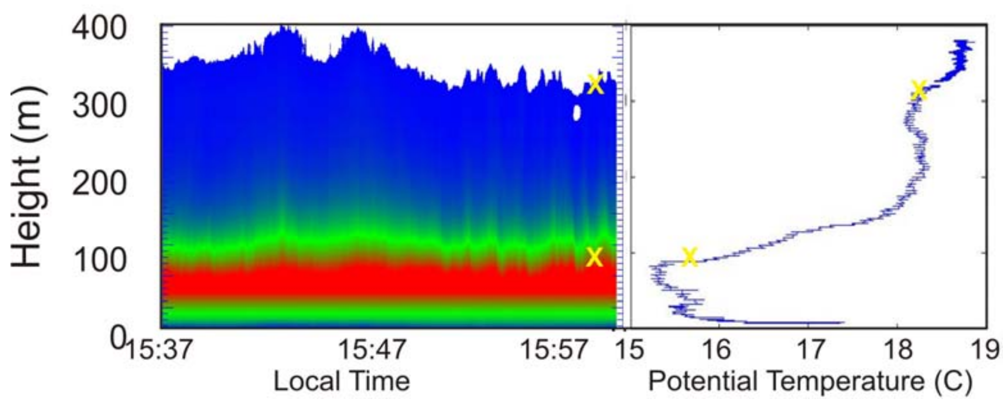

Figure 25: Comparison between final HOP potential temperature profile and lidar backscatter. Locations on the lidar image where HOP profiles made at that time show similar structures are marked with an x.

A closer view of this final profile is given in figure 26.The HOP profile is compared to a single lidar line of sight. The HOP profile shows the temperature, and the lidar profile shows the natural log of the relative backscatter. A large backscatter indicates a region of relatively high aerosol concentration, and an abrupt change in backscatter indicates the presence of a layer or structure. The lidar data is incomplete at altitudes lower than about 75 m, but even in this area, the two profiles identify structures in the same locations. The top of the PBL is clearly shown at about 85 m in both datasets. The temperature inversions seen in the HOP profile at 140 m and 320 m correspond exactly with changes in backscatter seen by the lidar.

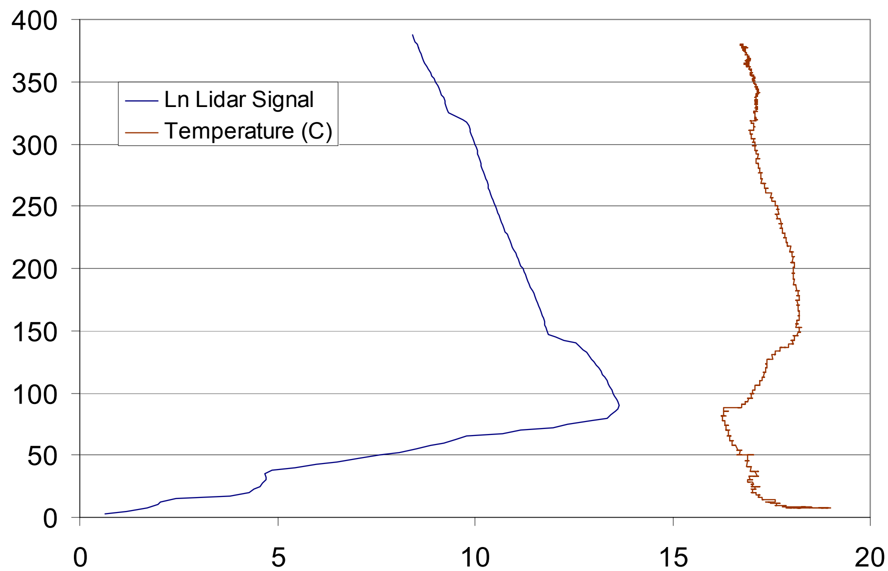

Figure 26: Comparison between HOP profile and lidar line of sight

4.2.3.2 CBL HOP-Lidar Profile Comparison

One interesting contribution of the HOP to the measurement of atmospheric profiles is the ability to measure profiles of carbon dioxide and water vapor concentrations as well as profiles of temperature. As well as providing a more complete picture of the atmosphere, this ability provides important context to flux measurements, whether made from the HOP, from a higher-flying airplane, or from a stationary tower.

Figure 27 shows a time/spatial series of lidar data, along with HOP profiles of potential temperature, mixing ratio and carbon dioxide concentration made concurrently. It can be seen from the lidar data that the atmosphere during this time is fairly homogeneous and stationary, so that the two sets of measurements can be compared. The top of the ABL can be seen at about 500 m above the surface, where there is a strong capping inversion. This layer can be clearly seen in the lidar data, as an area where convective structures are forming. Note the relatively high concentration of water vapor and carbon dioxide just below in the inversion. The top of the residual layer can be seen at around 700 m above the surface, where there is another, smaller, inversion. The lidar data clearly shows this layer, with an abrupt decrease in elastic backscatter above it. Both the water vapor and the carbon dioxide profiles show a relative maxima at this point, with a decrease in concentration just above.

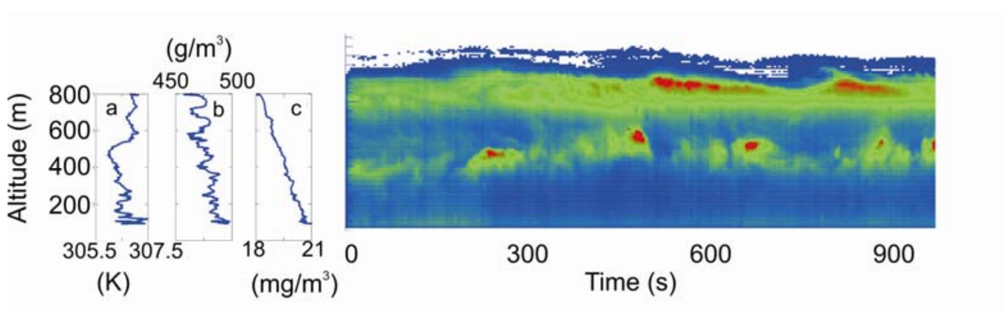

Figure 27: HOP profiles of potential temperature (a), water vapor concentration (b) and carbon dioxide concentration (c) compared with a time series of backscatter measured by the lidar.

4.2.4 Conclusions

The two cases discussed here demonstrate the ability of the HOP to make atmospheric profiles, and to locate the top of the ABL with a high degree of accuracy. The HOP is shown to be a useful tool for identifying interesting structures and other atmospheric phenomena. For example, the measured carbon dioxide flux at the surface in the CLASIC is downward, as shown in Table 3. The increasing carbon dioxide concentration profile near the surface can explain this, providing information for the interpretation of flux measurements.

Lidar and HOP profiles are extremely complementary, in addition, as the different measurements can add context to one another. For example, HOP profiles might identify a neutral layer which might explain the sudden rise of a buoyant plume observed by the lidar, or lidar data might be used to find the average size of plumes so that aircraft flights can be made with sufficient length to capture a statistically significant sample in the shortest possible time. Also, because the HOP is able to measure water vapor and carbon dioxide concentrations in addition to potential temperature, it can provide some insight into what causes the backscatter measured by the lidar.

Profiles measured from the HOP have several advantages over those measured using more traditional methods. Where the HOP is present in the field, it can make a profile from the surface well into the troposphere, in a matter of minutes. In doing this, the HOP can identify the top of the ABL in real time, determining the best location for further HOP and other airborne flights. The HOP can identify areas of the ABL where interesting phenomena exist and more sampling should take place, and then sample those areas immediately. The HOP can validate remotely-sensed measurements with exact, in-situ quantities, and it can provide more information with which to interpret the remotely-sensed measurements. The HOP is a useful tool for the measurement of boundary layer profiles.

4.3 HOP/Micrometeorological Tower Comparison

One important way of determining the accuracy of a system is by comparison with other reliable measurements. All wind measurements made from aircraft are affected by the aerodynamics of the platform to some extent (Lenschow et al 1991), and Nicholls et al (1983) suggest that it is difficult to quantify these effects without intercomparison of measurements made from different aircraft or from an aircraft and a tower. Lenschow et al (1991) add that this is especially important given that wind-measurement sensors must be calibrated in-flight, so in order to have confidence in them, they must be found to agree with established measurements. Comparisons between airborne sensors and point-based or other airborne sensors, although not straightforward, have been attempted many times. When attempting aircraft-aircraft comparisons, it is often difficult to reconcile the different airspeed, sampling frequency and altitude requirements of different platforms (Dobosy et al 1997). Nicholls et al (1983) point out that the similarity of the aerodynamics between different airplanes makes it difficult to rule out systematic flow distortion effects, even when the measurements between aircraft agree. In spite of this, several experiments have yielded good agreement between a variety of aircraft (Said et al 2005, Thornhill et al 2003, Dobosy et al 1997, Lenschow et al 1991, Nicholls et al 1983, LeMone and Pennell 1980).

Aircraft-tower comparisons have the added complexity that the footprint of a moving platform, generally well above the surface, is very different from that of a stationary tower near the surface (Gioli et al 2004). Oechel et al (1998) found a significant difference between tower and aircraft measurements made over Alaskan arctic tundra, which was partly explained by the neglect of spatial heterogeneity. Nevertheless, these comparisons have been made with good results, typically in homogeneous areas. Over cropland, Isaac et al (2004) and Prueger et al (2005) found good agreement between tower and aircraft mean and turbulent variables. Gioli et al (2004) and Samuelsson and Tjernstrom (1999) also found good agreement for a variety of agricultural and boreal forest sites in Europe. Over the western Pacific, Burns et al (1999) successfully reconciled data from five aircraft with ship- and buoy-based measurements, by adjusting all measurements to a 10 m altitude. Measurements made with the HELIPOD compare favorably with measurements made from the Cooperative Institute for Research in Environmental Sciences (CIRES) tethered balloon/kite borne turbulence measurement system (Muschinski et al 2001). HELIPOD measurements also compare favorably to ground-based tower and remote sensing measurements (Bange et al 2002).

4.3.1 Marine Boundary Layer Study

Also performed in order to evaluate the operating range of the HOP was a series of short flights at the US Army Corps of Engineers Coastal Station at Duck, North Carolina. Their purpose was to compare the observations collected on the HOP to those collected with similar sensors on a tower. These flights were conducted in conjunction with the profiles discussed in Section 4.2. The experiment was conducted on a day with a wind direction coming from the ocean, so that all sensors can be considered to measure only ocean conditions (Figure 28). More details and results from this experiment are shown in Section 6. The Duke University Mobile Micrometeorological Station (MMS) was deployed on the station's 560-m pier the. Figure 28 illustrates the precise location of the MMS on the pier and shows the HOP flying by during one of the three-kilometer legs that were performed on that day around 2 p.m. (EST). Note that the HOP flew at the same height as the sensors on top of the MMS mast.

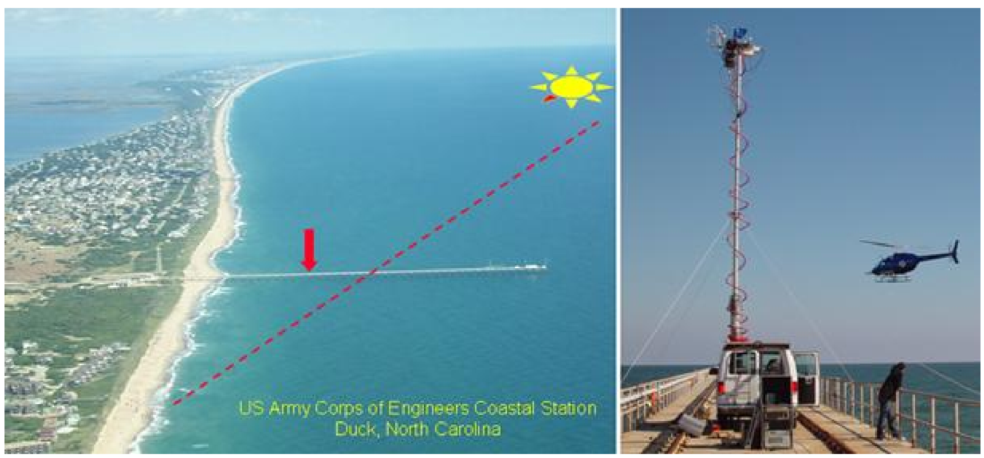

Figure 28: Observations set-up at the US Army Corps of Engineers Coastal Station in Duck (North Carolina), on March 26, 2007. The picture on the left depicts the station with its 560-m piers as well as the location of the Duke University Mobile Micrometeorological Station (MMS) on that pier (red arrow) and the wind direction (red triangle in the yellow orientation star). The red dashed line indicates the approximate 3-km flight legs performed into the wind. The picture on the right shows the HOP flying by at the same altitude as the sensors on the MMS (15 meters ASL). These sensors include a sonic anemometer and a Licor 7500 similar to those mounted on the nose of the HOP.

Figure 29 summarizes the mean and standard deviation of the sensible heat flux, latent heat flux, and carbon dioxide flux measured on the MMS during the nearly onehour time period that the flights were conducted. The time series were split into 20-min sequences to calculate the relevant statistics.

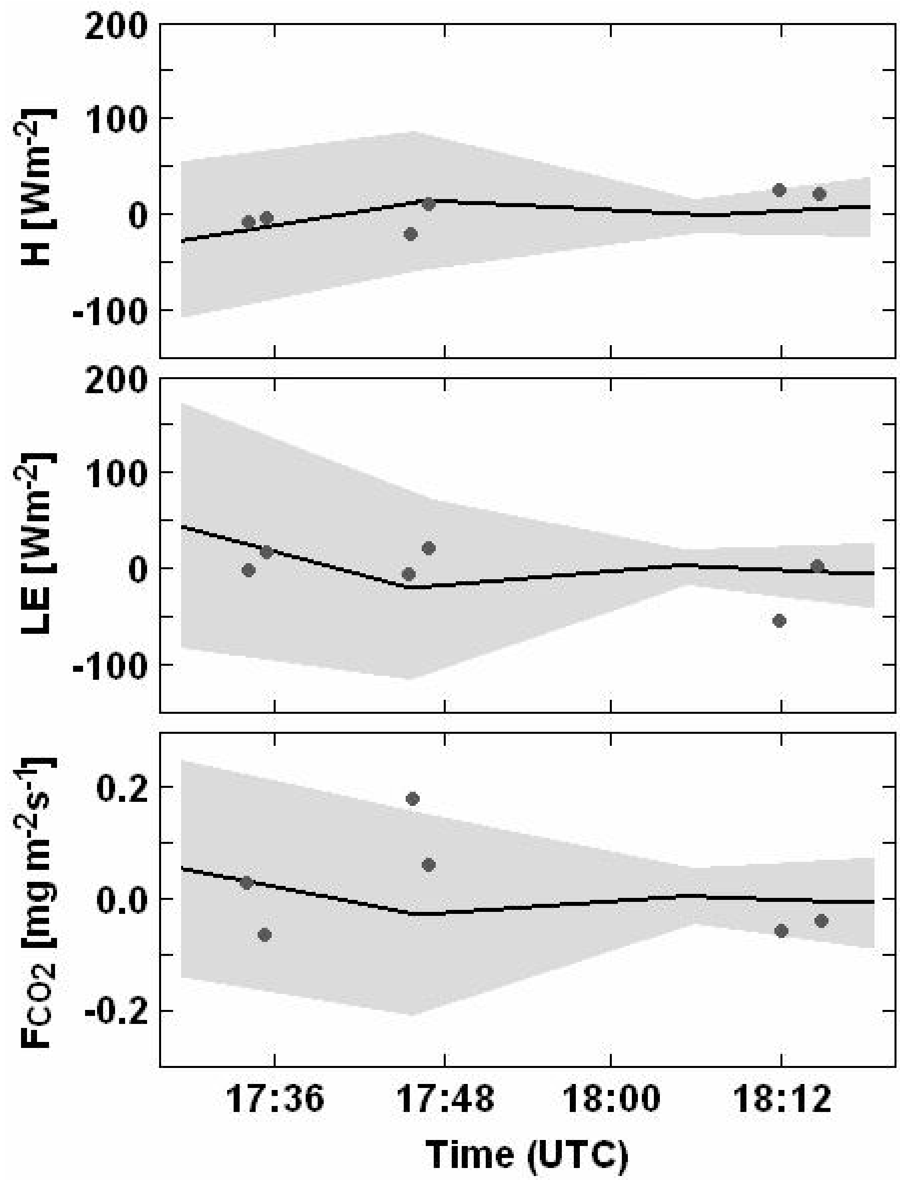

Figure 29: Sensible heat flux (H), latent heat flux (LE), and carbon dioxide flux (F_{CO2}) observed at Duck (North Carolina), on March 26, 2007. Dots are mean values for the different flight legs and solid lines are 20-min averages calculated from MMS data. Grey shadings indicate one standard deviation (1/2 on each side of the mean).

In general, and as expected near the ocean surface, mean fluxes were small during this period. Yet the tail of a front, which was generating strong winds, was still passing in the area when the flights began, resulting in high standard deviations during the first flight legs. After the front passed, a rapid decrease of the standard deviations is depicted in Figure 29. Each dot in the figure represents a variable calculated for a different flight leg, which each lasted about 3 min. Absolute differences between the HOP and the MMS are typically within one standard deviation. This experiment, while clearly limited, seems to indicate that similar fluxes are observed on the HOP and the MMS.

4.3.2 Canopy Horizontal Array Turbulence Study

Presented here are experimental results from the Duke University HOP that compare turbulent fluxes from the HOP to those measured by a stationary tower over an orchard. Comparisons between the Duke HOP and tower-based measurements, while still complex, are somewhat more straightforward because in many cases, the HOP is able to fly at the same vertical elevation as the tower. The measurement footprints may still not be the same, but sampling at the same point in the atmospheric profile reduces some uncertainty. The HOP is evaluated using tower-based measurements made over a large tree nut orchard in northern California during the Canopy Horizontal Array Turbulence Study (CHATS). For certain wind conditions during CHATS, the measurement footprint of both platforms can be considered to consist entirely of the internal boundary layer that forms over the orchard.

4.3.2.1 Description of Experiment

The main objective of the CHATS was to provide the relevant data needed to improve the parameterization of sub-filter-scale (SFS) processes in the roughness sub-layer that is affected by canopy-atmosphere interactions. For that purpose, in March-June 2007 NCAR deployed an array of sonic anemometers at different heights and lateral separations in a homogeneous walnut orchard in the Central Valley of California for the purpose of capturing the influence of the wake-scale motions in the lee of vegetation. Together with this array, other instruments, including a high tower and a new eye-safe lidar, were operating during the field campaign. While this equipment provided an excellent dataset at the tree-to-orchard scale, this experiment needed a general characterization of the entire ABL so that a full picture of the dynamics involved in the land-atmosphere interactions taking place above the orchard could be assessed. This missing link was occasionally provided by the Duke HOP, which flew about 25 hours in 6 days distributed over the period April-June 2007. For each day, two, 2-hour flights were performed (morning and early afternoon). During these flights, the Duke HOP measured 3D turbulence, temperature, moisture, and CO_2 in six transects at several heights from tree top to the top of the atmospheric boundary layer. The following perspective maps (Figure 30) show the CHATS experimental site.

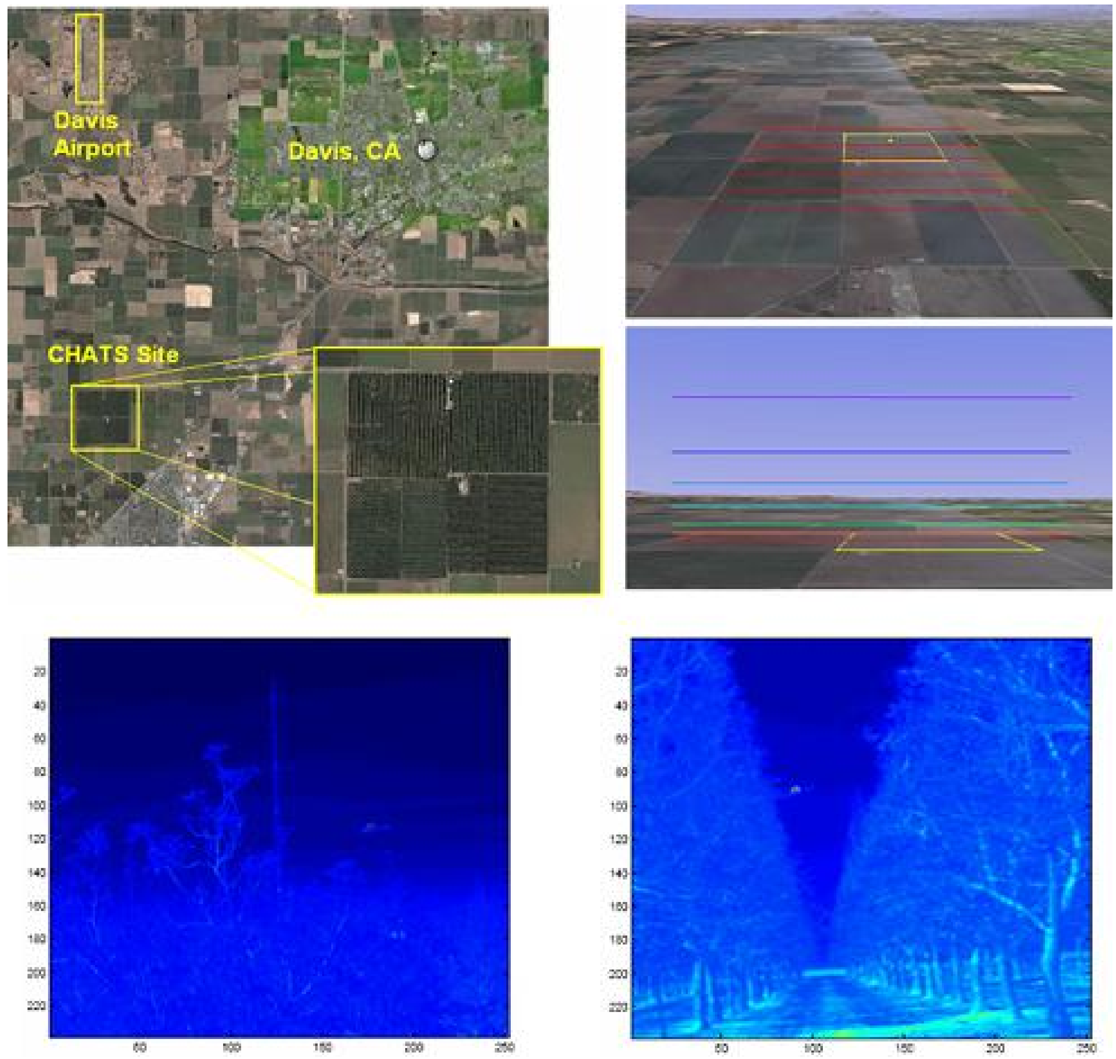

Figure 30: The CHATS experimental site (upper figures) south-west of Davis, CA (highlighted in yellow), and the horizontal and vertical flight tracks above the site. Note Davis Airport, which was conveniently located about 5 miles north of the site for refueling. The orchard is outlined in yellow, and the upper right figures show the flight tracks over the field. The lower two pictures show the infrared signature of the HOP in flight above the orchard. The tall tower erected at the experimental site can be seen in the lower left of the figure.

The HOP data can be directly compared to the data collected at the same elevation on the tall tower seen in the lower left photo in Figure 30. The flight results presented here were collected on May 25 at around 15:00 local time. On this day, the prevailing winds were from the south. When the winds are from the south, the tower, located at the north end of the field, is hypothetically within the internal boundary layer generated by the orchard. It is important to use HOP flights that are also within this internal boundary layer for comparison with the tower, so that all data are evaluated within the same framework. For evaluation of the HOP data, the flight legs closest to the tower, flown at the same elevation, are the focus, as these legs are more likely to have the same footprint as the measurements from the tower.

In addition, the HOP was flown in a "step-profile" pattern. Beginning at the surface, a series of two minute horizontal flight legs were flown with a vertical separation of 200 m. During the step-profile made on May 25 (Figure 31), the HOP made the flights while ascending and then descending. This flight pattern is useful for the calculation of flux profiles throughout the PBL, as is discussed in Section 1.2.

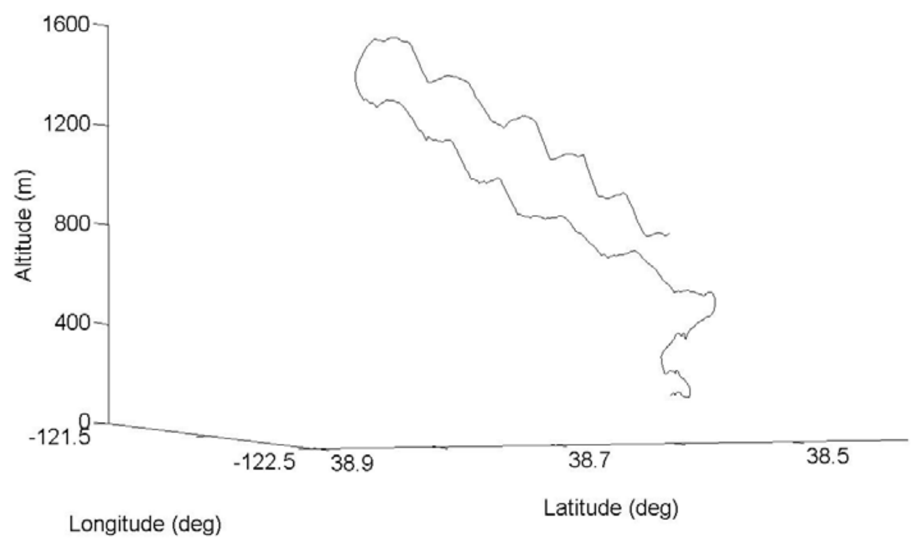

Figure 31: Flight track during the "step-profile" flight made on May 25, 2007. The HOP first ascended and then descended partway.

The tower-based sonic anemometer used in the comparison with the HOP flights was located at 23 m above the surface. The altitude of the HOP fluctuates somewhat but the pilots attempted to fly at about the same elevation. The coordinate system of the wind data was rotated so that u is positive to the east, v is positive to the north, and w is positive up, which is the same as the HOP coordinate system. Nighttime data collected on the tower was adjusted so that the average vertical wind velocity was zero. During the day, however, this was not done, so that no attempt was made to correct for movement of the instrument. Water vapor data was collected using a krypton hygrometer. Readers interested in additional details about the sensors on the tower and the field experiment can find them at http://www.eol.ucar.edu/deployment/field-deployments/field-projects/chats-project.

Conceptually, the comparison between the one minute HOP flights, which sample both in space and in time, and a 30 minute section of stationary data is not a straightforward one. Flux sampling errors in general can be thought to have three main components (assuming all instruments are functioning properly and the experimental setup is appropriate) (Vickers and Mahrt 1997; Mahrt 1998). First, there is a systematic error associated with the failure to capture all scales of the flux, especially large transporting scales. In general, this results in measured flux values smaller than actual values. Second, there is a random error associated with measurement records that are too short. The larger-scale eddies are not sufficiently sampled, leading to random error. Finally, there is error associated with non-stationarity or heterogeneity of the atmosphere. The HOP experiment during CHATS was designed such that this last problem can be safely disregarded, as the HOP and tower data records used are short enough to minimize mesoscale variability. In addition, the EMD was applied to both datasets, and any non-stationarities or heterogeneities were subsequently removed.

In order to ensure that the HOP was not sampling atmospheric heterogeneities due to a heterogeneous surface, the HOP was only flown over the orchard canopy. This resulted in very short flight legs, so that the systematic and random errors can be considered to be relatively high. As is discussed in Section 1.2, Lenschow et al (1994) find that the maximum systematic and random errors can be estimated by $2.2z_i(z/z_i)^{0.5}/L$ and $1.75(z/z_i)^{0.25}(z_i/L)^{0.5}$, respectively, where z_i is the height of the convective boundary layer, z is the flight altitude, and L is the length of the flight leg. For the case of the HOP flights during CHATS presented here, z is about 10 m, L is about 1500 m and z_i is about 400 m. Therefore, the estimated systematic error is about 9 % and the estimated random error is about 36 %.

It is evident that a direct comparison cannot be made between the short HOP flights and the long tower record. To make a comparison less problematic, several one minute records of tower data were randomly selected. Each analysis was performed on a 30 minute record of tower data and on the one minute tower records. These short sections of tower data will show the variability of data measured at small scales and are more directly comparable to HOP flights.

4.3.2.2 Results

4.3.2.2.1 Spectra and Cospectra

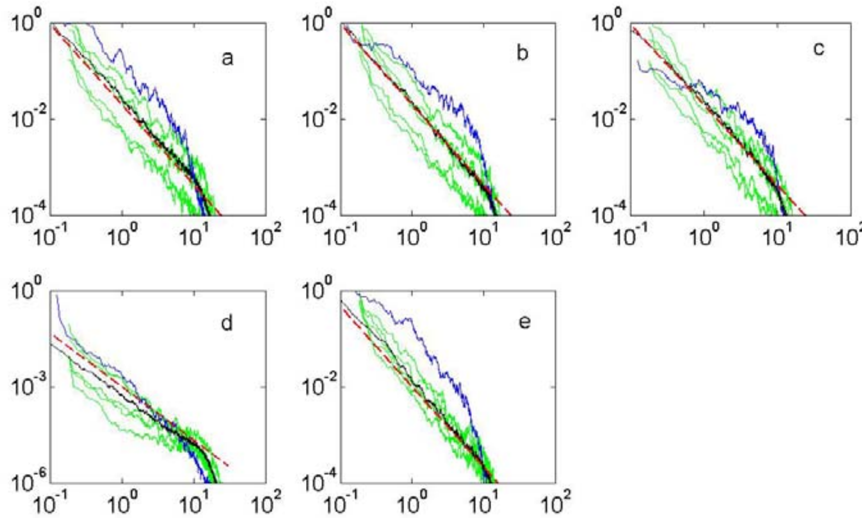

Figure 32: Comparison of 30 minute spectra from the tower (black line), one minute sections of tower data (green lines) and the HOP (blue lines). The red dashed line has a -5/3 slope.

Figure 32 shows example of filtered and detrended spectra from the HOP and from the tower. The HOP flights were approximately 60 seconds in length. Both the tower and the HOP *u* (Figure 32a) and *v* (Figure 32b) spectra follow the -5/3 slope. The HOP horizontal wind spectra have a slightly higher energy than the wind spectra from the tower. The HOP *w* spectrum (Figure 32c) also has a slightly higher energy than the tower spectrum. The *w* spectrum in this case exhibits a slope slightly flatter than -5/3. However, this is not typical of flights made during this field campaign. The temperature spectrum (Figure 32d) from the HOP has a slope slightly steeper than -5/3, while the spectra from the tower (both the 30 minute average and the one minute averages) have slightly flatter slopes. The energy from the HOP flight falls near the upper limit of the range of energies from the one minute tower averages. The water vapor spectra from the

HOP (Figure 32e) are also slightly higher than that measured by the tower. The HOP spectrum follows the -5/3 slope well into the higher frequencies. Note that the HOP data has been filtered to remove the high frequency rotor noise. This filtration corrects in large part the increase in energy at high frequencies. Spectra sampled on other days yield similar results, having slopes of -5/3. The HOP variables typically contain more energy than the tower variables.

The variable cospectra (Figure 33) show similar trends to the spectra. The absolute values of the cospectra are shown to make comparison on a log-log plot possible. The cospectra of *u* and *w*, and *v* and *w* exhibit a shape similar to the spectrum of *w*. It is interesting to note that the *uw* cospectra is larger when measured by the HOP than measured by the tower, while the *vw* cospectra is similar. The *u* component of the wind on this day was almost zero, and this is also the direction of flight. The components of the wind are often only weakly correlated (Lenschow and Stankov 1986), and their measurement from aircraft involves several layers of complexity, so that measurements of momentum flux are more prone to inaccuracy than other flux measurements (Dobosy et al 1997).

As with the temperature spectra, the *Tw* cospectra from both platforms follow cospectrum a -5/3 slope. Also similarly, the cospectra from the HOP are slightly larger than those measured by the tower. The water vapor and w HOP cospectrum contains more energy than the tower cospectra and has a shape similar to that of the momentum cospectra.

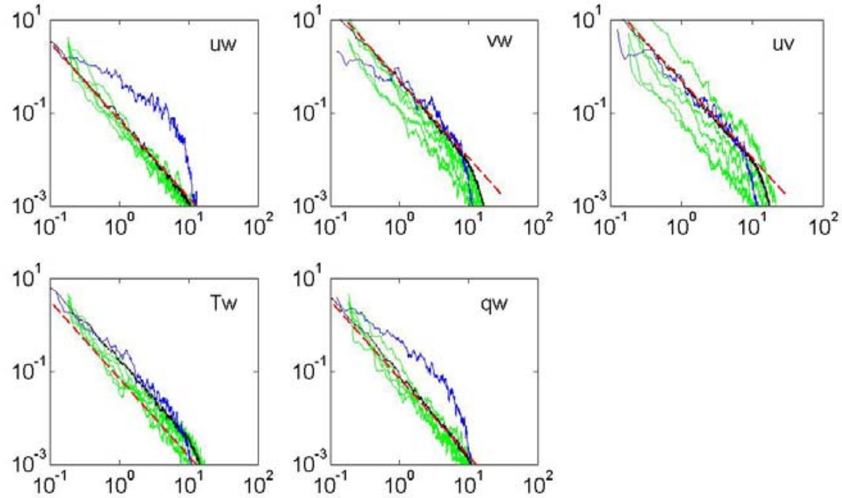

Figure 33: Comparison of 30 minute cospectra from the tower (black line), one minute sections of tower data (green lines) and the HOP (blue lines). The red dashed line has a -5/3 slope.

4.3.2.2.2 Variable Statistics and Fluxes

The statistics of the variables also show trends that are consistent with the spectra. Table 4 shows the variances of the variables measured by the HOP and by the tower. Variances for the 30 minute record of tower data were computed, as well as variances for the five randomly chosen one-minute records. The maximum and minimum of the short records are shown in Table 4. The variances of the components of the winds measured by the HOP are all within the range of one-minute variances measured by the tower. The variances of temperature and water vapor concentration are larger than those measured on the tower.

Table 4: Variances of variables measured by the HOP and the CHATS tower.

	u (m^2/s^2)	v (m^2/s^2)	w (m^2/s^2)	T (K^2)	q $(g/m^3)^2$
HOP	0.52	1.00	0.16	0.17	1.28
Tower 30-minute	0.64	0.40	0.25	0.01	0.31
Maximum Tower 1-minute	1.29	1.07	0.56	0.09	0.50
Minimum Tower 1-minute	0.07	0.07	0.03	0.00	0.01

It is difficult to draw definitive conclusions regarding HOP measurements made on different spatial and temporal scales than tower-based measurements, particularly when the flight legs are short. Examination of the energy spectra provides a visual reference for this problem. Turbulence production scales and the low frequency portion of the turbulent cascade contain orders of magnitude more energy than the high frequency regions. The short HOP flights measure only this high frequency region, so it is expected that the HOP measurements would contain less variance than a 30 minute tower record, which captures much more energy at lower frequencies. However, this problem is complicated by the spatial nature of the HOP data. Especially near the surface, where the atmosphere is less well-mixed and therefore more strongly influenced by small-scale surface heterogeneities. The atmosphere measured by the HOP contains more variability. The atmosphere measured by the tower is directly influenced only by one limited section of land surface. In addition, as discussed above, the random error contained in such short data records is high. The variability exhibited by the one minute tower averages is considerable, and in all cases except temperature, blankets the HOP measurements. Interestingly, these competing influences appear to balance out in this case. The HOP flight exhibits more energy at small scales than the tower data (except in the case of temperature) but lower frequency variations are not captured. Under different atmospheric, land surface or flight conditions, either the large-scale temporal variability or the small-scale spatial variability might be expected to dominate.

Similarly to Table 4, Table 5 shows the fluxes measured from the HOP and from the tower. Given the differences in variances measured from the two platforms, it is interesting that the fluxes are similar. Especially in light of the large variances of water vapor concentration, it is surprising that the latent heat flux value measured from the HOP falls well within the range of those measured by the tower. The sensible heat flux and TKE values measured by the HOP are also within the range measured by the tower. The one minute tower averages of momentum flux values also blanket the HOP measurements, with the exception of uv, which is large measured from the HOP.

Table 5: Fluxes measured from the HOP and from the tower.

	SH (W/m^2)	LH (W/m^2)	TKE (m/s)	uv (m^2/s^2)	uw (m^2/s^2)	Vw (m^2/s^2)
HOP	-27.99	162.64	0.84	0.15	0.07	-0.09
Tower	-13.32	196.86	0.65	-0.03	0.03	-0.15
Tower Maximum	9.00	634.98	1.35	0.08	0.24	-0.04
Tower Minimum	-29.52	105.99	0.11	-0.47	-0.04	-0.51

Betts et al (1990) and Grossman (1992) find that the application of a low-pass filter eliminating wavelengths longer than 5 km decreases aircraft flux to magnitudes significantly (10-35 %) lower than tower values. They hypothesize that this discrepancy is caused by the removal of low-frequency contributions to the flux. Additionally, Grossman (1992) finds that the application of a low-pass filter creates an offset of the flux data, so that even when the average flux is zero, the filtered flux has a value. He suggests that the low-frequency contribution to the fluxes has the opposite sign from the high-frequency contribution. This might explain why here we see that although the HOP flights measure more energy, the fluxes are comparable to longer tower-based measurements, although Mann and Lenschow (1994) present conflicting results.

The negative SH values near the surface are an interesting result. The ability of the HOP to make profiles of turbulent quantities is especially useful in such a situation, as it can provide some context to the surface point measurements. Figure 34 shows the profile of SH. The SH is negative near the surface and increases until about 400 m. It decreases from 400 m to about 1100 m, crossing zero at about 800 m. Above 1200 m, the SH increases again. Latent heat flux (Figure 35) is positive at the surface, as is expected over an actively growing forest. It decreases to a minimum at 400 m, then increases until about 1200 m, above which it is fairly constant. There appears to be a distinct layer going up to a height of about 400 m and another at 1200 m in all profiles, with most profiles showing a well-mixed atmosphere between and above these layers.

From inspection of these profiles, it appears that the surface is affecting the PBL up to an altitude of 400m, which is the current height of the PBL. The step profile was flown around 4 pm local time, and it appears that the surface is decoupling from the earlier boundary layer which was located at 1200 m. The well-mixed layer between 400 and 1200 m is the residual layer.

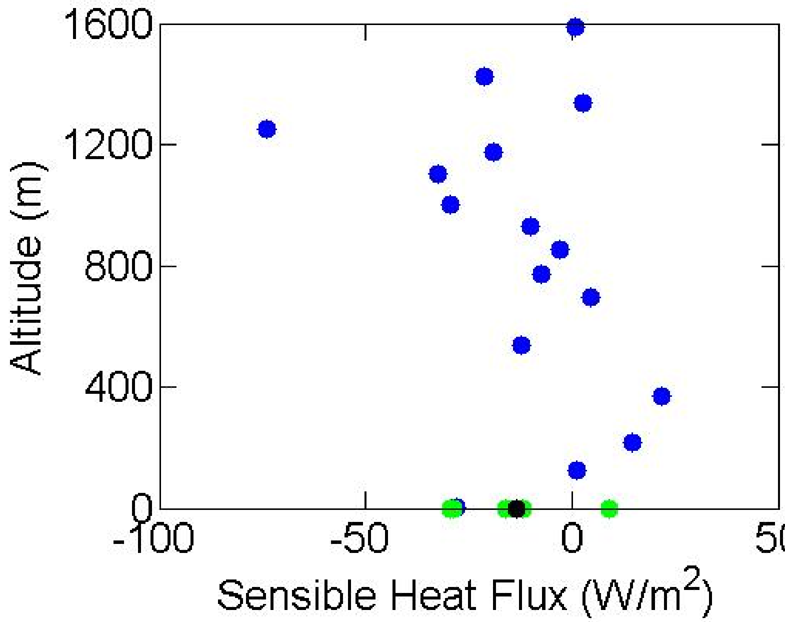

Figure 34: Profile of sensible heat flux as measured by the HOP (blue dots). The black dot represents the 30 minute tower average, and the green dots are the five randomly selected one minute tower averages.

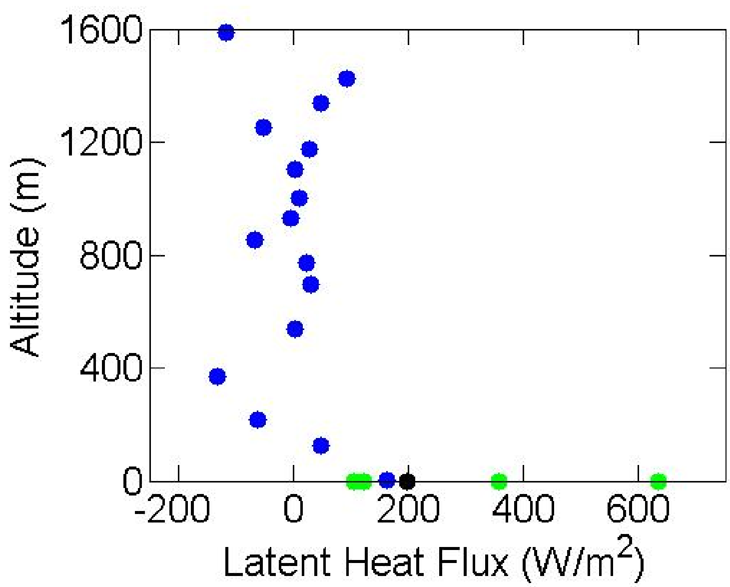

Figure 35: Profile of latent heat flux as measured by the HOP (blue dots). The black dot represents the 30 minute tower average, and the green dots are the five randomly selected one minute tower averages.

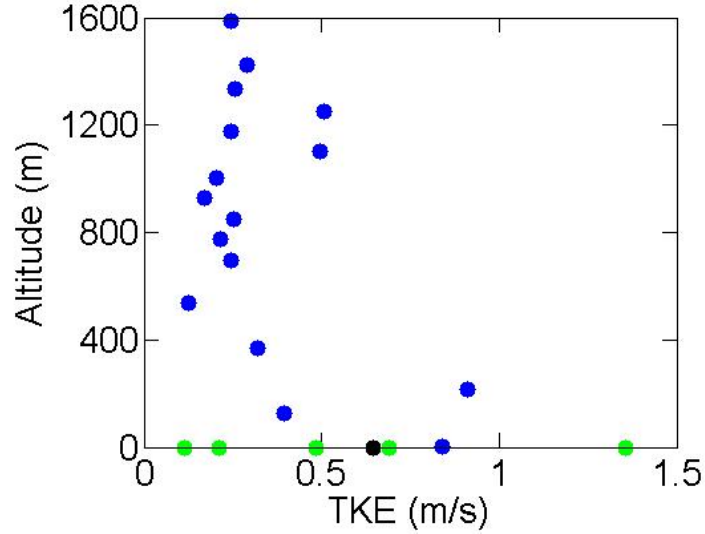

Figure 36: Profile of TKE as measured by the HOP (blue dots). The black dot represents the 30 minute tower average, and the green dots are the five randomly selected one minute tower averages.

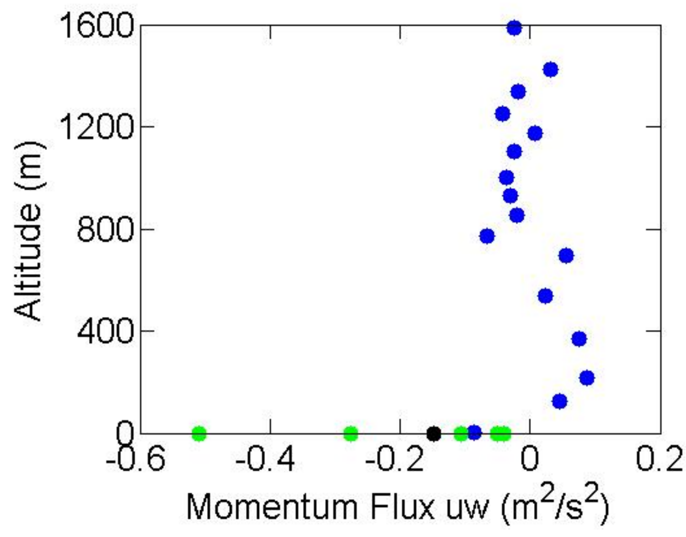

Figure 37: Profile of uw momentum flux as measured by the HOP (blue dots). The black dot represents the 30 minute tower average, and the green dots are the five randomly selected one minute tower averages.

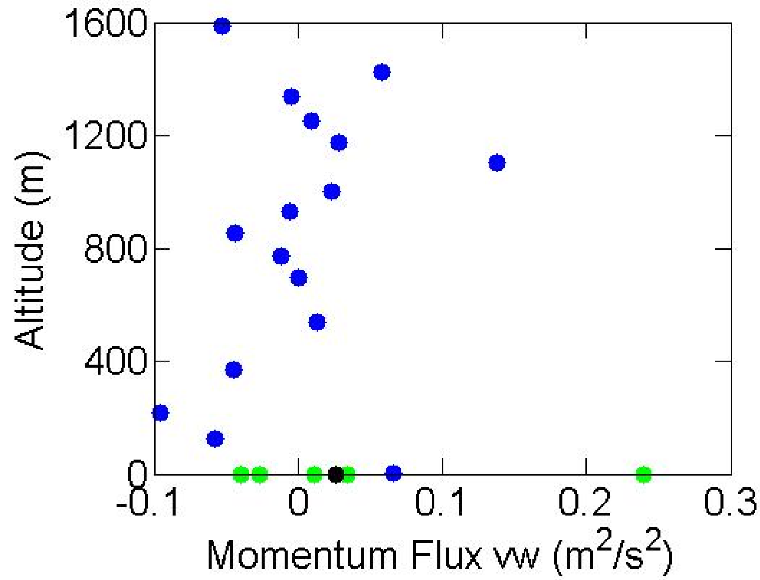

Figure 38: Profile of vw momentum flux as measured by the HOP (blue dots). The black dot represents the 30 minute tower average, and the green dots are the five randomly selected one minute tower averages.

4.3.2.3 Conclusions

During the CHATS field campaign in the spring of 2007, the HOP was flown past a stationary tower, at the same vertical elevation. The HOP flight was compared to the tower data gathered concurrently, with mixed result. Spectra and cospectra measured from the HOP tend to have more energy than those measured from the tower, except for temperature, which follows an opposite trend. The variances of variables measured by the HOP are not necessarily similar to those measured by the tower 30 minute average, but with the exception of water vapor concentration, the HOP values fall within the range of values calculated from one minute sections of tower data. The measured energy and momentum fluxes also fall within the range of values calculated from one minute tower averages.

Calculating one minute averages of point data allows a comparison to be made between the tower data and HOP data collected on similar temporal scales. Because the HOP data and the one minute tower averages contain a similar amount of variance, it can be inferred that in this case the effects of spatial variance are minimal. The wide spread of variance and flux values obtained using the one minute tower averages can be attributed to high random error, a problem that is also present in the HOP data. One way to alleviate this error is to average multiple flight legs to ensure that transporting eddies are adequately sampled, although this may have the effect of introducing some error due to non-stationarity, depending on the length of time taken to fly the multiple legs.

Profiles of fluxes provide context to surface measurements. This ability is one major advantage of the HOP over other instrument platforms. In the flux profiles obtained during this flight, the surface is shown to have an effect on the entire PBL, up to a height of 400 m. The residual layer remaining from the day's CBL is evident at 1200 m. In this case, it is clear that the HOP has the ability to sufficiently capture the surface fluxes from the flux profiles. This would be especially useful over areas where the placement of a tower is not practical, or over heterogeneous surfaces whose spatial variability would not be sampled by a tower.

5. Conclusions

The Duke University Helicopter Observation Platform fills an existing gap in existing atmospheric turbulence measurements. Tower-based measurements cover extremely small areas, but are inexpensive to make and can measure long time scales. Satellites cover large areas, but with poor spatial and temporal resolution. Their measurements are also indirect and thus their interpretation is not straightforward. Airplanes are useful for making in situ measurements on larger scales, but they cannot sample near the ground. In addition, small aircraft that can make measurements with good spatial resolution have extremely limited payload and power constraints. The Duke HOP fits into a niche that is currently empty, by sampling with good spatial resolution in all areas of the PBL. The HOP is able to bridge the gap between point measurements and satellite measurements to quantify boundary layer dynamics on a regional scale.

The Empirical Mode Decomposition is a valuable tool for the processing of HOP and other turbulent data. The EMD technique separates the data into a finite number of Intrinsic Mode Functions, each of which is unique and orthogonal, and thus physically based. This is an advantage of the EMD over the Empirical Orthogonal Function technique. The EMD technique does not require the data to be stationary or linear, unlike Fourier methods. The IMFs are derived empirically from the data itself, so that they do not need to be known *a priori*, and they can change frequency and amplitude as the data changes, unlike wavelet methods. The EMD technique is shown to be effective at removing random noise, rotor noise and vibrations from the HOP data, along with longer term trends due to changes in the PBL and changes in the aircraft altitude and attitude.

The EMD technique could prove to be a useful tool for the characterization of the PBL, as well. Because each mode is physically based, in theory, trends due to changing land surface could be identified in the IMFs. For example, if the HOP is flown over a landscape populated with irrigated and non-irrigated fields, the EMD should be able to discern the pattern of changing water vapor and other variables. The use of this technique for this type of analysis should be explored further.

Through analytical, computational and empirical studies, the aerodynamic envelope of the HOP at various airspeeds is quantified. The HOP is found to be clear of the main rotor downwash at forward airspeeds over about 10 m/s. At higher airspeeds, a pocket of high pressure develops in front of the nose of the HOP, which could influence the data measured by the sensors. The optimal airspeed for sampling is found to be around 30 m/s. At this airspeed and a sampling frequency of 40 Hz, the sampling resolution is 0.75 m, so that only small eddies are not sampled.

Turbulence data measured from the HOP is compared to measurements made with stationary micrometeorological towers over the ocean and over an orchard. Preliminary comparisons with a tower over the ocean yield good results. HOP-measured fluxes fall within the range of those measured from the tower. Potential temperature profiles measured from the HOP identify the top of the PBL and other atmospheric structures that are also identified by an elastic lidar.

The Duke University HOP is shown to be a useful tool for the measurement of turbulent atmospheric data. Issues with data collection and processing have been identified and overcome, and the ideal operating range has been identified. The HOP measurements compare well with tower-based measurements, and can extend these measurements over a region. The HOP is a state-of-the-art measurement platform that provides data in a way that no other platform has the capability to do.

5.1 Future Research Directions

It is also important to note that the Duke HOP has a modular design and, therefore, sensors and instruments can be mounted on it for specific experiments and disconnected afterward. It also has an attachment device under its belly, which includes power and data connectors. Thus, instruments can be mounted inside pods that can be rapidly attached to that universal device and that can communicate with the on-board data acquisition system, if desired.

For instance, an aerosol lidar has been constructed in such a pod. It is shown in Figure 30 and discussed in Eichinger et al (2008). This lidar can be attached to the HOP in a few minutes, and dismounting it is even faster. The lidar is mounted on a pod that hangs underneath the helicopter and is capable of looking forward, sideways or down. The unit is based on the University of Iowa elastic lidar systems using a Big Sky ULTRA laser (Nd:YAG, 50 mJ per pulse, 20 Hz) and an 8" Meade telescope. A Signatec PDA12 digitzer allows 1.25 m range resolution to about 5 km.

Figure 39: The HOP equipped with its lidar (engineering drawing in lower frame shows the components) in its first test flight on April 9, 2008. The laser (Big Sky Laser, Ultra CFR Nd:YAG) is a 20-Hz pulsed system with 50-mJ energy at 1064 nm.

This lidar is intended for use in boundary layer studies involving atmospheric evolution and structure and aerosol properties and dispersion. The lidar is expected to extend conventional measurements made aboard the helicopter and also to provide a larger context for those measurements. The real time data display capability of the lidar can also allow the helicopter pilot to better position the helicopter to make measurements in the most appropriate part of the atmosphere. Progress in optical aerosol physics is also anticipated from this lidar. The ability of the lidar to sense the air ahead of the helicopter and then sample that air as it flies through it will enable comparisons of optical and conventional aerosol sampling in ways not otherwise possible.

References

Affre, Ch., A. Carrara, F. Lefebre, A. Druilhet, J. Fontan and A. Lopez, 1999: Aircraft measurement of ozone turbulent flux in the atmospheric boundary layer. *Atmospheric Environement*, **33**:1561-1574.

Amiro, B.D., J.I. MacPherson and R.L. Desjardins, 1999: BOREAS flight measurements of forest-fire effects on carbon dioxide and energy fluxes. *Agricultural and Forest Meteorology*, **96**:199-208.

Abehserra, N., and R. Avissar, 2008. Simulations of the operating range of the Duke University Helicopter Observation Platform for the design of sensors and research missions. *J. Atmos. Ocean. Tech.,* in preparation.

Antonia, R.A., and Y. Zhu, 1994. Inertial range behavior of the longitudinal heat flux cospectrum. *Bound.-Layer Meteorol.*, **70**, 429-434, 1994.

Avissar, R., and F. Chen, 1993. Development and analysis of prognostic equations for mesoscale kinetic energy and mesoscale (subgrid-scale) fluxes for large-scale atmospheric models. *J. Atmos. Sci.*, **50**, 3751-3774.

Avissar, R. and R.A. Pielke, 1989. A parameterization of heterogeneous land-surface for atmospheric numerical models and its impact on regional meteorology. *Mon. Wea. Rev.*, **117**, 2113-2136.

Avissar, R. and T. Schmidt, 1998. An evaluation of the scale at which ground-surface heat flux patchiness affects the convective boundary layer using a Large-Eddy Simulation model. *J. Atmos. Sci.*, **55**, 2666-2689.

Avissar, R. and D. Werth, 2005. Global Hydroclimatological Teleconnections Resulting from Tropical Deforestation. *J. Hydromet.*, **6**, 134-145.

Axford, D.N., 1968: On the accuracy of wind measurements using an inertial platform in an aircraft, and an example of a measurement of the vertical mesostructure of the atmosphere. *Journal of Applied Meteorology*, **7**:645-666.

Babin, S. M., 1996. Surface duct height distributions for Wallops Island, Virginia, 1985 to 1994. *J. Appl. Meteorol.,* **35**, No. 1, 86-93.

Bange, J., and Roth, R., 1999: Helicopter-borne flux measurements in the nocturnal boundary layer over land-A case study. *Boundary-Layer Meteorology*, **92**, 295-325.

Bange, J., F. Beyrich, and D.A.M. Engelbart, 2002: Airborne measurements of turbulent fluxes during LITFASS-98: Comparison with ground measurements and remote sensing in a case study. *Theoretical Applied Climatology*, **73**:35-51.

Bange, J., T. Speiss, M. Herold, F. Beyrich, and B. Hennemuth, 2006: Turbulent fluxes from Helipod flights above quasi-homogeneous patches within the LITFASS area. *Boundary-Layer Meteorology*, **121**:127-151.

Bolch, M.A. and R. Avissar, 2008. Characterization of the atmospheric boundary layer with the Duke University Helicopter Observation Platform during CLASIC. *Bound.-Layer Meteorol.*, in preparation.

Betts, A.K., R.L. Desjardins, J.I. MacPherson and R.D. Kelly, 1990: Boundary-layer heat and moisture budgets from FIFE. *Boundary-Layer Meteorology*, **50**:109-137.

Bogel, W. and R. Baumann, 1991: Test and calibration of the DLR Falcon wind measuring system by maneuvers. *Journal of Atmospheric and Oceanic Technology*, **8(1)**:5-18

Bond, N.A. and Walter, B.A., 2002: Research aircraft observations of the mean and turbulent structure of a low-level jet accompanying a strong storm. *Journal of Applied Meteorology*, **41**:1210-1224.

Brown, E. N., C.A. Friehe, and D.H. Lenschow, 1983: The Use of Pressure Fluctuations on the Nose of an Aircraft for Measuring Air Motion. *Journal of Climate and Applied Meteorology*, **22 (1)**, 171-180.

Burns, S.P., D. Khelif, C.A. Friehe, A.G. Williams, P. Hignett, A.L.M. Grant, J.M. Hacker, D.P. Rogers, E.F. Bradley, R.A. Weller, M.F. Cronin, S.P. Anderson, C.W. Fairall, and C.A. Paulson, 1999: Comparisons of aircraft, ship and buoy meteorological measurements from TOGA COARE. *Journal of Geophysical Research*, **104(D24)**:30,853-30,883.

Chen, F., D.N. Yates, H. Nagai, M.A. LeMone, K. Ikeda and R.L. Grossman, 2003: Land surface heterogeneity in the Cooperative Atmosphere Surface Exchange Study (CASES-97). Part 1: Comparing modeled surface flux maps with surface-flux tower and aircraft measurements. *Journal of Hydrometeorology*, **4**:196-218.

Cho, J.Y.N., R.E. Newell, B.E. Anderson, J.D.W. Barrick and K.L. Thornhill, 2003: Characterizations of tropospheric turbulence and stability layers from aircraft observations. *Journal of Geophysical Research*, **108(D20)**:8784.

Cohn, S.A. and Angevine, W.M., 2000: Boundary layer height and entrainment zone thickness measured by lidars and wind-profiling radars. *Journal of Applied Meteorology*, **39**:1233-1247.

Collins, D.R., H.H. Jonsson, H. Liao, R.C. Flagan, J.H. Seinfeld, K.J. Noone and S.V. Hering, 2000: Airborne analysis of the Los Angeles aerosol. *Atmospheric Environment*, **34**:4155-4173.

Crawford, T.L. and R.J. Dobosy, 1992: A Sensitive Fast-Response Probe to Measure Turbulence and Heat Flux from Any Airplane. *Boundary-Layer Meteorology*, **59**, 257-278.

Crawford, T.L., R.J. Dobosy and E.J. Dumas, 1996a: Aircraft wind measurement considering lift-induced upwash. *Boundary-Layer Meteorology*, **80**:79-94.

Crawford, T.L., R.J. Dobosy, R.T. McMillen, C.A. Vogel and B.B. Hicks, 1996b: Air-surface exchange measurement in heterogeneous regions: Extending tower observations with spatial structure observed from small aircraft. *Global Change Biology*, **2**:275-285.

Cruette, D., A. Marillier, J.L. Dufresne, and J.Y. Grandpeix, 2000: Fast temperature and true airspeed measurements with the airborne ultrasonic anemometer-thermometer (AUSAT). *Journal of Atmospheric and Oceanic Technology*, **17**:1020-1038.

Datig, M. and T. Schlurmann, 2004: Performance and limitations of the Hilbert-Huang transformation (HHT) with an application to irregular water waves. *Ocean Engineering*, **31**:1783-1834.

Davis, K.J., D.H. Lenschow, S.P. Oncley, C. Kiemle, G. Ehret, A. Giez and J. Mann, 1997: Role of entrainment in surface-atmosphere interactions over the boreal forest. *Journal of Geophysical Research*, **102(D24)**:29,219-29,230.

Davis, K.J., N. Gamage, C.R. Hagelberg, C. Kiemle, D.H. Lenschow and P.P. Sullivan, 2000: An objective method for deriving atmospheric structure from airborne lidar measurements. *Journal of Atmospheric and Oceanic Technology*, **17**:1455-1467.

De Saeger, E., G. Dumont, E. Roekens, D. Tielemans and G. Verduyn, 1993: Study of the Photochemical Pollution in Belgium, Guest Contribution. *Proceedings of EUROTRAC Symposium '92*, 93-97.

Desjardins, R.L., P.H. Schuepp, J.I. MacPherson and D.J. Buckley, 1992: Spatial and temporal variations of the fluxes of carbon dioxide and sensible and latent heat over the FIFE site. *Journal of Geophysical Research*, **97(D17)**:18,467-18,475.

Desjardins, R.L., R. Pelletier, P.H. Schuepp, J.I. MacPherson, H. Hayhoe, and J. Cihlar, 1995a: Measurement and estimation of CO2 fluxes from aircraft and satellite-based systems. *Journal of Geophysical Research*, **100(D12)**:25,549-25,558.

Desjardins, R.L., J.I. MacPherson, H. Neumann, G. den Hartog and P.H. Schuepp, 1995b: Flux estimates of latent and sensible heat, carbon dioxide, and ozone using an aircraft-tower combination. *Atmospheric Environment*, **29(21)**:3147-3158.

Desjardins, R.L., J.I. MacPherson, L. Mahrt, P. Schuepp, E. Pattey, H. Neumann, D. Baldocci, S. Wofsy, D. Fitzjarrald, H. McCaughey and D.W. Joiner, 1997: Scaling up flux measurements for the boreal forest using aircraft-tower combinations. *Journal of Geophysical Research*, **102(D24)**:29,125-29,133.

Desmet, G., G. Dumont, D. Tielemans, R. De Lathouwer, and E.J. Roekens, 1995. Technical Note: Measurements of Atmospheric Pollutants Using Helicopters: Evaluation of the Possible Contamination of the Sample Air by Turbine Exhausts. *Atmos. Environ.*, **29(18)**, 2547-2552.

Dobosy, R.J., T.L. Crawford, J.I. MacPherson, R.L. Desjardins, R.D. Kelly, S.P. Oncley, and D.H. Lenschow, 1997: Intercomparison among four flux aircraft at BOREAS in 1994. *Journal of Geophysical Research-Atmospheres*, **102(D24)**:29,101-29,111.Desjardins, R.L., R. Pelletier, P.H. Schuepp, J.I. MacPherson, H. Hayhoe, and J. Cihlar, 1995: Measurement and estimation of CO2 fluxes from aircraft and satellite-based systems. *Journal of Geophysical Research*, **100(D12)**:25,549-25,558.

Donelan, M. and M. Miyake, 1973: Spectra and fluxes in the boundary layer of the trade-wind zone. *Journal of the Atmospheric Sciences*, **30**:444-464.

Duffy, D.G., 2004: The Application of Hilbert-Huang Transforms to Meteorological Datasets. *Journal of Atmospheric and Oceanic Technology*, **21**:599-611.

Eichinger, W., R. Avissar, and H.E. Holder, 2008. Development of a Helicopter Borne Lidar for Boundary Layer Studies, Proceedings, 24th International Laser Radar Conference, 23-27 June 2008, Boulder, Colorado, USA.

Etkin, B., 1959: *Dynamics of Flight*, John Wiley and Sons, Inc., New York, NY, 519 pp.

Foster, S., 2003: Accuracy requirements for airborne wind measurement in aerial application. *2003 ASAE/NAAA Technical Section, 37th Annual National Agricultural Aviation Association Convention, Reno, NV, 8 December 2003*, Paper Number AA03-0012.

Froude, R.E., 1889. On the part played in propulsion by differences of fluid pressure. *Transactions of the Institute of Naval Architects*, 30, p. 390.

Froude, W., 1878. On the elementary relation between pitch, slip and propulsive efficiency. *Transactions of the Institute of Naval Architects*, 19, pp. 47-57.

Frech, M. and A. Jochum, 1999: The evaluation of flux aggregation methods using aircraft measurements in the surface layer. *Agricultural and Forest Meteorology*, **98-99**:121-143.

Garman, K.E., K.A. Hill, P. Wyss, M. Carlsen, J.R. Zimmerman, B.H. Stirm, T.Q. Carney, R. Santini and P.B. Shepson, 2006: An airborne and wind tunnel evaluation of a wind turbulence measurement system for aircraft-based flux measurements. *Journal of Atmospheric and Oceanic Technology*, **23**:1696-1708.

Gillani, N.V., M. Luria, R.J. Valente, R.L. Tanner, R.E. Imhoff and J.F. Meagher, 1998: Loss rate of NO_y from a power plant plume based on aircraft measurements. *Journal of Geophysical Research*, **103(D17)**:22,585-22,592.

Gioli, B., F. Miglietta, B. de Martino, R.W.A. Hutjes, H.A.J. Dolman, A. Lindroth, M. Schumacher, M.J. Sanz, G. Manca, A. Peressotti, and E.J. Dumas, 2004: Comparison between tower and aircraft-based eddy covariance fluxes in five European regions. *Agricultural and Forest Meteorology*, **127**, 1-16.

Gioli, B., F. Miglietta, F. P. Vaccari, A. Zaldei, and B. De Martino, 2006: The Sky Arrow ERA, an innovative airborne platform to monitor mass, momentum and energy exchange of ecosystems. *Annals of Geophysics*, **49(1)**:109-116.

Glauert, H., 1935. *Airplane Propellers*, In Division L of *Aerodynamic Theory*, ed. W.F. Durand, Springer Verlag, Berlin, Germany. Reprinter by Peter Smith, Glouster, MA, 1976.

Gunter, R.L., 2007: Assessment of boundary layer variations in the Tampa Bay Area during the Bay Region Atmospheric Chemistry Experiment (BRACE). *Atmospheric Environment*, **41**:4165-4176.

Guo, Y., R.L. Desjardins, J.I. MacPherson and P.H. Schuepp, 1995: The correspondence of aircraft-measured fluxes of sensible heat, latent heat, CO2 and ozone to the surface characteristics in the San Joaquin Valley of California. *Atmospheric Environment*, **29(21)**:3159-3168.

Heinemann, G. and M. Kerschgens, 2006: Simulation of surface energy fluxes using high-resolution non-hydrostatic simulations and comparisons with measurements for the LITFASS-2003 experiment. *Boundary-Layer Meteorology*, **121**:195-220.

Holder, H.E., M.A. Bolch and R. Avissar, 2008a. Measurements of turbulent fluxes in the atmospheric boundary layer with the Duke University Helicopter Observation Platform. *J. Atmos. Ocean. Tech.,* in preparation.

Holder, H.E., D. Lenschow, N. Patton, N. Matayoshi and R. Avissar, 2008b. An evaluation study of the turbulent fluxes measured on board the Duke University

Helicopter Observation Platform during CHATS. *J. Atmos. Ocean. Tech.,* in preparation.

Hoff, R.M., M. Harwood, A. Sheppard, F. Froude and J.B. Martin, 1997: Use of airborne lidar to determine aerosol sources and movement in the Lower Fraser Valley (LFV), BC. *Atmospheric Environment*, **31(14)**:2123-2134.

Huang, N. E., Long, S. R.and Shen, Z. 1996: The mechanism for frequency downshift in nonlinear wave evolution. *Adv. Appl. Mech*., 32, 59-111.

Huang, N.E., Z. Shen, S.R. Long, M.C. Wu, H.H. Shih, Q. Zheng, N-C. Yen, C.C. Tung, and H.H. Liu, 1998: The empirical mode decomposition and the Hilbert spectrum for nonlinear and non-stationary time series analysis. *Proceedings of the Royal Society of London*, **454**:903-995.

Huang, N. E., Z. Shen, R. S. Long, 1999: A New View of Nonlinear Water Waves -- The Hilbert Spectrum, *Ann. Rev. Fluid Mech*. 31, 417-457.

Huang, N. E., M. L. Wu, S. R. Long, S. S. Shen, W. D. Qu, p. Gloersen, and K. L. Fan, 2003: A confidence limit for the Empirical Mode Decomposition and Hilbert Spectral Analysis. *Proceedings Royal Society of London*, A459, 2,317-2,345.

Huang, N.E., M-L. Wu, W. Qu, S.R. Long, and S.S.P. Shen, 2003: Applications of Hilbert-Huang transform to non-stationary financial time series analysis. *Applied Stochastic Models in Business and Industry*, **19**:245-268.

Huang, N.E. and N.O. Attoh-Okine, ed, 2005: *The Hilbert-Huang Transform in Engineering*. CRC Press, Boca Raton.

Hasel, M., Ch. Kottmeier, U. Corsmeier and A. Wieser, 2005:Airborne measurements of turbulent trace gas fluxes and analysis of eddy structure in the convective boundary layer over complex terrain. *Atmospheric Research*, **74**:381-402.

Hiyama, T., M.A. Strunin, R. Suzuki, J. Asanuma, M.Y. Mezrin, N.A. Bezrukova and T. Ohata, 2003: Aircraft observations of the atmospheric boundary layer over a heterogeneous surface in eastern Siberia. *Hydrological Processes*, **17**:2885-2911.

Hubler, G., R. Alvarez, P. Daum, R. Dennis, N. Gillani, L. Kleinman, W. Luke, J. Meagher, D. Rider, M. Trainer and R. Valente, 1998: An overview of the airborne activities during the Southern Oxidants Study (SOS) 1995 Nashville/Middle Tennessee Ozone Study. *Journal of Geophysical Research*, **103(D17)**:22,245-22,259.

Huebert, B.J., G. Lee, and W.L. Warren, 1990: Airborne Aerosol Inlet Passing Efficiency Measurement. *Journal of Geophysical Research*, **95(D10)**, 16,369-16,381.

Hui, K. and S. Baillie, 1996: *Validation of the simultaneous calibration of aircraft position error and airflow angles using a differential GPS technique on a helicopter*. AGARD FVP Symposium on "Advances in Flight Testing", Lisbon, Portugal, 23-26 September, CP-593.

Imhoff, R.E., R. Valente, J.F. Meagher and M. Luria, 1995: The production of O_3 in an urban plume: airborne sampling of the Atlanta urban plume. *Atmospheric Environment*, **29(17)**:2349-2358.

Imhoff, R.E., R.L. Tanner, R.J. Valente and M. Luria, 2000: The evolution of particles in the plume from a large coal-fired boiler with flue gas desulfurization. *Journal of the Air and Waste Management Association*, **50**:1207-1214.

Imhoff, R.E., M. Luria, R.J. Valente and R.L. Tanner, 2001: NO_y removal from the Cumberland Power Plant Plume. *Atmospheric Environment*, **35**:179-183.

Isaac, P.R., J. McAneney, R. Leuning, and J.M. Hacker, 2004: Comparison of aircraft and ground-based flux measurements during OASIS95. *Boundary-Layer Meteorology*, **110**:39-67.

Kader, B.A. and A.M. Yaglom, 1991. Spectra and Correlation Functions of Surface Layer Atmospheric Turbulence in Unstable Thermal Stratification. In: O. Metals and M. Lesieur (eds.), *Turbulence and Coherent Structures,* Dordrecht, Kluwer, pp. 387-412.

Kaimal, J.C., J.C. Wyngaard, Y. Izumi, and O.R. Coté, 1972. Spectral Characteristics of Surface-Layer Turbulence, *Quart. J. R. Meteorol. Soc.*, **98**, 563-589.

Kalogiros, J.A. and Q. Wang, 2002a: Calibration of a radome-differential GPS system on a Twin Otter research aircraft for turbulence measurements. *Journal of Atmospheric and Oceanic Technology*, **19**:159-171.

Kalogiros, J.A. and Q. Wang, 2002b: Aerodynamic Effects on Wind Turbulence Measurements with Research Aircraft. *Journal of Atmospheric and Oceanic Technology*, **19**:1567-1576.

Kang, S.-L., K.J. Davis and M.A. LeMone, 2007: Observations of the ABL structures over a heterogeneous land surface during IHOP-2002. *Journal of Hydrometeorology*, **8**:221-244.

Kelly, R.D., E.A. Smith and J.I. MacPherson, 1992: A comparison of surface sensible and latent heat fluxes from aircraft and surface measurements in FIFE 1987. *Journal of Geophysical Research*, **97(D17)**:18,445-18,453.

Khelif, D., S.P. Burns, and C.A. Friehe, 1999: Improved Wind Measurements on Research Aircraft. *Journal of Atmospheric and Oceanic Technology*, **16,** 860-875.

Kiemle, C., M. Kastner and G. Ehret, 1995: The convective boundary layer structure from lidar and radiosonde measurements during the EFEDA '91 campaign. *Journal of Atmospheric and Oceanic Technology*, **12**:771-782.

Kiemle, C., W.A. Brewer, G. Ehret, R.M Hardesty, A. Fix, C. Senff, M. Wirth, G. Poberaj and M.A. LeMone, 2007: Latent heat flux profiles from collocated airborne water vapor and wind lidars during IHOP 2002. *Journal of Atmospheric and Oceanic Technology*, **24**:627-639.

Kim, J., Q. Guo, D.D. Baldocchi, M.Y. Leclerc, L. Xu, and H.P. Schmid, 2006. Upscaling fluxes from tower to landscape: Overlaying flux footprints on high-resolution (IKONOS) images of vegetation cover. *Agric. For. Meteorol.*, **136**, 132–146.

King, A.D., 1998: Inertial Navigation—Forty Years of Evolution. *GEC Review*, **13(3)**.

Kolmogorov, A.N., 1941: Energy dissipation in locally isotropic turbulence. *Doklady AN SSSR*, **32(1)**:19-21.

Kovalev, V.A. and Eichinger, W.E., 2004: *Elastic Lidar: Theory, Practice and Analysis Methods*. Wiley-Interscience, John Wiley and Sons, Inc, Hoboken, NJ.

Kustas, W.P, J.H. Prueger, J.I. MacPherson, M. Wolde and F. Li, 2005: Effects of land use and meteorological conditions on local and regional momentum transport and roughness for Midwestern cropping systems. *Journal of Hydrometeorology—Special Section*, **6**:825-839.

Leishman, J.G. *Principles of Helicopter Aerodynamics*. Cambridge Aerospace Series. W. Shyy and M.J. Rycroft, Editors, Second Edition, 826 pages, 2006.

Leishman, J.G. and A. Bagai. Rotor Wake Visualization in Low-Speed Forward Flight, AIAA Paper 91-3232, 9th AIAA Applied Aerodynamics Conference, Baltimore, MD, Sept 23-25, 1991.

Lemone, M.A. and W.T. Pennell, 1980: A Comparison of Turbulence Measurements from Aircraft. *Journal of Applied Meteorology*, **19**:1420-1437.

LeMone, M.A., F. Chen, J.G. Alfieri, M. Tewari, B Geerts, Q. Miao, R.L. Grossman and R.L. Coulter, 2007: Influence of land cover and soil moisture on the horizontal distribution of sensible and latent heat fluxes in southeast Kansas during IHOP-2002 and CASES-97. *Journal of Hydrometeorology*, **8**:68-87.

Lenschow, D.H., 1972: *The Measurement of Air Velocity and Temperature Using the NCAR Buffalo Aircraft Measuring System*. Technical Note NCAR/EDD-74, NCAR, Boulder, CO, 39 pp.

Lenschow, D.H., 1986: Aircraft Measurements in the Boundary Layer. in Probing the Atmospheric Boundary Layer, D.H. Lenschow, ed. American Meteorological Society, Boston, MA, 1986.

Lenschow, D.H., E.R. Miller, and R.B. Friesen, 1991: A Three-Aircraft Intercomparison of Two Types of Air Motion Measurement Systems. *Journal of Atmospheric and Oceanic Technology*, **8**:41-50.Lenschow, D.H., 1986: Aircraft Measurements in the Boundary Layer. in Probing the Atmospheric Boundary Layer, D.H. Lenschow, ed. American Meteorological Society, Boston, MA, 1986.

Lenschow, D.H., E.R. Miller, and R.B. Friesen, 1991: A Three-Aircraft Intercomparison of Two Types of Air Motion Measurement Systems. *Journal of Atmospheric and Oceanic Technology*, **8**:41-50.

Lenschow, D. H., Mann, J., and Kristensen, L., 1994. How long is long enough when measuring fluxes and other turbulence statistics, *J. Atmos. Ocean. Tech*., **11**, 661–673.

Lumley, J.L., 1964. The Spectrum of Nearly Inertial Turbulence in a Stably Stratified Fluid, *J. Atmos. Sci.*, **21**, 99-102.

Lundquist, J.K., 2003: Intermittent and Elliptical Inertial Oscillations in the Atmospheric Boundary Layer. *Journal of the Atmospheric Sciences*, **60**:2661-2673.

Luria, M., R.J. Valente, N.V. Gillani, R.L. Tanner, R.E. Imhoff, and J.F. Meagher, 1999. The evolution of photochemical smog in a power plant plume. *Atmos. Environ*.**,** **31**, 3023-3036.

Mahrt, L., J.I. MacPherson and R. Desjardins, 1994: Observations of fluxes over heterogeneous surfaces. *Boundary-Layer Meteorology*, **67**:345-367.

Mahrt, L., D. Vickers and J. Sun, 2001: Spatial variations of surface moisture fluxes from aircraft data. *Advances in Water Resources*, **24**:1133-1141.

Mahrt, L. and D. Vickers, 2002: Relationship of area-averaged carbon dioxide and water vapor fluxes to atmospheric variables. *Agricultural and Forest Meteorology*, **112**:195-202.

Marillier, A., M. Cabane, and D. Cruette, 1991: Preliminary tests of an ultrasonic thermo anemometer for aircraft measurements. *Journal of Atmospheric and Oceanic Technology*, **8**:597-605.

Matayoshi, N., H. Inokuchi, K. Yazawa, and Y. Okuno, 2005: Development of an airborne ultrasonic velocimeter and its application to helicopters. *AIAA 2005-6118*.

Matejka, T. and S.A. Lewis, 1997: Improving research aircraft navigation by incorporating INS and GPS information in a variational solution. *Journal of Atmospheric and Oceanic Technology*, **14(3)**:495-511.

Measures, R.M., 1984: *Laser Remote Sensing: Fundamentals and Applications*. Krieger Publishing Company, Malabar, FL.

Mitsuta, Y., 1966: Sonic anemometer-thermometer for general use. *Journal of Meterological Research of Japan*, **44**:12-23.

Muschinski, A., and C. Wode, 1998: First in situ evidence for coexisting submeter temperature and humidity sheets in the lower free troposphere. *Journal of the Atmospheric Sciences*, **55(18)**:2893-2908.

Muschinski, A., R. G. Frehlich, M. L. Jensen, R. Hugo, A. M. Hoff, F. Eaton, and B. B. Balsley, 2001: Fine-scale measurements of turbulence in the lower troposphere: An intercomparison between a kite- and balloon-borne and a helicopter-borne measurement system. *Bound.-Layer Meteor.,* **98,** 219–250.

Nakamura, R., and L. Mahrt, 2001: Similarity theory for local and spatially averaged momentum fluxes. *Agricultural and Forest Meteorology*, **108**:265-279.

National Research Council (NRC), 2008. Integrating Multiscale Observations of U.S. Waters. Washington, D.C., National Academy Press.

Nicholls, S., 1978: Measurements of turbulence by an instrumented aircraft in a convective atmospheric boundary layer over the sea. *Quarterly Journal of the Royal Meteorological Society*, **104**:653-676.

Nicholls, S., W. Shaw, and T. Hauf, 1983: An Intercomparison of Aircraft Turbulence Measurements Made During JASIN. *Journal of Climate and Applied Meteorology*, **22**:1637-1648.

Nyeki, S., S.de Wekker, D. Steyn, M. Kossmann, M. Kalberer, I. Colbeck and U. Baltensperger, 1999: Airborne lidar study of convective boundary layer development over pre-alpine terrain. *Journal of Atmospheric Science*, **30**, supplement 1:S209-S210.

Nyeki, S., K. Eleftheriadis, U. Baltensperger, I. Colbeck, M. Fiebig, A. Fix, C. Kiemle, M. Lazaridis and A. Petzold, 2002: Airborne lidar and in-situ aerosol observations of an elevated layer, leeward of the European Alps and Apennines. *Geophysical Research Letters*, **29(17)**:Article Number 1852.

Oechel, W.C., G.L. Vourlitis, S. Brooks, T.L. Crawford, and E. Dumas, 1998: Intercomparison among chamber, tower, and aircraft net CO2 and energy fluxes measured during the Arctic System Science Land-Atmosphere-Ice Interactions (ARCSS-LAII) Flux Study. *Journal of Geophysical Research*, **103(D22)**:28,993-29,003.

Ogunjemiyo, S., P.H. Schuepp, J.I. MacPherson and R.L. Desjardins, 1997: Analysis of flux maps versus surface characterisitcs from Twin Otter grid flights in BOREAS 1994. *Journal of Geophysical Research*, **102(D24)**:29,135-29,145.

Ogunjemiyo, S.O., S.K. Kaharabata, P.H. Schuepp, I.J. MacPherson, R.L. Desjardins, D.A. Roberts, 2003: Methods of estimating CO2, latent heat and sensible heat fluxes from estimates of land cover fractions in the flux footprint. *Agricultural and Forest Meteorology*, **117**:125-144.

Pan, J., X-H. Yan, Q.Zheng, W.T. Liu, and V.V. Klemas, 2002: Interpretation of scatterometer ocean surface wind vector EOFs over the Northwestern Pacific. *Remote Sensing of Environment*, **84**:53-68.

Pennell, W.T. and M.A. LeMone, 1974: An experimental study of turbulence structure in the fair-weather trade wind boundary layer. *Journal of the Atmospheric Sciences*, **31**:1308-1323.

Pottier, J.L., S.C. Pryor and R.M. Banta, 1997: Synoptic variability related to boundary layer and surface features observed during Pacific '93. *Atmospheric Environment*, **14**:2163-2173.

Prueger, J.H., J.L. Hatfield, W.P. Kustas, L.E. Hipps, J.I. MacPherson, C.M.U. Neale, W.E. Eichinger, D.I. Cooper, and T.B. Parkin, 2005: Tower and Aircraft Eddy Covariance Measurements of Water Vapor, Energy, and Carbon Dioxide Fluxes during SMACEX. *Journal of Hydrometeorology—Special Section*, **6**:954-960.

Rankine, W.J.M., 1865. On the mechanical principles of the action of propellers. *Transactions of the Institute of Naval Architects*, 6, pp. 13-39.

Ritter, J.A., J.D.W. Barrick, C.E. Watson, G.W. Sachse, G.L. Gregory, B.E. Anderson, M.A. Woerner and J.E. Collins, Jr., 1994: Airborne boundary layer flux measurements of trace species over Canadian boreal forest and northern wetland regions. *Journal of Geophysical Research*, **99(D1)**:1671-1685.

Roekens, E.J., G.F. Dumont, D.M Tielmans, G.E. Verduyn, and E.G. De Saeger, 1992: Ozone Levels in Belgium. Air Pollution Control: papers from the 9th World Clean Air Congress, Montreal, Quebec, Canada, September 4, 1992.

Roth, R., M. Hofmann, and C. Wode, 1999a: Geostrophic wind, gradient wind, thermal wind and the vertical wind profile—A sample analysis within a planetary boundary layer over Arctic sea-ice. *Boundary-Layer Meteorology*, **92**:327-339.

Roth, R., M. Hofmann, and C. Wode, 1999b: The determination of the geostrophic windspeed on the basis of pressure measurements with the HELIPOD-system. *Meteorologische Zeitschrift*, **8(1)**:36-39.

Said, F., J.L. Attie, B. Benech, A. Druilhet, P. Durand, M.H. Marciniak and B. Monteny, 1997: Spatial variability in airborne surface flux measurements during HAPEX-Sahel. *Journal of Hydrology*, **188-189**:878-911.

Said, F., U. Corsmeier, N. Kalthoff, C. Kottmeier, M. Lothon, A. Wieser, T. Hofherr, and P. Perros, 2005: ESCOMPTE experiment: intercomparison of four aircraft dynamical, thermodynamical, radiation and chemical measurements. *Atmospheric Research*, **74**:217-252.

Salisbury, J.I. and M. Wimbush, 2002: Using modern time series analysis techniques to predict ENSO events from the SOI time series. *Nonlinear Processes in Geophysics*, **9**:341-345.

Samuelsson, P. and M. Tjernstrom, 1999: Introduction to the in situ airborne meteorological measurements in NOPEX. *Agricultural and Forest Meteorology*, **98-99**:181-204.

Schmitgen, S., H. Geiss, P. Ciais, B. Neininger, Y. Brunet, M. Reichstein, D. Kley and A. Volz-Thomas, 2004: Carbon dioxide uptake of a forested region in southwest France derived from airborne CO2 and CO measurements in a quasi-Lagrangian experiment. *Journal of Geophysical Research*, **109**:D14302.

Siebert, H., and A. Muschinski, 2001. Relevance of a tuning fork effect for temperature measurements with the Gill Solent HS ultrasonic anemometer-thermometer. *J. Atmos. Oceanic Technol.,* **18,** 1367–1376.

Siebert, H., H. Franke, K. Lehman, R. Maser, E.W. Saw, D. Schell, R.A. Shaw, and M. Wendisch, 2006. Probing finescale dynamics and microphysics of clouds with helicopter-borne measurements. *Bull. Amer. Meteorol. Soc.*, 1727-1738.

Schmid, H.P., 2002. Footprint modeling for vegetation atmosphere exchange studies: a review and perspective, *Agric. For. Meteorol.*, **113**, 159–183.

Smith, R.B., S. Skubis, J.D. Doyle, A.S. Broad, C. Kiemle and H. Volkert, 2002: Mountain waves over Mont Blanc: Influence of a stagnant boundary layer. *Journal of the Atmospheric Sciences*, **59**:2073-2092.

Strawbridge, K.B. and B.J. Snyder, 2004: Daytime and nighttime aircraft lidar measurements showing evidence of particulate matter transport into the Northeastern valley of the Lower Fraser Valley, BC. *Atmospheric Environment*, **38**:5873-5886.

Strunin, M.A. and T. Hiyama, 2004: Response properties of atmospheric turbulence measurement instruments using Russian research aircraft. *Hydrological Processes*, **18**:3099-3117.

Strunin, M.A. and T. Hiyama, 2005: Spectral structure of small-scale turbulent and mesoscale fluxes in the atmospheric boundary layer over a thermally inhomogeneous land surface. *Boundary-Layer Meteorology*, **117**:479-510.

Sun, J., R. Desjardins, L, Mahrt and I. MacPherson, 1998: Transport of carbon dioxide, water vapor, and ozone by turbulence and local circulations. *Journal of Geophysical Research*, **103(D20)**:25,873-25,885.

Suomi, V.E. and J.A. Businger, 1959: Principle of the sonic anemometer-thermometer. Geophysical Research Paper No. 59, AFCRC-TR-58-235, 673 pp.

Telford, J.W. and P.B. Wagner, 1974: The measurement of horizontal air motion near clouds from aircraft. *Journal of the Atmospheric Sciences*, **31**:2066-2080.

Telford, J.W., P.B. Wagner and A. Vaziri, 1977: The measurement of air motion from aircraft. *Journal of Applied Meteorology*, **16**:156-166.

Thornhill, K.L., B.E. Anderson, J.D.W. Barrick, D.R. Bagwell, R. Friesen and D.H. Lenschow, 2003: Air motion intercomparison flights during Transport and Chemical Evolution in the Pacific (TRACE-P)/ACE-ASIA. *Journal of Geophysical Research*, **108(D20)**:9001.

Tjernstrom, M. and C.A. Friehe, 1991: Analysis of a radome air-motion system on a twin-jet aircraft for boundary-layer research. *Journal of Atmospheric and Oceanic Technology*, **8**:19-94.

Valente, R.J., R.E. Imhoff, R.L. Tanner, J.F. Meagher, P.H. Daum, R.M. Hardesty, R.M. Banta, R.J. Alvarez, R.T. McNider, and N.V. Gillani, 1998. Ozone production during an urban air stagnation episode over Nashville, Tennessee. *J. Geophys. Res.*, **103,** 22,555-22,568.

Van Atta, C.W. and J.C. Wyngaard, 1975. On Higher-Order Spectra of Turbulence. *J. Fluid Mech.*, **72**, 673-694.

Van den Kroonenberg, A., and J. Bange, 2007. Turbulent flux calculation in the polar stable boundary layer: Multiresolution flux decomposition and wavelet analysis. *J. Geophys. Res.,* **112(D6)** D06112.

Veltcheva, A.D., and C.G. Soares, 2004: Identification of the components of wave spectra by the Hilbert Huang transform method. *Applied Ocean Research*, **26**:1-12.

Vickers, D., and L. Mahrt, 2006. A solution for flux contamination by mesoscale motions with very weak turbulence. *Bound.-Layer Meteorol.*, **118**, 431-447.

Wolff, M. and J. Bange, 2000: Inverse method as an analysing tool for airborne measurements. *Meteorologische Zeitschrift*, **9(6)**:361-376.

Wood, R., I.M. Stromberg, P.R. Jonas, and C.S. Mill, 1997: Analysis of an Air Motion System on a Light Aircraft for Boundary Layer Research. *Journal of Atmospheric and Oceanic Technology*, **14**:960-968.

Wu, Z, N.E. Huang, S.R. Long and C.-K. Peng, 2007: On the trend, detrending, and variability of nonlinear and nonstationary time series. *Proceedings of the National Academy of Sciences*, **104(38)**:14889-14894.

Wyngaard, J.C. and O.R. Coté, 1972, CoSpectral Similarity in the Atmospheric Surface Layer. *Quart. J. R. Meteorol. Soc.*, **98**, 590-603.

Wyngaard, J.C., W.T. Pennell, D.H. Lenschow, and M.A. LeMone, 1978. The Temperature- Humidity Covariance Budget in the Convective Boundary Layer. *J. Atmos. Sci.*, **35**, 47-58.

Yazawa, K., Tamaru, T. and H. Hashiguchi, 2001: Development of ultrasonic anemometer for environmental observation by aircraft. AIAA 2001-5272.

Zhaoyang, J., Y. Qiang, L. Shuhe, W. Tianduo, S. Xiaomin and Z. Renhua, 2006: Comparative analysis of temperature and CO2 fluxes for winter wheat in Tibetan Plain and North China Plain using the EMD method. *Progress in Natural Science*, **16(10)**:1066-1071.

Biography

Heidi Eichinger Holder was born in Tacoma, WA and graduated from Los Alamos High School in Los Alamos, NM. She received a B.S. in Biosystems Engineering (2001) and an M.S. in Environmental Engineering and Science (2003), both from Clemson University. She is married and has one child.